INTEGRATED STUDY ON GROUNDWATER DYNAMICS IN THE COASTAL AQUIFERS OF WEST BENGAL FOR SUSTAINABLE GROUNDWATER MANAGEMENT

NHP

A PURPOSE DRIVEN STUDY, UNDER NATIONAL HYDROLOGY PROJECT

NATIONAL INSTITUTE OF HYDROLOGY
ROORKEE (UTTARAKHAND)

Integrated Study on Groundwater Dynamics in the Coastal Aquifers of West Bengal for Sustainable Groundwater Management

A PURPOSE DRIVEN STUDY
UNDER
NATIONAL HYDROLOGY PROJECT

Director: Dr. M.K. Geol

STUDY TEAM

National Institute of Hydrology, Roorkee

Dr. Sudhir Kumar, Director & Sc. 'G' (Rtd)
Dr. M.Someshwar Rao, Scientist-G

SWID, Government of West Bengal

Er. Subrat Haldar, Exec. Eng. (A-1)

HYDROLOGICAL INVESTIGATIONS DIVISION
NATIONAL INSTITUTE OF HYDROLOGY,
Roorkee-247 667, Uttarakhand,
INDIA

June, 2024

FOREWORD

It is with great pride and satisfaction that I present this comprehensive report on the groundwater resources and their management in the coastal zone of West Bengal. This report is the culmination of extensive research and meticulous analysis carried out by a dedicated team of experts. The scope and depth of the study not only highlight the critical state of groundwater resources in this coastal region but also serve as a strategic guide for addressing the challenges posed by salinization, seawater intrusion, and resource depletion.

The coastal areas of West Bengal play a crucial role in supporting both agriculture and urban development, yet they face increasing threats from changing hydrological patterns, population growth, and climate change. This report provides a systematic understanding of these issues by employing state-of-the-art tools and technologies, including remote sensing, GIS, hydrochemical analysis, and isotope hydrology. These techniques have yielded invaluable insights into groundwater dynamics, highlighting regions that are most vulnerable to depletion and contamination.

What sets this report apart is its interdisciplinary approach. By integrating advanced methodologies with local data, the research team has offered a holistic view of the groundwater system, allowing for more accurate predictions and the development of sustainable management strategies. This study not only expands the knowledge of coastal groundwater systems but also demonstrates how cutting-edge technology can be applied to solve real-world problems.

I am confident that the findings and recommendations contained in this report will serve as a valuable resource for water managers, researchers, policymakers, and other stakeholders in the field of water resources management. It offers practical solutions to the growing water challenges faced by coastal regions, not just in West Bengal but across similar geographies in India.

I extend my heartfelt appreciation to all members of the research team for their hard work, dedication, and collaboration. Their contributions have not only made this report a resounding success but have also laid the groundwork for sustainable water resource management in the coastal regions of West Bengal. I believe that this report will inspire further research and action in the field, ensuring that our water resources are protected and managed for future generations.

Director
National Institute of Hydrology

TABLE OF CONTENTS

LIST OF FIGURES

LIST OF TABLES

EXECUTIVE SUMMARY

Coastal zones are vital regions that support approximately 40% of the global population, serving as crucial hubs for economic activities, agriculture, and settlements. However, these areas are increasingly threatened by rapid urbanization, climate change, rising sea levels, and seawater intrusion. Coastal West Bengal, particularly in districts like East Medinipur, South 24 Parganas, and Howrah, is acutely experiencing these challenges, compounded by excessive groundwater extraction and pollution. Understanding the structure of the saline-freshwater interface is essential for assessing diminishing fresh groundwater reserves, the discharge of fresh groundwater into the sea, salt enrichment in inland aquifers, and pollutant discharge into the marine environment. This study provides a comprehensive assessment of groundwater and surface water quality, runoff potential, seawater intrusion, and the impacts of population growth. A robust methodology was employed, including the collection of archival data on surface water, groundwater, and aquifer characteristics, supplemented by field and laboratory investigations. Detailed analyses of hydrogeology, water quality, and isotopic composition were conducted to evaluate the dynamic interactions between freshwater and seawater in the region, aiming to deliver actionable insights for planners, decision-makers, and implementation agencies.

Key Findings:

1. **Rainfall and Runoff**: The average annual rainfall in the study area was recorded at 1728 ± 293 mm, with significant spatial variation. Higher rainfall near the coast contributes to runoff, especially in watersheds like the Damodar River, where runoff percentages reached 52.53%. This data is critical for flood management and urban planning.
2. **Groundwater Potential**: The study identified four groundwater potential zones: very high (16.78%), high (53.48%), moderate (29.52%), and low (0.22%). Areas with flat or gently sloping terrain showed higher recharge potential, indicating suitable regions for sustainable groundwater extraction.
3. **Water Quality**: High salinity levels were observed in shallow aquifers near the Haldi River, with notable declines in bicarbonate levels at greater depths. Isotopic analysis confirmed significant seawater intrusion, emphasizing the urgency of managing groundwater extraction to prevent further degradation.
4. **Seawater Intrusion**: Population growth is accelerating seawater intrusion, particularly in densely populated areas like Kolkata and Howrah. Mapping seawater intrusion in relation to population density reveals high-risk zones requiring targeted management strategies.
5. **Long-Term Water Quality Trends**: From 2010 to 2022, groundwater salinity fluctuated, with some areas showing freshening trends while others, particularly Howrah and Kolkata, continued to struggle with high salinity. Heavy metal concentrations, including arsenic and manganese, exceeded safe levels, necessitating immediate intervention for public health.

6. **Aquifer Lithology and Tritium Analysis**: Thicker aquifers in South 24 Parganas and East Medinipur are particularly vulnerable to seawater intrusion. Tritium analysis indicated that 88% of groundwater samples showed no recent recharge, highlighting reliance on older groundwater and the need for effective recharge management.

Recommendations:

- **Flood Management and Urban Planning**: Utilize rainfall-runoff data to develop flood mitigation strategies, particularly in high-risk watersheds. Enhanced drainage systems and flood management infrastructure are essential to prevent waterlogging and damage.
- **Groundwater Management**: Focus on high-potential recharge zones for sustainable groundwater extraction. Implement policies regulating groundwater withdrawal and promote rainwater harvesting.
- **Seawater Intrusion Mitigation**: Develop protective measures, such as salinity barriers and enhanced groundwater recharge practices, in identified high-risk zones to safeguard freshwater resources.
- **Water Quality Monitoring**: Establish stringent monitoring protocols for drinking water sources, particularly in areas with high heavy metal concentrations. Prioritize water treatment and health advisories to mitigate public health risks.
- **Urban Planning**: Integrate urban expansion with sustainable water resource management, focusing development in areas with lower vulnerability to seawater intrusion to reduce pressure on freshwater supplies.

Conclusion:

The findings from this comprehensive study provide critical insights into the hydrological, geological, and environmental challenges faced by Coastal West Bengal. By utilizing GIS and remote sensing tools, planners and state implementation agencies can better understand dynamic water systems and take proactive measures for sustainable freshwater resource management. Immediate actions based on these results are necessary to mitigate long-term risks and ensure water security for future generations. Addressing these challenges will not only protect the region's water resources but also enhance the resilience of coastal communities against the impacts of climate change and urbanization.

1 INTRODUCTION

1.1 Coastal Zones and Their Hydrological Significance

Approximately 40% of the world's population lives within 100 kilometres of the coast. Major cities under coastal influence include Tokyo (Japan), Mumbai (India), São Paulo (Brazil), Kolkata (India), New York (US), Shanghai (China), Karachi (Pakistan), Lagos (Nigeria), Manila (Philippines), Buenos Aires (Argentina), Los Angeles (US), Rio de Janeiro (Brazil), Istanbul (Turkey), Osaka-Kobe (Japan), Shenzhen (China), Guangzhou (China), Jakarta (Indonesia), and Lima (Peru), among others.

The coastal zone is an interface between the land and sea, which is comprised of a continuum of coastal land, intertidal areas, aquatic systems including the network of rivers and estuaries, islands, transitional and intertidal areas, salt marshes, wetlands, and beaches. Coastal zones are continually changing because of the dynamic interaction between the sea and the land by tides, currents, and waves. The high concentration of people in coastal regions is due to extensive possibilities for transportation and trade links, industrial and urban development, revenue from tourism, sea-food, oil & gas zones, defense, salt mines, power production etc. The economic growth, population growth and urbanization comes with land-use change, increased use of freshwater resources, agricultural expansion, deforestation, encroachment on water bodies, infrastructure developments, land-use changes, development of embankments, industrial settlements, waste and effluent disposal from industrial and municipal sources, and more. In addition to human-induced stressors, climate-induced factors such as sea-level rise, subsidence, coastal tectonic activities, climate change, cyclones and storms, coastal flooding, tides, seawater intrusion, soil salinization, coastal inundation, high fluxes of sedimentation, etc., also cause loss of fertile land, human, livestock and property, and reduction in freshwater reserve.

India has a total coastline length of 7516.6 km constituting 5422.6 km length of mainland coastline and 2094 km of island territories. Indian coastline touches nine states-- Gujarat, Maharashtra, Goa, Karnataka, Kerala, Tamil Nadu, Andhra Pradesh, Odisha, West Bengal; two unions territories-- Daman and Diu and Puducherry; and two islands of Andaman and Nicobar Islands in the Bay of Bengal and Lakshadweep in the Arabian Sea.

The coastal zone is associated with several geomorphic features and coastal processes including estuarine zone, tidal influenced zone, tidal marsh, backwater etc. Esturies are the tidal mouth that has a free connection with the open sea and within which tides cause inflow

of seawater whereas freshwater derived from land drainage cause dilution of seawater salinity. Tides in seawater develop in response to the forces exerted by the moon and sun; and their relative position with respect to earth. Further, the shape of bays and estuaries, and roughness of the bed surface also modifies the intensity of tides. Backwater is a part of estuarine system, that refers to a system of shallow, brackish-water lagoons and swamps along the coastline. The quality of backwater system is influenced by short-term changes induced by the tides effects and the seasonal changes brought about by the monsoon system. During monsoon, it is freshwater dominated whereas in the remaining period it is dominated by seawater.

Important factor that affect mean sea level include change in the ratio of glacial-ice cap to the total volume of sea water; relative movements of ground (subsidence/uplift) and sea-floor; thermal expansion of seawater; and other dynamic factors like winds, atmospheric pressures, ocean currents, and waves, tide, tsunami, storm surges, etc.

Mean sea level at a given position is the height of the sea surface averaged over a long period of time. The long term averaging, averages miner temporal variations mainly associated due to tidal and seasonal effects. The mean sea level averaged over the global oceans is called global mean sea level (GMSL). Sea level rise is of major concern for countries and islands located in low-lying areas. In such areas, sea-level rise results into coastal inundation, erosion, and submergence of land-mass.

Coastal Regulated Zone (CRZ) and Coastal Zone Management Plan (CZMP): A coastal zone is a part of the land affected by its proximity to the sea, and that part of the sea affected by its proximity to the land as the extent to which man's land-based activities have a measurable influence on water chemistry and marine ecology. In order to protect biodiversity, demographic patterns, natural resources, and conserve our coastal environment etc., Ministry of Environment, Forest and Climate Change (MoEFCC) under the section 3 of the Environment Protection Act, 1986 of India, introduced Coastal Regulation Zone (CRZ) which was notified and issued in February 1991. This was amended, revised and notified as Coastal Regulation Zone (CRZ) in 2011. The notification declares the coastal stretches of the country and the water (and bed) area upto its 12-mile territorial water limit as well as tidal-influenced water bodies, as Coastal Regulation Zone (CRZ), and imposes restrictions on industries, operations and processes in this zone. The 2011 notification classifies the CRZ into four categories:

CRZ-I: Ecologically sensitive areas

CRZ-II: Built-up areas

CRZ-III: Basically rural areas

CRZ-IV: Water areas, including territorial waters and tidal-influenced water bodies

Further, the Government of India issued the Coastal Regulation Zone Notification in 2019 for CZMP, with a view:

- to conserve and protect the unique environment of coastal stretches and marine areas
- to ensure livelihood security to the fisher communities and other local communities in the coastal areas
- to promote sustainable development based on scientific principles taking into account the dangers of natural hazards, sea level rise due to global warming, do hereby, declares the coastal stretches of the country and the water area up to its territorial water limit, excluding the islands of Andaman and Nicobar and Lakshadweep and the marine areas surrounding these islands, as Coastal Regulation Zone:

- CRZ-IA - Ecologically Sensitive Areas
- CRZ-IB - Intertidal Zone
- CRZ-II - Developed Land Areas (Municipal Limits / Urban Areas)
- CRZ-IIIA - Undeveloped rural areas; population density > 2161/km2; area up to 50 meters from the HTL on the landward side is the 'No Development Zone (NDZ)'
- CRZ-IIIB - Undeveloped rural areas; population density < 2161/km2; and the area up to 200 meters from the HTL on the landward side is earmarked as the 'No Development Zone (NDZ)'
- CRZ-IVA - The water area and the sea bed area between the Low Tide Line up to twelve nautical miles on the seaward side shall constitute CRZ-IV A
- CRZ-IVB - areas shall include the water area and the bed area between LTL at the bank of the tidal influenced water body to the LTL on the opposite side of the bank, extending from the mouth of the water body at the sea up to the influence of tide, i.e., salinity of five parts per thousand (ppt) during the driest season of the year.

Table 1: Classification of Coastal Regulation Zones (CRZ)

CRZ	Regulation
I	IA: The areas that are ecologically sensitive and the geomorphological features which play a role in the maintaining the integrity of the coast
	IB: The area between Low Tide Line (LTL) and High Tide Line (HTL)
II	Areas which are developed up to the shoreline and falling within the municipal limits; includes built-up area Villages and towns are that are already well established
III	Areas that are relatively undisturbed and also include rural and urban areas that are not substantially developed CRZ-IIIA - Population density is more than 2161 per square kilometre as per 2011 census base, and area up to 50 meters from the HTL on the landward side shall be earmarked as the 'No Development Zone (NDZ)' CRZ-IIIB - Population density of less than 2161 per square kilometre, as per 2011 census base, and the area up to 200 meters from the HTL on the landward side shall be earmarked as the 'No Development Zone (NDZ)
IV A	The water area from the LTL to twelve nautical miles on the seaward side
IVB	The water areas of the tidal influenced water body from the mouth of the water body at the sea up to the influence of tide which is measured as five parts per thousand during the driest season of the year

Figure 1 Coastal Regulation Zone (CRZ) for Coastal Zone Management Plan (CZMP), as per the notification 2019

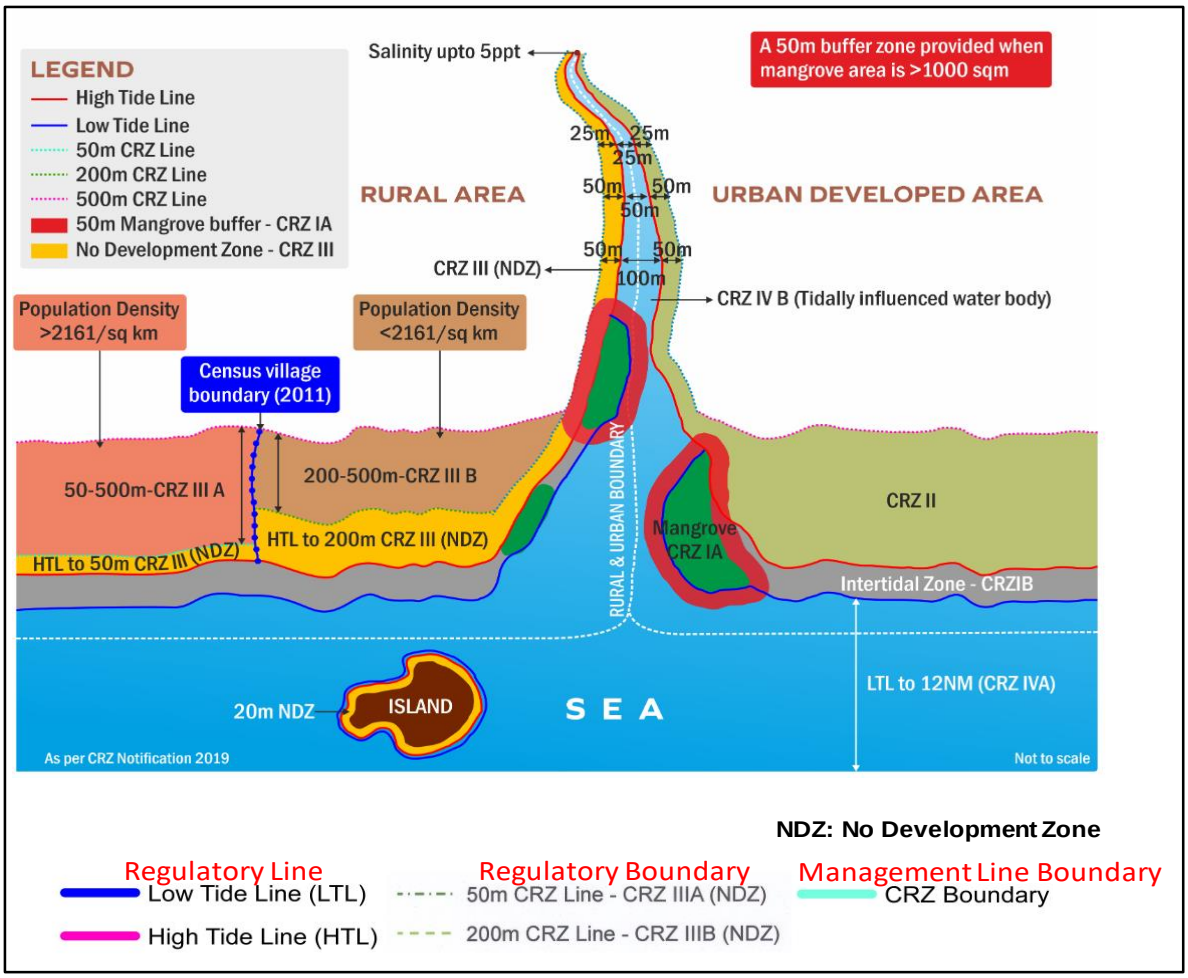

Figure 2 Conceptual Diagram of Coastal Zone Management Plan (Source: https://czmp.ncscm.res.in/)

Salt Water Intrusion is one of the major problem in water resources in the coastal regions. Saline water has high mineral contents (Seawater salinity= 35,000 ppm, whereas fresh water salinity is less than 1000ppm), high water density (density of seawater: 1025 kg/m^3 whereas the freshwater density is 1000kg/m^3) pressure. Due to higher density of saline water, the sea water pushes the freshwater and makes it float. Recharge through evaporating lagoons, salt playas, leaching of salts from saline clays, contamination from paleo-seawater, are the process which are in addition to the direct seawater intrusion that cause saltwater contamination.

The main issues in Ganga Basin is rapidly increasing population, rising living standards and exponential growth of industrialization and urbanization. River Ganga, and its tributaries in some stretches, particularly during lean seasons is known to become unfit even for bathing. The threat of global climate change is also becoming important issue impacting infrastructural projects in the upper reaches of the river, raise issues that need a comprehensive response.

1.2 Bengal Basin

The Bengal Basin is a significant geological and hydrological region bordered by various geological features. To the north, it is bounded by the Shillong Plateau, a prominent upland area separating it from the Brahmaputra Valley. To the east, the Burma Arc fold-belt marks the basin's boundary with Myanmar and the Chittagong hills in Bangladesh. The Bay of Bengal forms its southern boundary, while the Indian craton, encompassing the Chhota Nagpur Plateau and the Rajmahal hills, delineates its western edge, remnants of the ancient Gondwanaland.

1.2.1 Hydrology and River Systems

The river systems of the Ganges, Brahmaputra, and Meghna, originating from the Himalayas and the Indo-Burmese ranges, converge within the basin to form the Ganges-Brahmaputra delta. This delta is the world's largest subaerial delta system, spanning over 100,000 km² of riverine channels, floodplains, delta plains, and vast fertile plains that support extensive agriculture and sustain a dense population.

1.2.2 Geological Formation and History

The formation of the Bengal Basin began during the Middle-Upper Cretaceous period (66.0-145 million years ago) with differential subsidence. The basin originated from the subduction of the Indian Plate beneath the Eurasian and Burmese Plates, leading to the formation of a rifted eastern continental margin and a remnant ocean basin. During the breakup of Gondwanaland, non-marine sediments were deposited in isolated graben-controlled basins oriented in a north-south direction. Subsequent marine inundation during the late Cretaceous period covered much of the basin, resulting in the deposition of thick sedimentary layers that form the foundational soils of its fertile plains.

1.2.3 Key Geological Features

(a) Eocene Hinge Zone:

This zone, running in a north-northeast to south-southwest direction, represents a critical geological boundary where the basin's sedimentary prism undergoes abrupt changes in thickness and composition. Associated with gravity highs and magnetic lows, it reflects the complex subsidence patterns and tectonic activities during the Oligocene (23-33.9 Ma) and Miocene epochs (5.3-23.03 Ma), highlighting the basin's dynamic geological history. The north-northeast to south-southwest direction running basin margin fault, separates the crystalline/metamorphic complex of the Precambrian

age (4.0-4.5 billion years) to the west and the shelf sediments to the east. Formed during the Early Cretaceous (65-145 Ma), this fault zone contributed to the down-warping of the basin and influenced the deposition of Rajmahal basaltic lavas. West of this fault zone, the basin transitions into exposure to Gondwana sediments resting on the Precambrian (4.5-5.4 billion years) granitic basement.

(b) Shelf Zone:

The Shelf Zone of the Bengal Basin extends more than 100 km wide in the north, narrowing towards the south. This region reveals a history of gradual subsidence during the post-Paleocene period (Paleocene: 56-66 Ma). The Eocene (33.9-55 Ma) epoch witnessed the development of shelf carbonates, including reefal build-ups along the shelf edge, signifying a transition from fluvial to deltaic and marine depositional environments from west to east.

(c) Swatch of No Ground:

This trough-shaped marine valley or trench canyon, about 14 km wide, crosses the continental shelf, extending seaward for almost 2,000 km down the Bay of Bengal in the form of valleys with levees. The trench is 400–450 m deeper than the surrounding mean seafloor depth of 1000 m. It is believed that during the Pleistocene (11.7 ka to 2.6 million years ago), the Ganga-Brahmaputra River discharged its sediment load directly on the shelf edge. The combination of river flow and turbidity currents generated at the shelf break and upper slope was responsible for the formation of the Swatch of No Ground. This area, declared a marine protected area in 2014, is home to several globally threatened marine species.

(d) The Ganges-Brahmaputra Delta

i. The Ganges-Brahmaputra (GB) delta is one of the most vulnerable deltas in the world, tilting from the west (West Bengal) towards the east (Bangladesh). Due to these socio-environmental complexities, the Bengal Basin is hydrologically one of the most active regions globally.

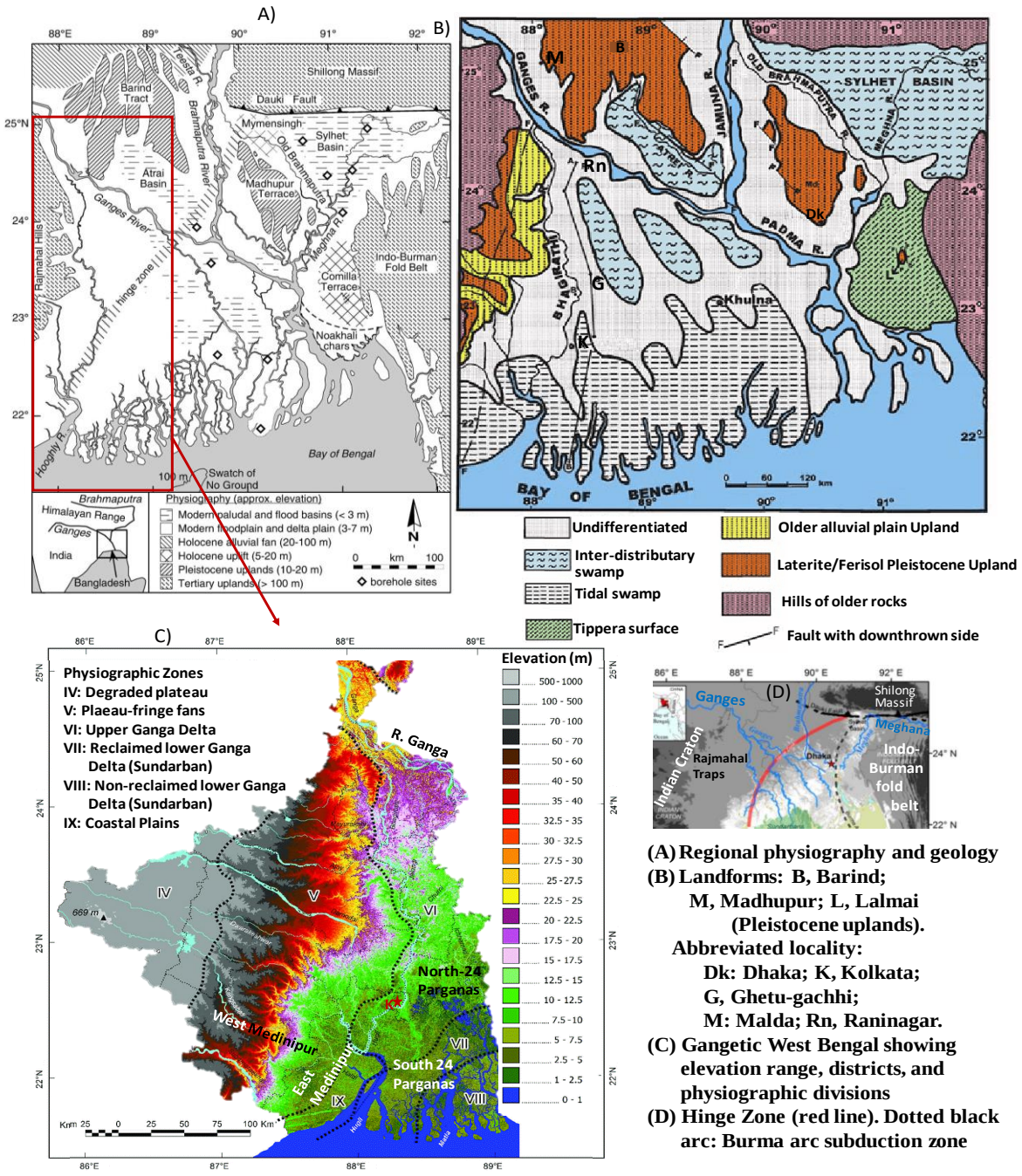

(A) Regional physiography and geology
(B) Landforms: B, Barind; M, Madhupur; L, Lalmai (Pleistocene uplands).
Abbreviated locality: Dk: Dhaka; K, Kolkata; G, Ghetu-gachhi; M: Malda; Rn, Raninagar.
(C) Gangetic West Bengal showing elevation range, districts, and physiographic divisions
(D) Hinge Zone (red line). Dotted black arc: Burma arc subduction zone

(Figures reproduced from: Goodbred et al., 2003, Acharya, 2010, Ghosh, 2019, Krien et al., 2019)

Figure 3: Physiography, geology and landforms of Gangetic West Bengal

ii. Rarh Region:

The Rarh region intervenes between the southern Ganges delta and the western plateau region. Extending from the 50-meter contour in the east to the 100-meter contour in the west, this region includes the districts of Birbhum, Barddhaman, Bankura, Murshidabad, and Medinipur. It is believed to have been created from soil originating from the Deccan plateau and is dominated by laterite soil.

iii. Sundarban Delta:

The Sundarban delta is the largest mangrove forest in the world. 'Sundari' trees are found in abundance, giving the region its name. The delta is formed from the dense network of the river Ganga distributaries and their silt deposition, including the Hoogly, Matla, Jamira, Gosaba, Saptamukhi, and Haribhanga rivers. The region is characterized by tidal creeks, mudflats, and islands. The Mangrove Forest of this region is listed in the UNESCO World Heritage list as the Sundarbans and Sundarbans National Park, respectively.

iv. Coastal and Sedimentary Environments

a) Part of the district of Purba Medinipur along the Bay of Bengal constitutes the coastal fringe. The emergent coastal plain is made up of sand and mud deposited by rivers and wind. This area has been shaped by its numerous rivers.

b) The sedimentary environment of the deltaic region is developed by the sediment load carried by the Ganga-Brahmaputra-Meghana river system from the Himalayas to the Bay of Bengal, amounting to about a billion tons annually. Due to tidal action, the suspended sediment load settles in the estuarine mouth and river floodplain in the coastal region, resulting in the creation of mudflats. The process of sediment accretion also leads to the formation of swamps, islands, and marginal bars. Among the coastal features, sand dunes are observed along the coastline in sectors such as Bakkhali-Fraserganj, Digha-Shankarpur, and Ganga Sagar-Chuksar Island.

c) The Bengal Basin, with its diverse geological history, complex hydrology, and unique ecosystems, plays a crucial role in supporting a dense population and various economic activities. However, it also faces significant challenges from natural and human-induced factors, making it one of the most dynamic and vulnerable regions in the world.

1.3 Hydrological Investigations of Coastal Water Resources

Seawater enters inland areas through creeks, tidal streams, and backwaters. The range over which the intrusion occurs depends on the temporal variation of tidal heights, stream geometry, and local topography and geology. The tidal oscillations result in periodic changes in the salinity levels of these coastal streams, and in the region of stream-groundwater interaction, contamination results in groundwater salinization (Hoitink et al., 2016; Jones et al., 2020; Werner, 2006). Excessive groundwater withdrawals in coastal regions can lead to a decline in piezometric heads, inducing saltwater upconing in production wells in coastal

aquifers (Sarker et al., 2021; Dieu et al., 2022). Conversely, control over excessive abstraction combined with artificial recharge measures can lead to the freshening of saline groundwater pockets, improving the fresh groundwater reserve and controlling seawater intrusion (Chen et al., 2014; Hussain et al., 2019).

The landward movement of seawater contaminates fresh groundwater resources on land, while the seaward discharge of contaminants and nutrients from discharging groundwater and surface water also contaminates coastal ecosystems, estuaries, and marine zones (Prusty & Farooq, 2020; Klassen & Allen, 2017; Paerl, 2006; Shtereva, 2015). Similarly, the discharge of conservable fresh surface water to the sea or submarine discharge of fresh groundwater to the sea (submarine groundwater discharge) contributes to the loss of terrestrial freshwater resources (Zou et al., 2019; Sawyer et al., 2016; Moosdorf & Oehler, 2017).

The evolution of the hydrochemical quality of groundwater, evaporation-associated enrichment of salts, salinization, sources of pollution, sources of salinity, hydrogeochemical processes, and interaction with seawater in coastal aquifers are widely assessed using major ion chemistry, ionic ratios, stable isotopes of water, and the combined use of isotopic-hydrochemical analysis (Mondal et al., 2010; Selvakumar et al., 2022; Schiavo et al., 2009; Currell et al., 2015; Chen et al., 2021; Wu et al., 2020; Batayneh, 2014).

1.3.1 Project Objectives

The present study is conducted in the coastal districts of West Bengal, encompassing a 157.5 km coastline, the northwest upland degraded plateau, the coastal deltaic region, the Sundarbans, densely populated urban areas (Howrah district and Kolkata region), and sparsely populated rural regions. The study focuses on investigating the following hydrological components:

- Long-term rainfall patterns
- Watershed-wise runoff generation
- Groundwater flow conditions, particularly groundwater in the top 200 m zone
- Hydrochemical and isotopic composition of groundwater
- Salinity of river-water
- Mapping of freshwater discharge zones and seawater intrusion zones
- Tides and tidal-affected regions

Table 2: Watershed (Area & Avg. slope) map

Watershed	Area (sq.km)	Avg. Slope (%)	Watershed	Area (sq.km)	Avg. Slope (%)
Tidal Streams	9779.93	0.005	Rasulpur	1562.82	0.18
Kasai Haldi	4638.06	0.122	Damodar	898.77	0.16
Rupnarayan	3914.25	0.08	Pichhabai	822.79	0.03
Subarnarekha	2686.82	0.14	Saraswati	280.82	0.06
Ichhamati	1757.94	0.009			

The study area shows wide variations in drainage characteristics as well as drainage congestion is a common problem in coastal plains -the flat areas with flat slopes. In these areas, particularly in low-lying coastal areas, disposal of surface runoff takes considerable time and surface drainage problem becomes acute. The accumulation of water affects the crops.

2 STUDY AREA

2.1 Geography

West Bengal is the only state of India that extends from the Himalaya to the Bay of Bengal. A large portion of the state occupies the transitional zones between the Himalayas in the north and the Chhotanagpur plateau in the west to the plains of the Ganga-Brahmaputra delta (GBD) in the southern and eastern sections The length of the coastline in West Bengal is 220 km (325 km long including islands) with a coastal zone of about 9,630 square km. The coastal zone supports an approximate population of 7 million. The coastal zone includes three coastal districts namely, East (or Purba) Medinipur (Dist HQ: Tamluk), South 24 Parganas (Dist H Q: Alipore) and Howrah. For the present study, the adjoining two districts West Medinipur (Dist H. Q: Medinipur) and North 24 Parganas (HQ: Barasat) are also included making total five districts and also included the Kolkata Municipal Corporation (KMC).

In 1983, the district 24 Parganas was split into two districts -North 24 Parganas with its Head Quarter Barasat, and South 24 Parganas with its Head Quarter as Alipore

In 2002, Medinipur (also known as Midnapore) was split into Paschim (or West) Medinipur and East (or Purba) Midinipur

In 2022-23 new districts were announced to come into existence. These are:

North 24 Parganas to be split into Icchamati district (HQ: Bongaon) and Basirhat district (HQ: Basirhat)

South 24 Parganas is proposed to split into: South 24 Parganas district and Sundarbans District

The study area (5 districts & KMC) covers a total area of 18,667 km^2 of the coastal zone of West Bengal (shown in fig.2). The river Hugli separates the eastern and western part of the coastline. The western coastline forms the southern boundary of the East Medinipur district, and it covers 60km (approximately 27%) of the coastline. The eastern part of the coastline forms the southern boundary of the district South 24 Parganas. Considerable portion of the district South 24 Parganas is covered by Sundarbans.

The study area occupies six major physiographic zone Sundarbans, Deltaic plan, Degraded plateau, Plateau fringe fan, Reclaimed coastal zones and Medinipur coastal plains shown in the **(Figure 3).**

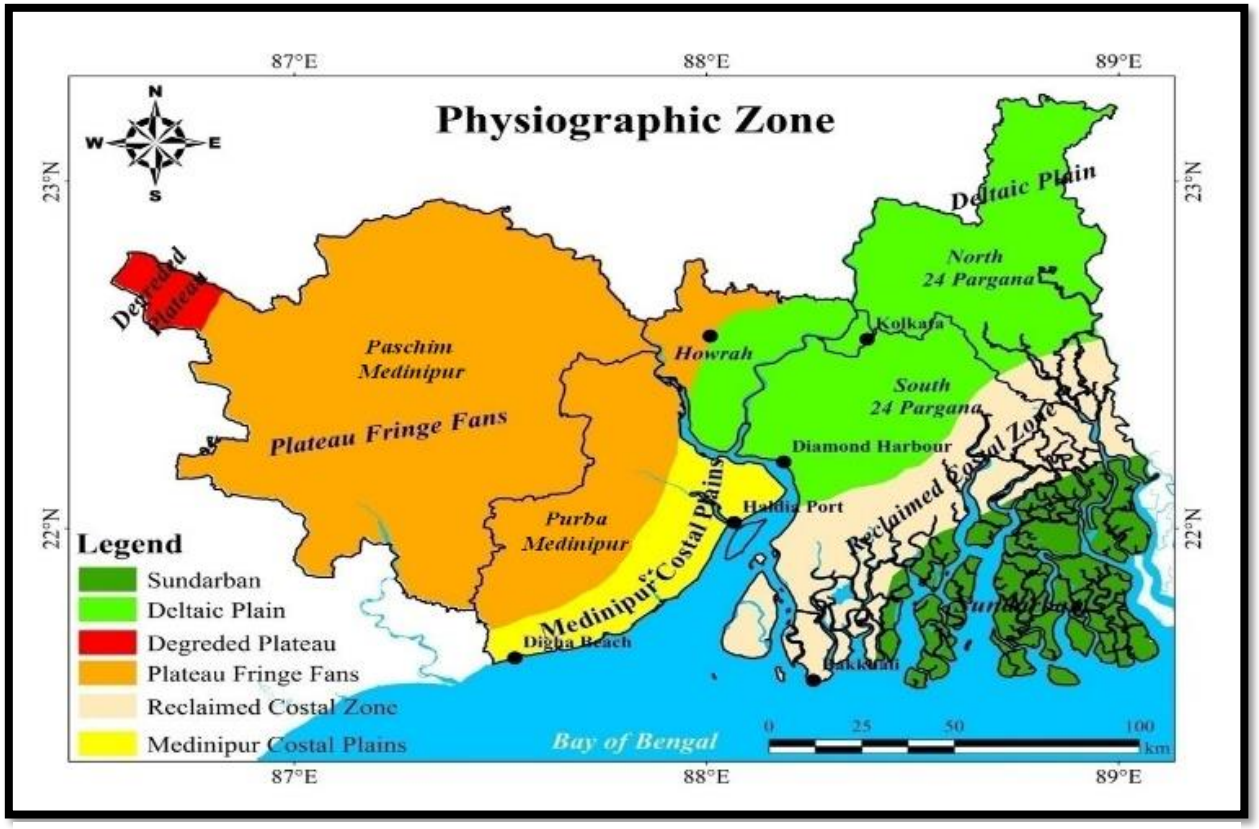

Figure 4: Physiographic zones of the study area.

In the Sundarbans region, the river Hugli with its tributary systems meanders severely in its confluence with the Bay of Bengal and is divided into a number of branches, enclosing and intersecting the delta. In the process it leaves a number of meandering scars, which include dead channels, creeks, brackish water lakes, swamps, etc. North and South 24 Parganas are traversed by a number of moribund rivers, which are primarily spill channels of Hugli River. Six major estuarine rivers, viz., Muri Ganga, Saptamukhi, Thakuran, Matla, Gosaba and Herobhanga meet the Bay of Bengal on their southern mouths and are interconnected with each other through numerous criss-cross creeks and small rivers creating about 102 islands of which 54 islands have been cleared and converted to habitable lands and the rest are still part of the Sundarbans mangrove ecosystem. These tidal estuarine rivers carry the seawater from the Bay of Bengal during high tide and inundate the mangrove forests at regular intervals. The river Hugli (Ganga) in the west is the main river carrying freshwater from upstream reaches of lower Ganga delta into the Sundarbans (Indian part).

Total area falling within the coastal zone of the study area (and also of the state West Bengal) is about 10,158.22 sq km, of which CRZ-I cover an area of 8,184.91 sq km,while CRZ-II and CRZ-III account for 3.41 sq km and 1,969.90 sq km respectively (Hussain & Kumar, 2019).

Sundarban Land Reclamation: The pristine Sundarban forest has drastically decreased over the last two centuries due to extensive forest destruction, land reclamation, and expanding settlements. The Dampier-Hodges Line is an imaginary line passing through the South 24 Parganas and North 24 Parganas districts. It indicates the eco-region of Sundarbans in India. This hypothetical line, developed by the British in 1828, mapped the extent of the mangrove forest in 1830 and is still considered the northern limit of the Indian Sundarbans. The line runs through the 24 Parganas North and South districts of West Bengal.

Currently, the Indian Sundarban covers 4266.40 km², though satellite images show only 1434.40 km² of forest-dominated areas. It is estimated that two centuries ago, the Indian Sundarban covered about 10,000 km², with only 42% remaining today (Mondal et al., 2010). Kolkata city was once covered with mangrove vegetation (Ghosh et al., 2015), and the saline marine condition extended up to the north of Barrackpore, North 24-Parganas, with tidal ingression at present-day Dum Dum between 6,000-10,000 years BP **(Banerjee, 1996,** Chanda S and A. K. Hait, 1996). Over time, more than half of the mangrove forest area has dwindled, leaving less than 50% today in the Indian Sundarbans.

The degradation of the Sundarban mangrove forests began in 1770 during British India. Claude Russel and later Tilmen Henckell initiated the reclamation of Sundarban forests. These forests were partially exploited for human settlement and the rest for rice cultivation and brackish water fisheries. Migrants from Midnapore, Jharkhand (then Bihar), and Chhattisgarh (then Madhya Pradesh) settled in the Sundarban, searching for work and land. This reclamation and settlement took place in five phases:1770–1780, 1780–1873, 1873–1939, 1945–1951, and 1951–1971 (Ghosh & Mukhopadhyay, 2016). The British initiated rapid reclamation of this region with the help of local Zamindars (landlords of pre-independence India) for revenue collection. By the time of India's independence in 1947, only 50% of the forest's pre-colonial size remained. Human encroachment has altered the low-lying marshy forested land of the Sundarban region.

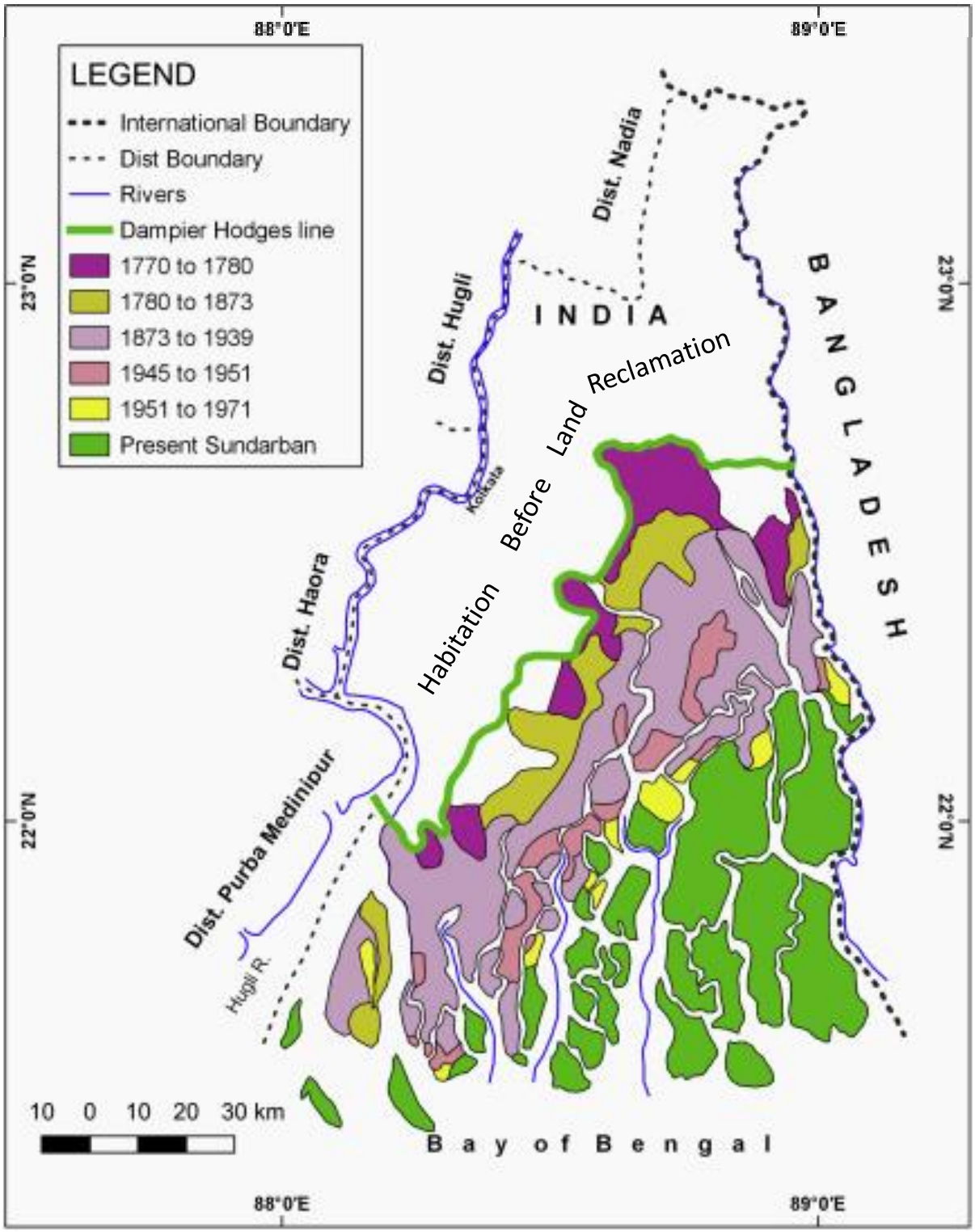

Figure 5: Roy A. & S. B. Dhar (2021)

Reclamation of Waterbodies (Salt Lake): Much before the Mughal's era, the eastern parts of Kolkata was a conglomerate of several wet land (locally known as bheris, these are also Ramsey sites) and salt lakes. Over the time, with urbanization, many of these turned into marshy area. Post-Independence, in the early 60's Dr. Bidhan Chandra Roy, the first Chief Minister of West Bengal reclaimed one such saline lake in the east of Kolkata to develop a satellite township. The low lying area was filled with sand and mud (dredged-out from Hooghly river), and developed it as a satellite township as Salt Lake City or Bidhan Nagar.

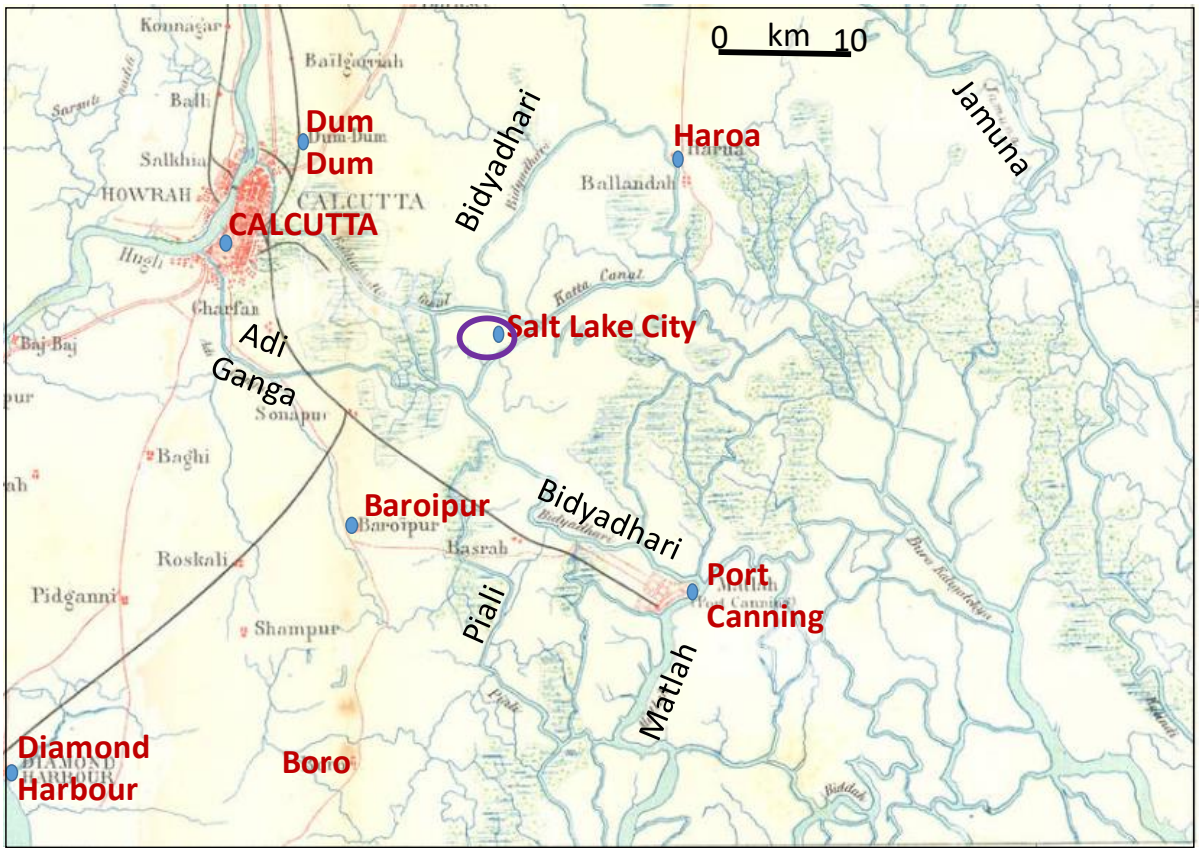

Figure 6: Location of Salt Lake City or Bidhan Nagar

West Bengal has about 41 Islands, of these Sagar Island is the largest amongst all with a area of about 300km^2. Many of these islands are still evolving and getting modified due to combination of natural anthropogenic processes including erosion, accretion, subsidence, sea-level rise and anthropogenic activities. An evolution of Sagar Island in the past two centuries is shown in the **Figure 7**.

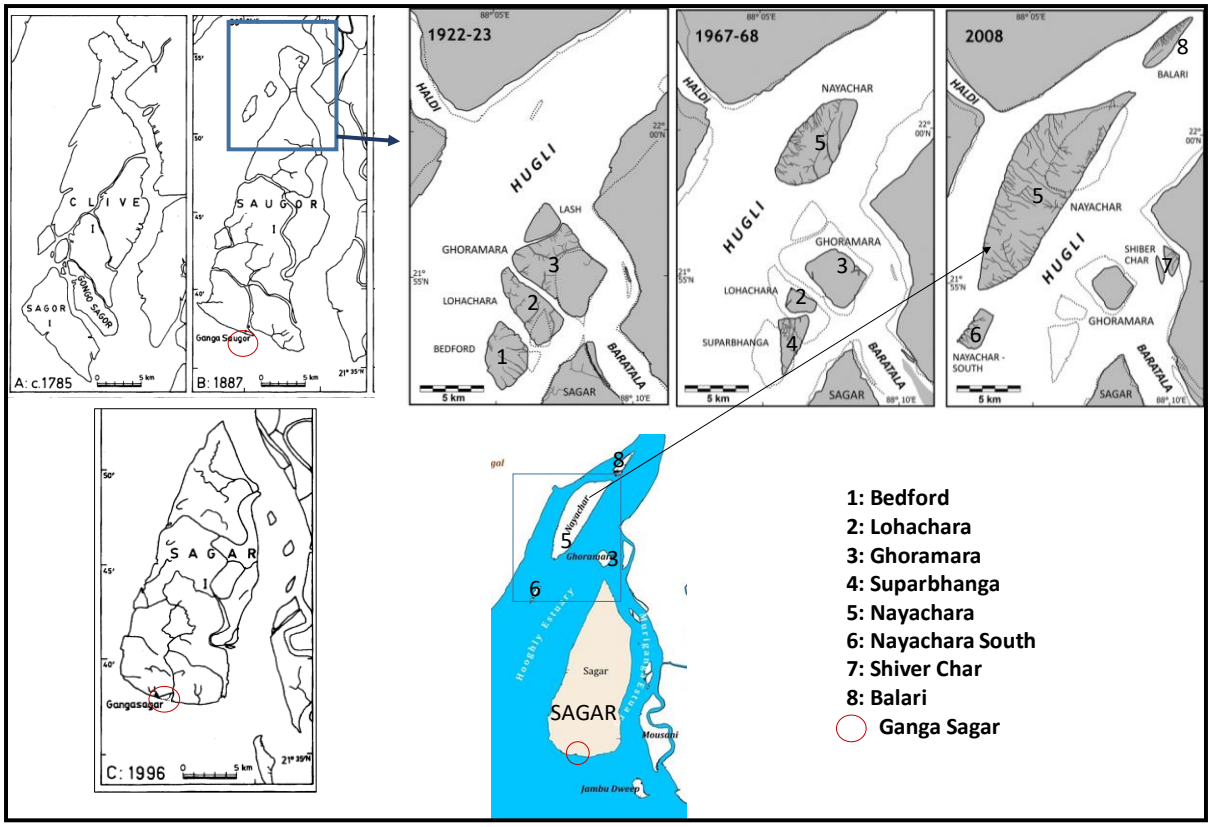

Figure 7: Evolution of Sagar Island and sarounding area (Ref.: Gopinath and Serlathan, 2005; Nandy and Bandopadhyay, 2011)

2.2 Climate

The climate of the study area is characterized by an oppressively hot summer, high humidity nearly the year-round, and well-distributed rainfall during the monsoon season. The cold season from about the middle of November to the end of February is followed by the summer from March to May. The southwest monsoon season is from June to September. October and the first half of November constitute the post-monsoon season.

The district experiences a humid sub-tropical type of climate with minimum and maximum temperature varying from 7^0C in the winter to 45^0C in summer respectively. In summer, average daily maximum temperature varies between 25ºC and 40ºC. Winter is generally dry and cold with average winter temperature around 17º C.

In the study region, the mean daily maximum temperature is high from March to October, peaking during April-May. After May, the temperature decreases until mid-July, then increases again, reaching another peak in October before continuously decreasing until the start of January. During April-May, the distribution of the mean daily maximum temperature in the

study area is highly resolved. This well-separated temperature distribution pattern reduces and becomes more or less uniform from July to February.

In the post-winter period, the mean daily minimum temperature increases from a value close to 13°C, reaching a maximum level of about 26°C. This plateau region continues from mid-April to September, after which the temperature rapidly drops.

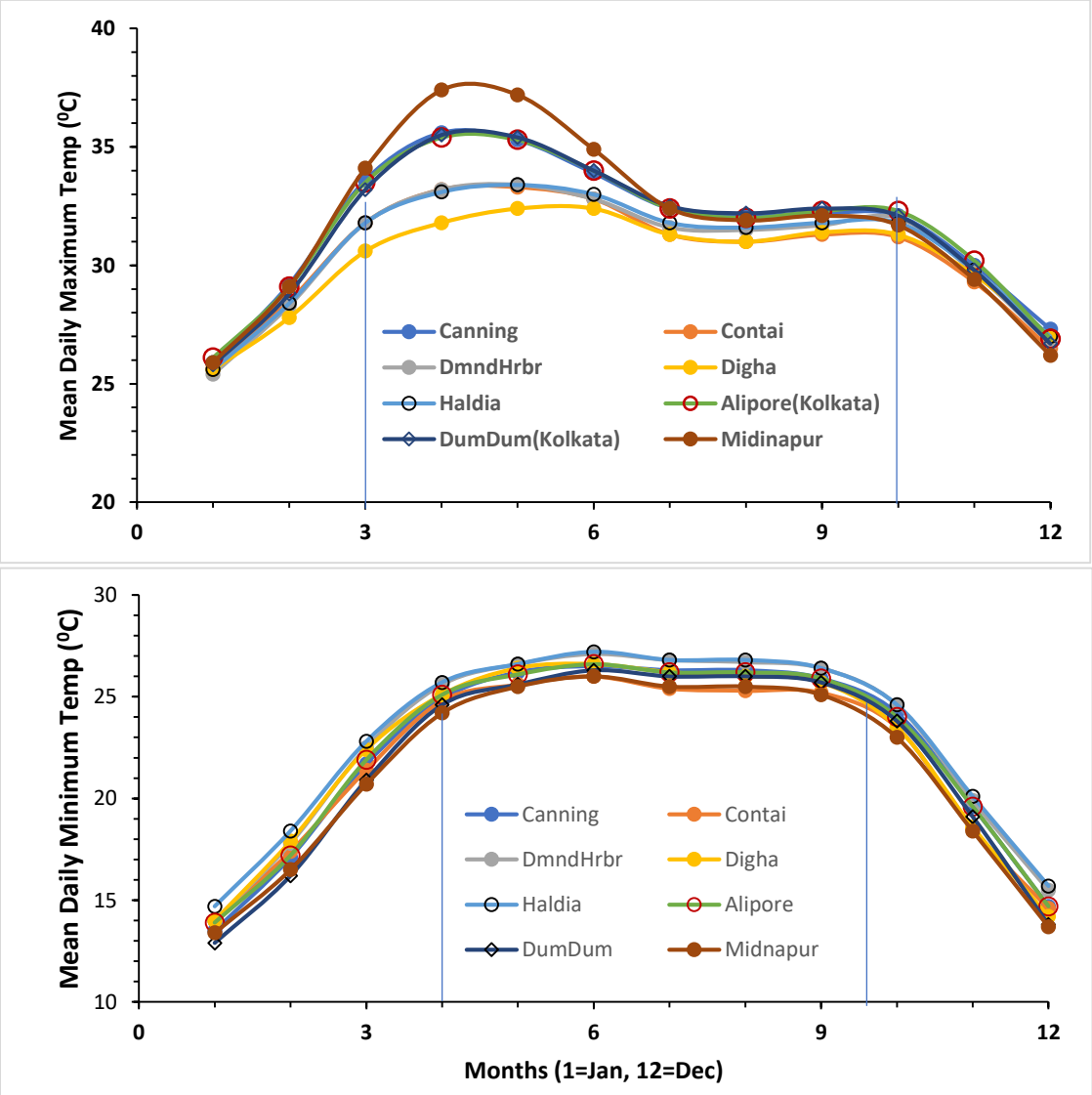

Figure 8: Mean daily minimum and maximum temperature (Source: IMD, 2008)

The long-term normal rainfall distribution pattern is not same in all the districts (Fig…). It is a bell shaped curve for West Medinipur and North 24 Parganas with peak rainfall during July-August. The peak is narrower for the case of West Medinipur compared to the North 24 Parganas. The rainfall distribution is bi-modal shaped with the main peak appearing in July and a small hump in September for the districts Howrah, South 24 Pargans and the Kolkata Municipal Corporation (KMC). In the case of East Medinipur also it is bimodal shaped but

with the difference that the main peak appears in November and minor hump in July. When compared the total annual rainfall, the districts West Medinipur and Howrah receive rainfall ~1587 mm, the districts North 24 Parganas, East Medinipur and KMC receive ~1752mm, and the South 24 Parganas receive ~2020mm. Data for the extreme rainfall years (draught and excessive rainfall years) shows that excessive rainfall years are very high in the study area compared to the drought years indicating requirement of better management strategies to tackle frequent flooding events than the drought events

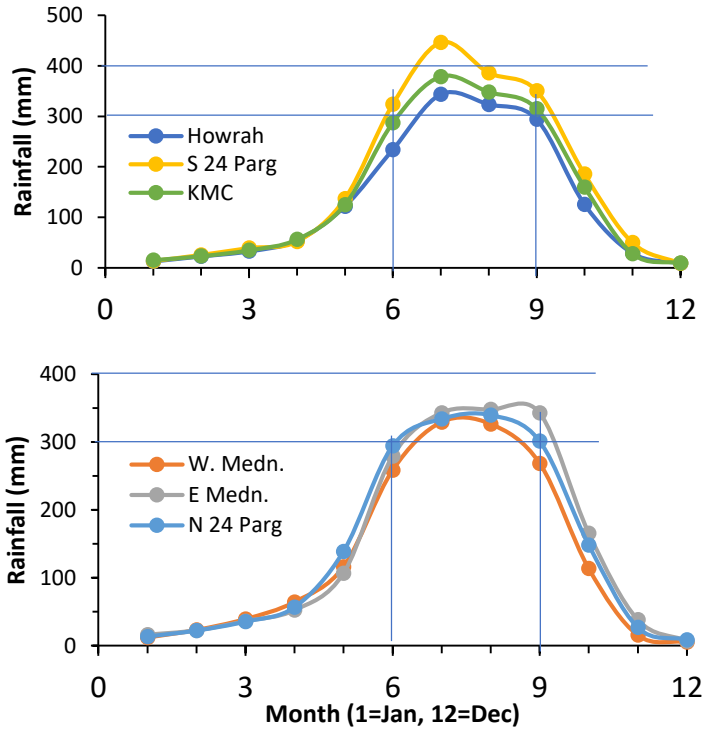

Figure 9: Normal Annual Rainfall distribution in the study area. For calculating the Normal Annual Rainfall, a back-calculation is done using the raw data for rainfall and the deviation percentage. The raw data is taken from the imd's website:

https://hydro.imd.gov.in/hydrometweb/(S(gfrefe3gxcxxznz5ennu10vj))/DistrictRaifall.aspx

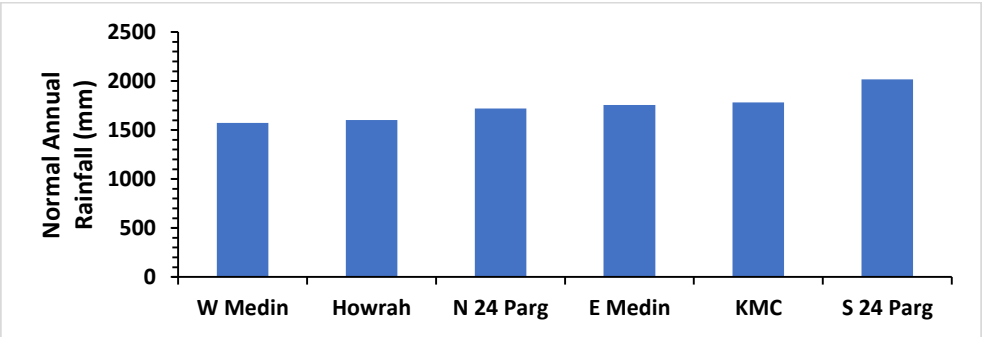

Figure 10: District-wise Annual Rainfall in the study area

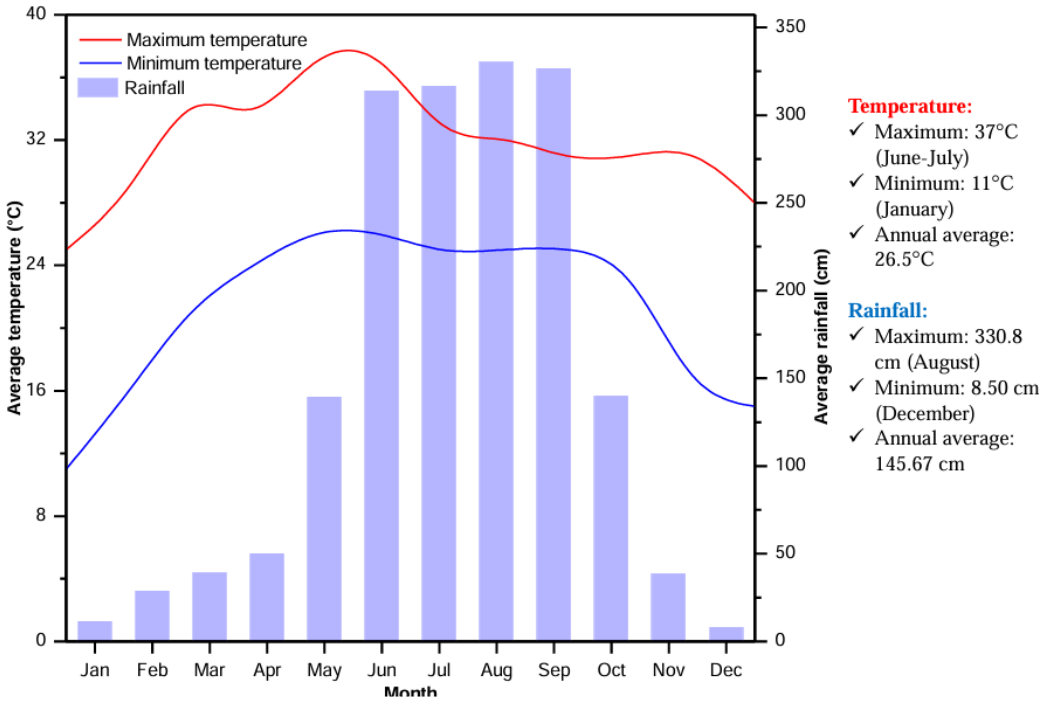

Figure 11: Month-wise variation of average rainfall and temperatures during 1949 – 2017 of the Purba Medinipur district.(Ref: Paul and Mandal, 2021)

Table 3: District-wise extreme rainfall years (Source: IMD, 2008)

District	Drought years		Excessive Rainfall Years	
	Year	Lowest RF as a % of normal annual rainfall	Year	Highest RF as a % of annual normal rainfall
Howrah	1954, 1982	57%	1952, 1971	152%
Kolkata	1953, 1954, 1966, 1982	66%	1971, 1978, 1984, 1986, 1990, 1990, 1993, 1999	152%
North 24 Parg	1966, 1979, 1982	72%	1959, 1968, 1970, 1971, 1977, 1978, 1981, 1981, 1984, 1986, 1990, 1995, 1999	167%
South 24 Parganas	1951, 1954, 1957, 1964, 1979	61%	1956, 1971, 1977, 1981, 1986, 1988, 1990, 1991, 1995	366%
West Medinipur	1954	63%	1956, 1968, 1971, 1973, 1978, 1986, 1989, 1990, 1993, 1997, 1999	190%
E. Medinipur	1957, 1964	71%	1956, 1965, 1966, 1971, 1973, 1986, 1990, 1993, 1995, 1999	165%

The study area shows wide variations in drainage characteristics as well as drainage congestion is a common problem in coastal plains -the flat areas with flat slopes. In these areas, particularly in low-lying coastal areas, disposal of surface runoff takes considerable time and surface drainage problem becomes acute. The accumulation of water affects the crops.
The watershed within study area with avg. slope (in percentage) and area (in sq.km) **shown in Table 2**.

Table 4: Watersheds in the study area and the relative area percentage

Watershed no.	Watershed	% area
1	Subarnarekha	10.7
2	Pichhabani	1.8
3	Rasulpur	5.2
4	Haldia	18.8
5	Rupnarayan	20
6	Hugli	10.2
7	Kulti	14.5
8	Icchamati	5.5
9	Sundarban	13.3
	Total	**100**

Source of Anthropogenic Pollution: The study area contains large number of industries including drug and pharma industries, cement, metal smelters, distilleries, fertilizers, oil refineries, thermal power plants (Titagarh (S. 24 Pargana), Garden Reach, Kolkata, Cossipore station, Kolkata, Bandel Plant, Hoogly, Kolaghat, East Medinipur, etc), petrochemical industries, pulp and paper mills, sugar industries, dyeing and bleaching units, anodizing and galvanizing units, cast iron foundries, hot rolling mills etc. These industries contaminate air, water and soil by chemicals, bio-medical waste, heavy metals, organic and hazardous wastes. On an average, Kolkata and Howrah Municipal Corporation together generates about 4,400 MT of solid and liquid waste every day (Ali, 2018; Gupta, 2022). About 25% of this passes through treatment and the rest gets disposed untreated contaminating the environment.

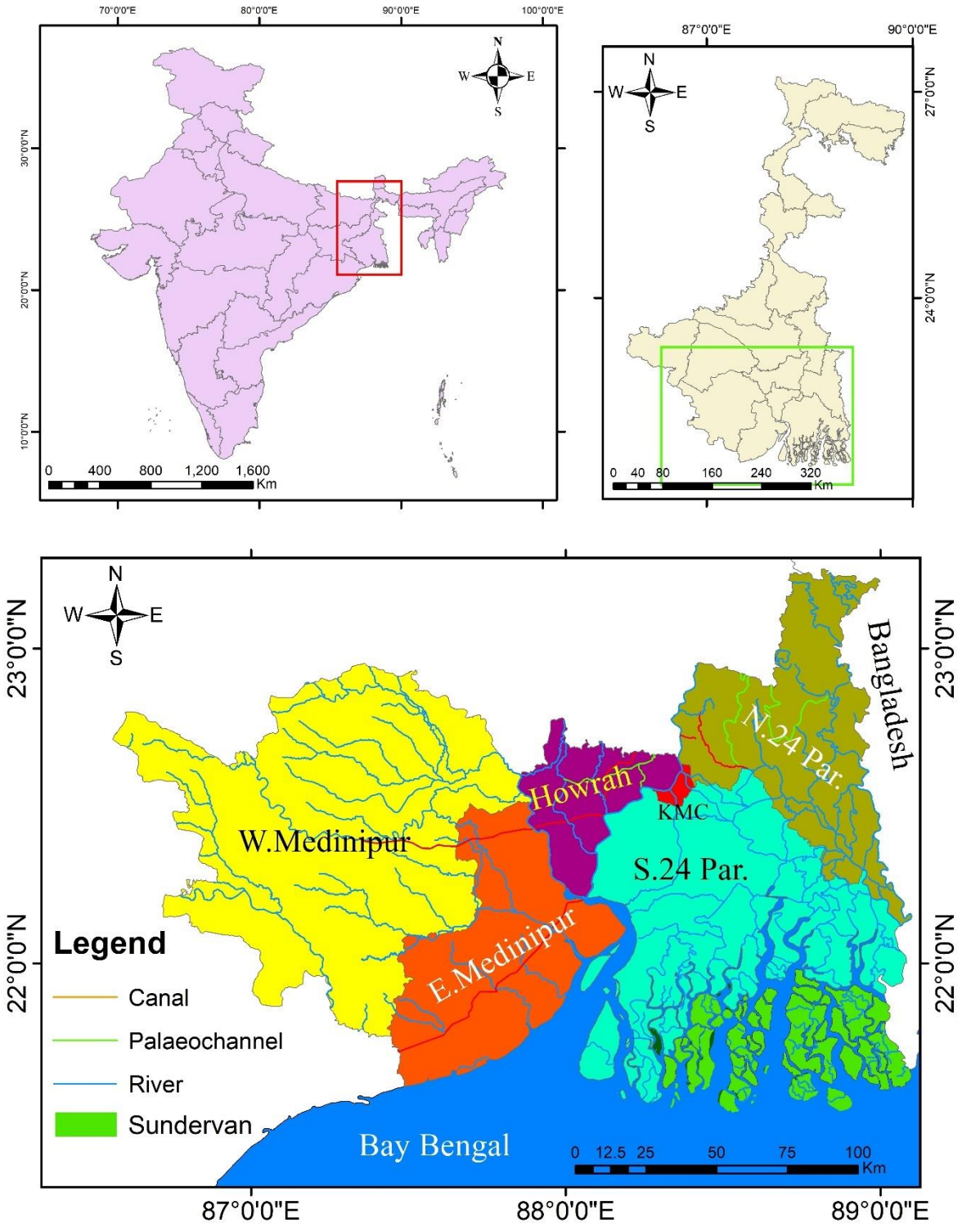

Figure 12: Study area: District map, and the surface drains

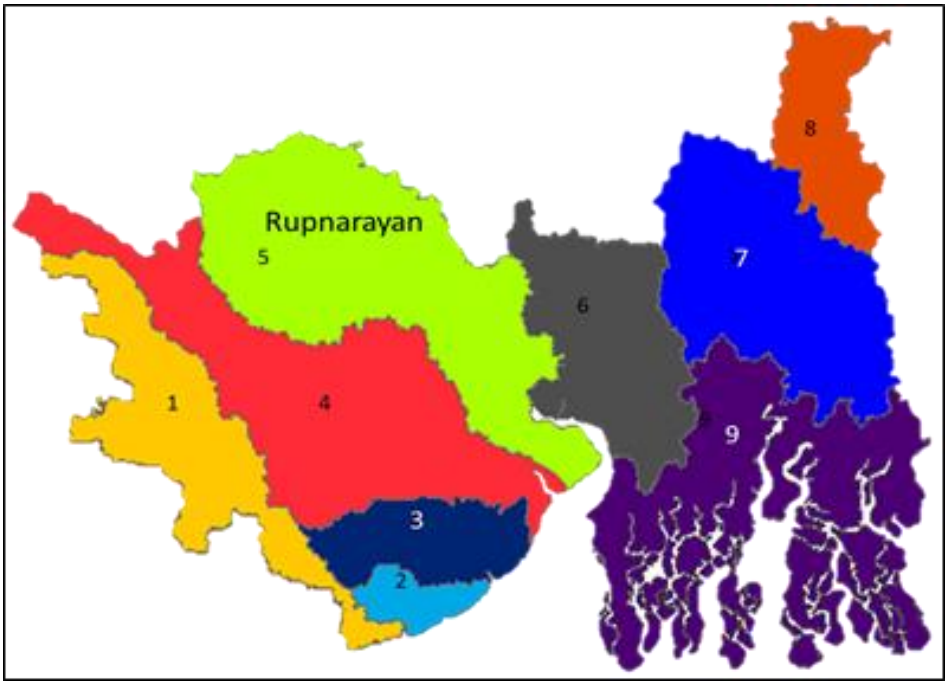

Figure 13: Watershed in the study area of WB (1,7 and 8 are transboundary watersheds)

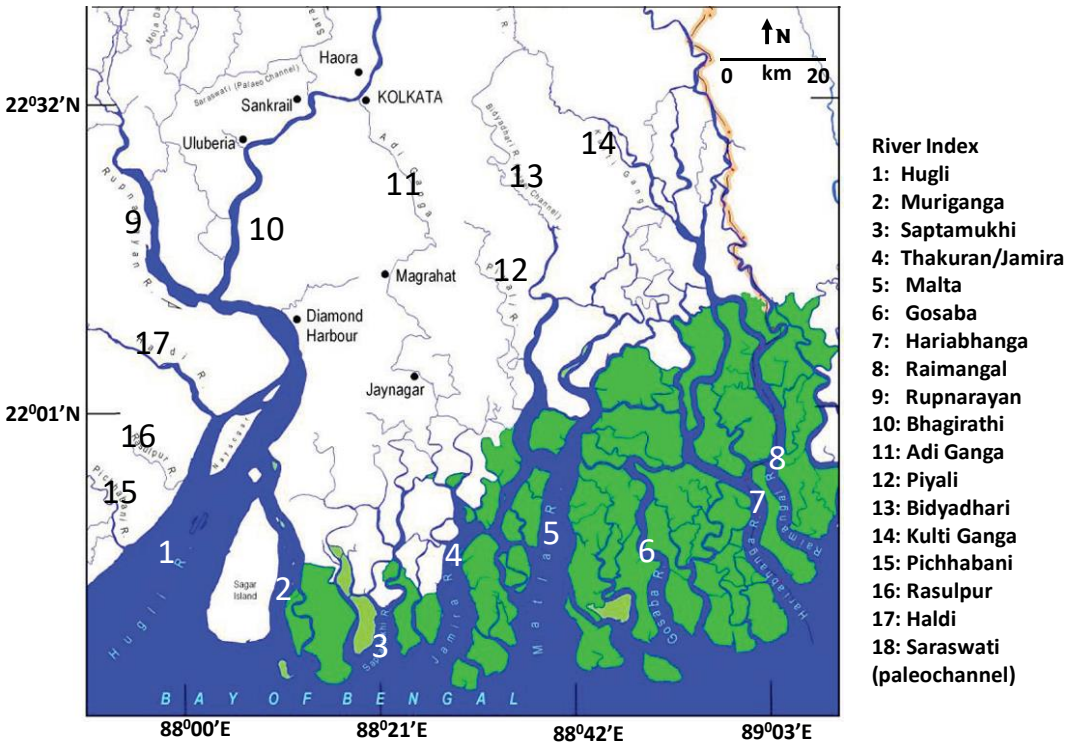

Figure 14: Rivers and the tidal channels in the district South -24 Parganas. River's are marked by their respective serial numbers.

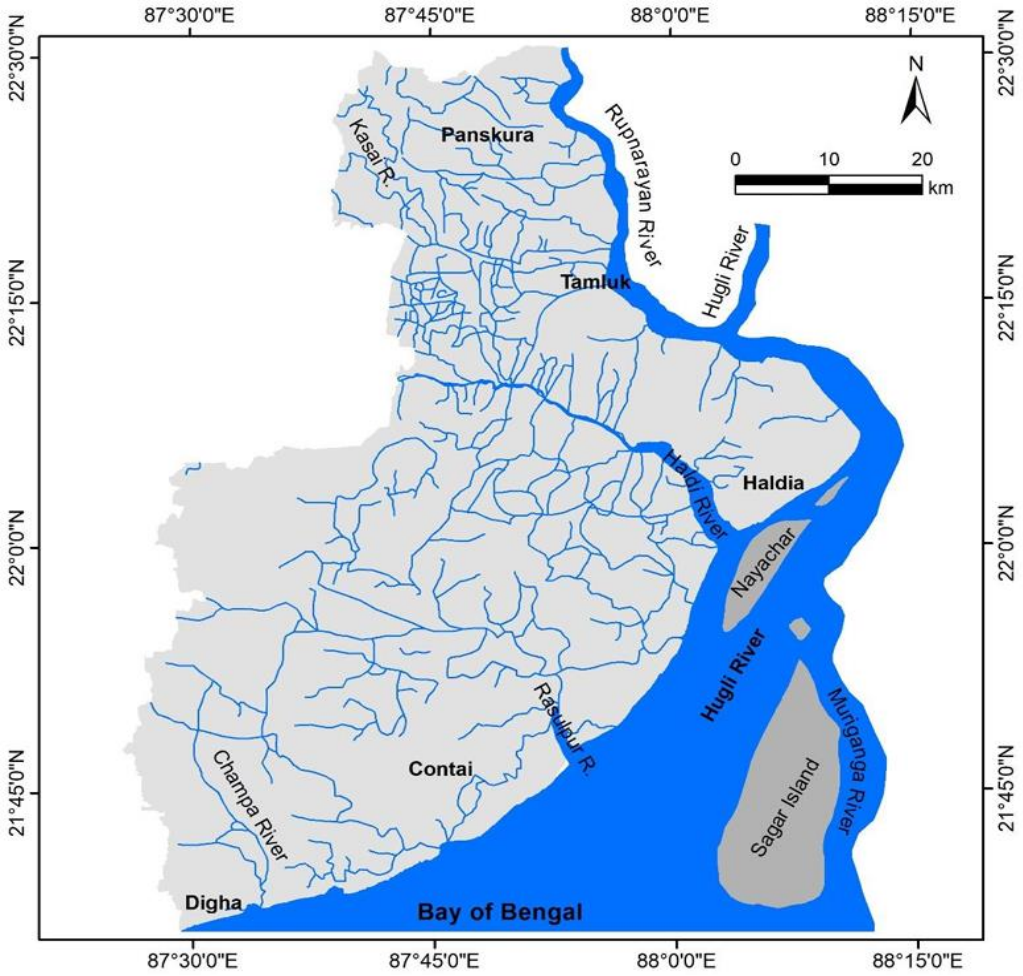

Figure 15: Drainage systems of the Purba Medinipur district (Ref: Paul & Mondal, 2021)

3 DATA AND METHODOLOGY

3.1 DATA SOURCE:

For the present study, data is downloaded from the open source domain including from IMD, CGWB, State Ware Resources Investigation Directorate (SWID), Government of West Bengal, West Bengal Pollution Control Board (WBPCB), National Bureau of Land Use Survey and Land Use Planning (NBS-LUP), West Bengal Public Health Engineering Department (PHED); **https://earthexplorer.usgs.gov/** etc. The details of the source of the data are given in the **Table 5**

Table 5: Data collected for various analysis and the data source

Sl. No.	Data	Details	Source
1	Rainfall	1993-2013, Annual average	IMD Grid data (0.25^0X0.25^0)
2	Groundwater level	1996 to 2019, Pre and Post monsoon	CGWB, *indiawris.gov.in*
3	Water quality data (2010 onwards)	Groundwater: at bi-annual intervals Lake water: at bi-annual intervals River water: Monthly data Canal water: Monthly data	WBPCB & CGWB
4	Tidal data	daily data, from 3 locations, Period: Dec. 2019-Dec 2022	Tideschart.com
5	Digital Elevation Model	Map prepared (Fig.3) Resoultion: 30m Elevation range:1 to 446m	SENTINEL2 https://earthexplorer.usgs.gov/
6	Litholog data		source: SWID, GoWB
7	Demography (Population, 2001 & 2011)		Population Census of India,
8	Soil data, Geomorphological and physiographic map		NBSS-LUP (https://nbsslup.icar.gov.in/) + Other published Literature
9	Land use Land-cover		LANDSAT-8, https://earthexplorer.usgs.gov/
10	Watersheds Map		https://earthexplorer.usgs.gov/
11	Land Surface Temperature Map (monthly, Period: 2018 and 2019)		
12	Sea Surface Temperature Map [Period: 2018 and 2019; Area considered: Offshore width: 150km; Coastline length = 240 km]		
13	Hydrogeological Map		maps.wbphed.gov.in

3.2 RUNOFF

For runoff estimation, the spatial and non-spatial data were collected from different data sources and then, various thematic layers such as land use land cover map (LULC), Hydrological Soil Group (HSG) map and soil map were prepared and overlaid. Finally, the runoff is estimated on the basis of the rainfall that occurred in the study area. The overall methodology is shown in Figure 29. For estimating the runoff for individual watresehds, the study area has been divided into the individual watersheds namely; Ichhamati Damodar, Rasulpur, Pichhabani, Subarnarekha, Kasai Haldi, Rupnarayan, Saraswati and Tidal Streams; and then the runoff using SCS-CN method is estimated.

3.2.1 SURFACE RUNOFF USING SCS-CN:

The runoff curve number method is a procedure for hydrologic abstraction developed by the USDA Soil Conservation Service. In this method, runoff depth (i.e. effective rainfall) is a function of total rainfall depth and an abstraction parameter referred to as runoff curve number or simply curve number and is usually represented by CN. The curve number varies in the range 1 to 100, being a function of the following runoff producing catchment properties: (1) hydrologic soil type, (2) land use and treatment, (3) ground surface condition, and (4) antecedent moisture condition.

The method is based on an assumption of proportionality of the following form:

$$\frac{P - I_a - Q}{S} = \frac{Q}{P - I_a} \qquad (1)$$

where; P = total storm rainfall, Q = actual direct runoff, S = potential maximum retention, and Ia = initial abstraction. P, Q and S are expressed in the same units e.g. cm or inches. This assumption underscores the conceptual basis of the runoff curve number method.

Solving for Q from Eq. (1) leads to the following.

$$Q = \frac{(P - I_a)^2}{P - I_a + S} \qquad (2)$$

1

which is physically subject to the restriction that $P \geq Ia$ (i.e. the potential runoff minus the initial abstraction cannot be negative). To simplify Eq. (2), initial abstraction is related

to potential maximum retention. Vandersypen et. al. (1972) developed the following relationship between initial abstraction and potential maximum retention for Indian conditions.

For black soil region (Antecedent moisture condition I) and for all other regions:

$$I_a = 0.3S \qquad (3)$$ 2

Therefore Eq. (2) reduces to

$$Q = \frac{(P - 0.3S)^2}{P + 0.7S}, \qquad P \geq 0.3S$$ 3 (4)

For black soil region (Antecedent moisture condition II & III):

$$I_a = 0.1S \qquad (5)$$ 4

Therefore Eq. (2) reduces to

$$Q = \frac{(P - 0.1S)^2}{P + 0.9S}, \qquad P \geq 0.1S$$ 5 (6)

Eq. (6) is used with the assumption that the cracks, which are typical of black soil when dry, are filled.

Since potential maximum retention varies widely, it is expressed in terms of a runoff curve number, an integer varying in the range 1 to 100, in the following form.

$$S = \frac{2540}{CN} - 25.4 \qquad (7)$$6

in which CN is the runoff curve number (dimensionless) and S is in cm. Hence, the values of P and Q in Eqns. (4) and (6) are also to be expressed in cms. The runoff curve number is a function of hydrologic soil group, land use and treatment, hydrologic surface condition, and antecedent moisture condition.

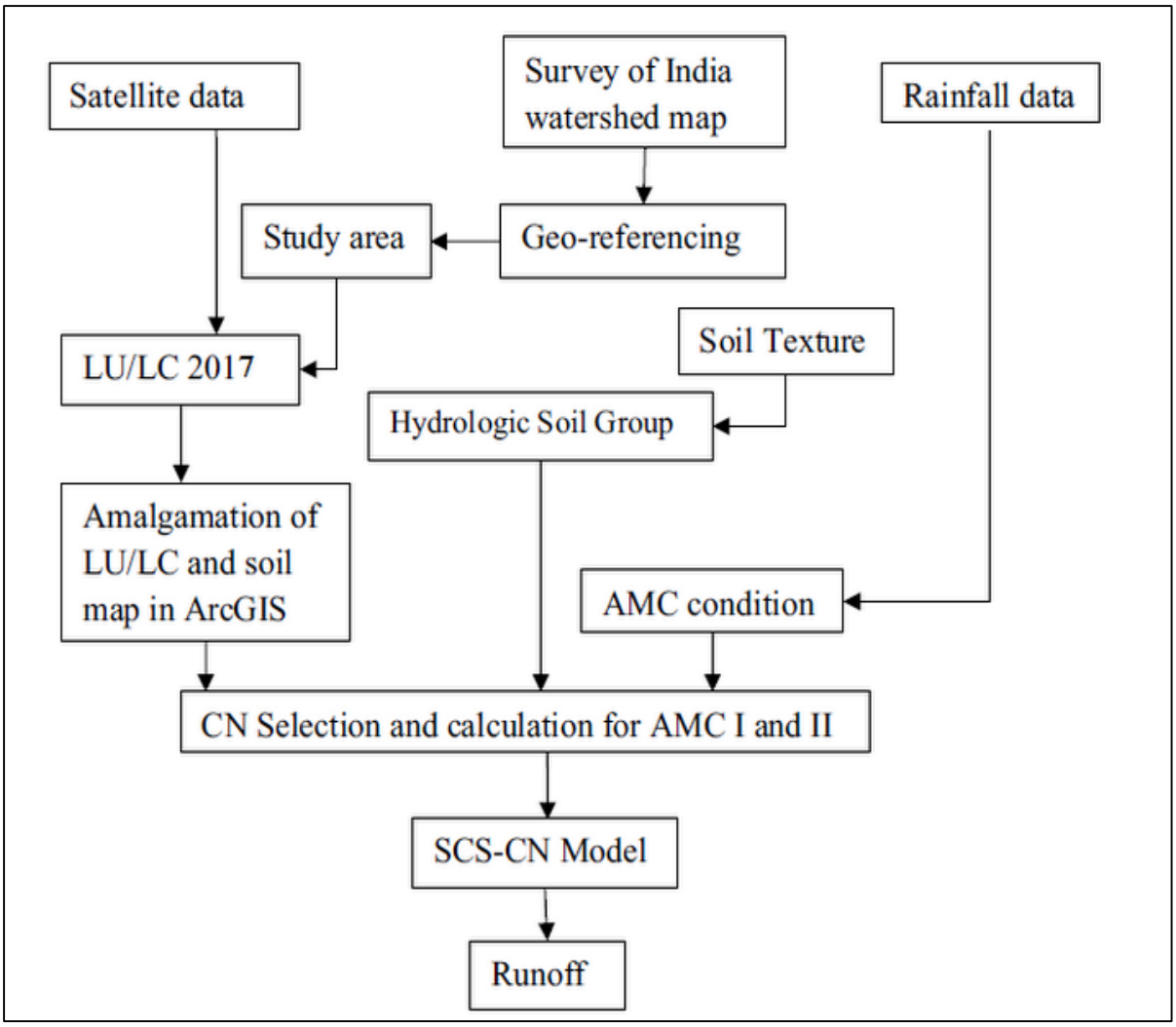

Figure 16: Flowchart of a methodology for rainfall-runoff estimation using the SCS-CN method and GIS

3.3 Land Use Land Cover

Both the land use map and hydrologic soil map were prepared to a scale of 1:2,50,000 were scanned, and then rectified to the same projection and co-ordinate system. On-screen digitization was carried out using the scanned land use map in the background in the GIS package-ARC/INFO version 7.2.1, developed by ESRI, to demarcate the various land use categories. Subsequently, on-screen digitization was also carried out using the scanned hydrologic soil map in the background to demarcate the various hydrologic soil groups. These digitized layers, i.e. the vector layers of land use map and soil map were then cleaned. The vector layers were then checked for errors like dangles and pseudo nodes which were subsequently removed. The vector layers were then built for topology using commands in the ARC INFO package. This tracing was superimposed on the satellite FCC and boundaries of

various land use/ land cover classes were demarcated keeping in view the fundamentals of visual interpretation. The interpretation was based on site, shape, shadow, tone, texture, pattern and association characteristics of the images. Then the results were compared with the limited ground truth data that were available and the modifications/ corrections were transferred to the base map. The study area was divided into eleven classes, namely; Agricultural Field, Forest Cover, Cultivated Land, Mangrove Forest, Inland River, Open Land, Built-up Land, Wet Land, Dry Land, Agricultural Farm Pond/Aquaculture, and Inland Pond.

3.4 Soil and Hydrological Soil Group (HSG) Map

The soil map of the study area was prepared using Arc GIS 10.3 software. The study area comprised of various kinds of soil textures- loamy, silty loam, fine loamy, clay, and sandy. The soil map is then classified into hydrological soil group map, which refers to the infiltration capacity of the soil and classified into 4 classes such as A, B, C, D. The table 1 shows their corresponding Hydrological Soil Group characteristics. The combination of soil type and land use and treatment is referred to as soil-vegetation-land use (SVL) complex. The combination of a hydrologic soil group (HSG) and a land use and treatment class (cover) is referred to as hydro-logic soil-cover complex (USDA-NRCS 2004). Classification of soil texture according to the percentage of sand, silt clay, quartz and the corresponding saturated hydraulic conductivity K_s is detailed in the **Table 6**. Classification of soil texture according to the USDA ternary diagram for sand-silt-clay is shown in the **Figure 17.**

Table 6: Description of the Hydrological soil group (HSG), USDA-NRCS, 1986

Hydrological Soil	Type of soil	Runoff Potential	Final Infiltration Rate (mm/hr)	Remarks
Group A	Deep, well-drained sands and gravels, sand, loamy sand, sandy loam	Low	>7.5	High infiltration rate, low run-off potential
Group B	Moderate infiltration rate when thoroughly wetted, well-drained with moderately fine to coarse textures, silt loam, or loam, gravelly loam	Moderate	3.81-7.62	Moderate rate of water transmission
Group C	Gravelly loam, clay loams, shallow sandy loam, soils	Moderately high	1.27-3.81	Low infiltration rates when

	with moderately fine to fine textures			thoroughly wetted, moderate rate of water transmission
Group D	Rocky outcrops, clay soils that swell significantly when wet, heavy plastic and soils with a permanent high water table	High	<1.27	High run-off potential, low rate of water transmission

The soil of the study area is broadly divided into six types – Clay skeletal, Clayey, Loamy, Loamy skeletal, Sandy soil. Maximum area covered by loam soil

Table 7: Soil Texture classes according to USDA (1969), based on percentage volumes of sand, silt, clay and quartz content. dm: median diameter (#Tafasca et al., 2020), values of θ_s and Ks are from Ali et al., 2013

[θ_s: Mean volumetric moisture content at near saturation or mean total porosity (cm^3/cm^3); K_s: Mean saturated hydraulic conductivity (m/day)]

Texture class	Class Abbre-viation	Sand (%)	Silt (%)	Clay (%)	Quartz (%)	dm (μm)	θ_s (cm^3/cm^3)	K_s (m/day)
Sand	S	92	5	3	92	936.4	0.437	5.040
Loamy Sand	LS	82	12	6	82	806.1	0.437	1.466
Sandy Loam	SL	58	32	10	60	490.7	0.453	0.622
Sandy Clay Loam	SCL	58	15	27	60	373.3	0.398	0.103
Sandy Clay	SC	52	6	42	52	112.9	0.430	0.029
Loam	L	43	39	18	40	39.3	0.463	0.317
Silt loam	SiL	17	70	13	25	29	0.501	0.163
Silt	Si	10	85	5	10	26.6		
Clay Loam	CL	32	34	34	35	25.1	0.464	0.055
Silty clay loam	SiCL	10	56	34	10	15.9	0.471	0.036
Silty Clay	SiC	6	47	47	10	5.4	0.479	0.022
Clay	C	22	20	58	25	1.6	0.475	0.014

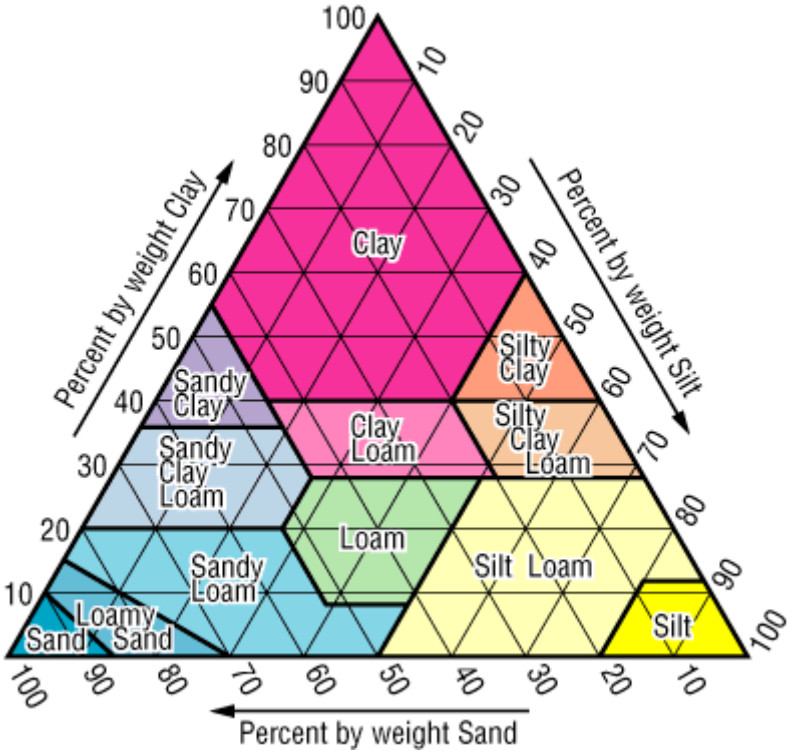

Figure 17: USDA soil texture triangle (USDA, 1951, 2017)

Antecedent Moisture Condition (AMCs): AMC indicates the moisture content of soil at the beginning of the rainfall event. The AMC is an attempt to account for the variation in curve number in an area under consideration from time to time. Three levels of AMC were documented by SCS AMC I (Soils are dry but not to the wilting point), AMC II (Average conditions), and AMC III (soils are saturated due to heavy rainfall or light rainfall and low temperatures within last 5 days). The limits of these three AMC classes are based on rainfall magnitude of previous five days and season (dormant season and growing season).

An increase in the AMC index means an increase in the runoff potential. The SCS developed three antecedent soil-moisture conditions and labeled them as I, II, III. Classification of AMC's, corresponding soil conditions and the rainfall units is shown in the **Table 8 ,**For present study, average condition (AMC II) is selected foe study area. Runoff curve numbers for (AMC II) for hydrologic soil cover are shown in **Table 9.**

The CN (dimensionless number ranging from 0 to 100) is determined from a table, based on land cover, HSG, and AMC. In the present study, runoff curve numbers compatible with SENTINEL data have been developed. For example, curve number for "poor cultivated land" is an arithmetic average of all curve number values under the heading "poor hydrologic condition". "Straight row" was not included in this calculation since any straight row cultivated land would be either poor cultivated or good cultivated in the

land use map prepared from SENTINEL data. The weighted curve number for AMC II (average conditions) of the study area is thus estimated as 75.

Table 8: Classification of Antecedent Moisture Condition (AMCs)

AMC Class	Soil conditions	Total five day antecedent rainfall (mm)	
		Dormant season	Growing season
I	Soils are dry but not to the wilting point; satisfactory cultivation has taken place.	<12.7	<35.56
II	Average conditions.	12.7-27.94	35.56-53.34
III	Heavy rainfall or light rainfall and low temperatures have occurred within last 5 days, saturated soils	>27.94	53.34

Table 9: Runoff Curve number (AMC II) for hydrologic soil cover complex (Ref-Chow et al., 1988; USDA, 1986)

Sl. No	Land use	Hydrologic Soil Group			
		A	B	C	D
1	Agricultural Land without conservation (Kharif)	72	81	88	91
2	Village	72	82	87	91
3	Forest Plantation	25	55	70	77
4	Scrub forest	33	47	64	67
5	Grass land/pasture	39	61	74	80
6	Land with scrub	36	60	73	79
7	Land without scrub (stony waste/rock outcrops) Or Forest (degraded)	45	66	77	83
8	Agriculture Plantation	45	53	67	72
9	Settlement	57	72	81	86
10	Prosophis	61	70	74	78
11	Double crop	62	71	88	91
12	Quarry	71	87	89	91
13	Commercial or urban	89	92	94	95
14	Industrial	81	88	91	93
15	Tanks without water	96	96	96	96
16	River/stream	97	97	97	97
17	Road/Railway line	98	98	98	98
18	Tank with water/reservoir/canal	100	100	100	100

Table 10: Hydrologic soil groups under different land use/cover classes

Sl. No.	Land use		Hydrologic soil group	Area (sq km)
1.	Agricultural Land	Good crop land	B	11463.31
			C	2491.82
		Open land	B	940.38
		Dry land	C	177.4
		Agricultural Farm Pond/Aquaculture	C	29.28
		Wet land	B	479.42
2.	Forest	Dense	B	7149.45
		Mangrove	C	1875.23
3.	Settlements		B	559.62

3.5 Groundwater potential zones

To estimate groundwater potential in the research region, ten thematic maps were created using remote sensing (RS) and conventional data. These maps include hydro-geology, soil, topographic elevation (using a digital elevation model [DEM]), land use/land cover (LULC), and the drainage network. The topographic elevation map was generated using 1:25,000 scale toposheets with a 5-meter contour interval, while the other maps were produced using supplementary data.

The geomorphology and geology maps were sourced from the Geological Survey of India (2000) at a scale of 1:250,000. These maps were scanned, corrected, and digitized using ArcGIS 10 to create thematic layers, which were further updated using satellite data. The soil map of the research area was obtained from the National Bureau of Soil Survey and Land Use Planning and was digitized. This soil map was then updated with urban land use data using the 2017 SENTINEL-2B dataset.

Surface water bodies were identified from high-resolution satellite data, and the LULC map was also created using the SENTINEL-2B dataset. To ensure consistency, the satellite dataset was geometrically corrected to a common projection (Universal Transverse Mercator and datum WGS84) and resampled using the nearest-neighbor technique in ERDAS Imagine software. Supervised classification with a maximum likelihood classifier was performed to categorize the images after band selection using a minimal noise fraction approach (Mallick et al., 2008). The classification's accuracy was then validated and assessed using a confusion or error matrix, comparing reference data with the classified map pixels (Lillesand and Kiefer, 1999).

Tracing the effect of groundwater on the land surface is crucial in exploring groundwater potential using RS. One of the most promising indicators is the heat fingerprint, as saturated soil has a higher heat capacity than dry soil. Remote thermal sensing can thus be used to evaluate groundwater potential (Alkhaier, 2011). In general, flat and mildly sloped areas support infiltration and groundwater recharge, while steep slopes result in runoff and minimal infiltration. The study area has a mild gradient, allowing for minimal overland flow discharge and a high rate of infiltration, suggesting a higher groundwater potential in flat and gently sloping terrains.

3.6 Selection of Thematic Layers

In the present study, multivariate techniques such as Principal Component Analysis (PCA) and expert judgment were used to prepare the groundwater potential map (GWPM). PCA is a statistical tool that identifies the most significant variables (or thematic maps) in a dataset and uncovers relationships among statistical units. Only principal components (PCs) explaining at least 60% of the variance were considered (Andreo et al., 2008). The PCA was performed in a single phase using all ten thematic layers.

3.7 Groundwater fluctuation and identification of recharge potential zones using GIS technique

The method of water level fluctuations is based on the acknowledgment that water level rise is due to recharge reaching groundwater. Estimation of the specific yield of the region of fluctuation for applying the method, the ground water level is required. Data pertaining to rainfall water level data collected for a period of four-year (2016 to 2019) during pre and post-monsoon season. Assessing the potential zone of groundwater recharge is critical for water quality preservation and groundwater system management. Remote sensing and Geographic Information System (GIS) methods are used to identify groundwater potential zones. In this paper, a standard methodology for determining groundwater potential based on the combination of RS and a GIS technique is suggested. GIS tools are used to create the composite map. Using satellite data and survey of India (SOI) toposheets of scale 1:50000, precise information is obtained to acquire the factors that may be evaluated for determining the groundwater potential zone, such as geology, slope, drainage density, geomorphic units, and lineament density.

3.8 Mapping groundwater quality for identification of vulnerable zones

Groundwater quality mapping is very essential to identify regions where groundwater is suitable for various uses. A study of the vulnerability of groundwater for pollution in a region is required as it will provide information for taking precautionary measures. Groundwater is being extensively used for domestic purposes. The present study was carried out with the objective of preparing a water quality graphs and vulnerability map. Groundwater samples over the entire area were collected and analyzed for electrical conductivity and major ions.

3.9 Sampling locations and analysis

For the study, water samples were collected from surface water (river, rainwater, rainwater, seawater) and groundwater sources during pre-monsoon and post-monsoon seasons. Total 498 samples were collected in 4 field visits during Pre-Monsoon 2019, Pre-Monsoon 2020, Post-Monsoon 2021 and Pre-Monsoon 2022. EC and pH were measured both in the field and in the laboratory. Isotopic and chemical analyses were conducted in NIH laboratories. Stable isotopic composition were measured on DI-IRMS and CF-IRMS; major ion concentration on DIONX-5000 Ion Chromatograph, and heavy metal concentration on Atomic Emission Spectrometer. The details of collected samples is shown in the **(Table 11)**.

Table 11: Details of samples collected from the study area and the analysis details

No. Of Samples	EC	pH	St. Isotope	^{3}H	Major Ions	Heavy Metals
Groundwater: 381 River water: 68 Sea water: 46 Rainwater: 3 ---------- Total: 498	373 out of 498	373 out of 498	372 out of 498 Analysis done on: DI-IRMS and CF-IRMS	19 out of 91 Measurement done using Tritium Enrichment Unit and Quantulus (the ultra low level liquid scintillation spectrometer)	227 out of 486 Analysis done on DIONEX-5000 Ion Chromatograph	40 out of 103 Analyses done on Atomic Emission Spectrometer

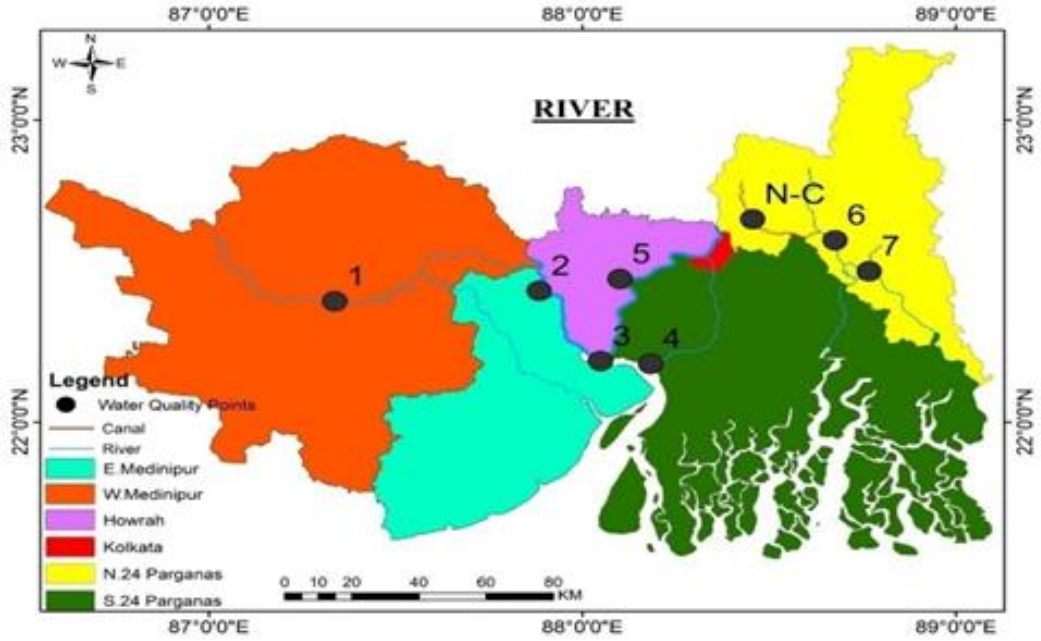

Figure 18: Locations of sampling points from rivers in study area in WB

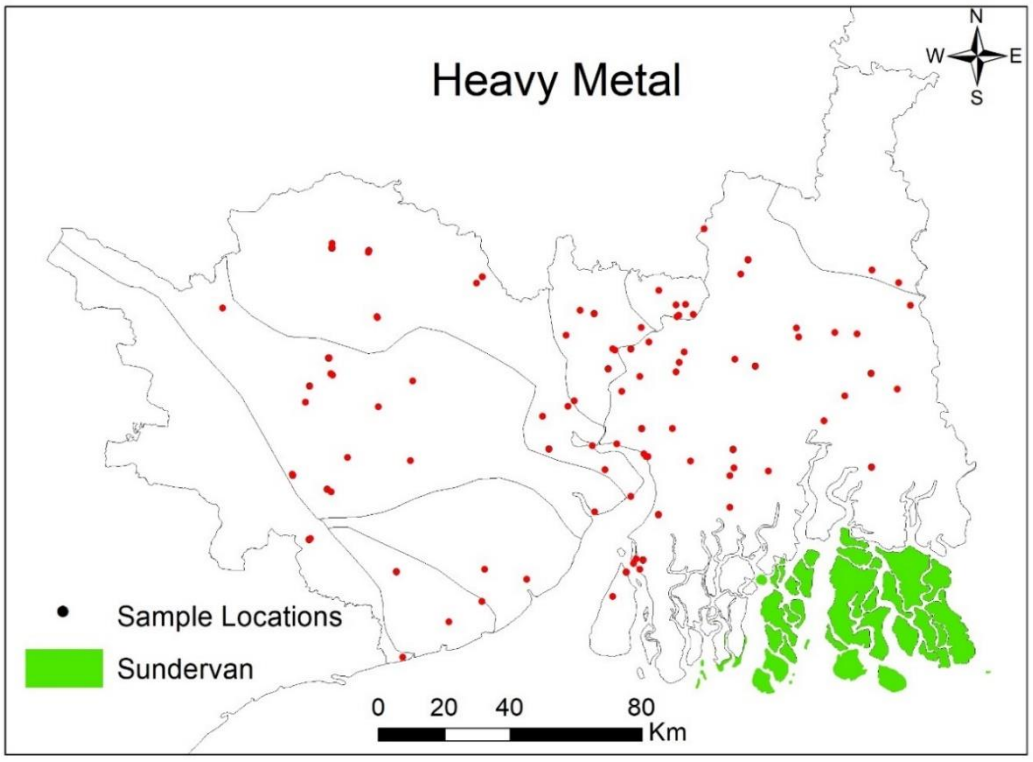

Figure 19: Heavy Metals Sampling Location Map

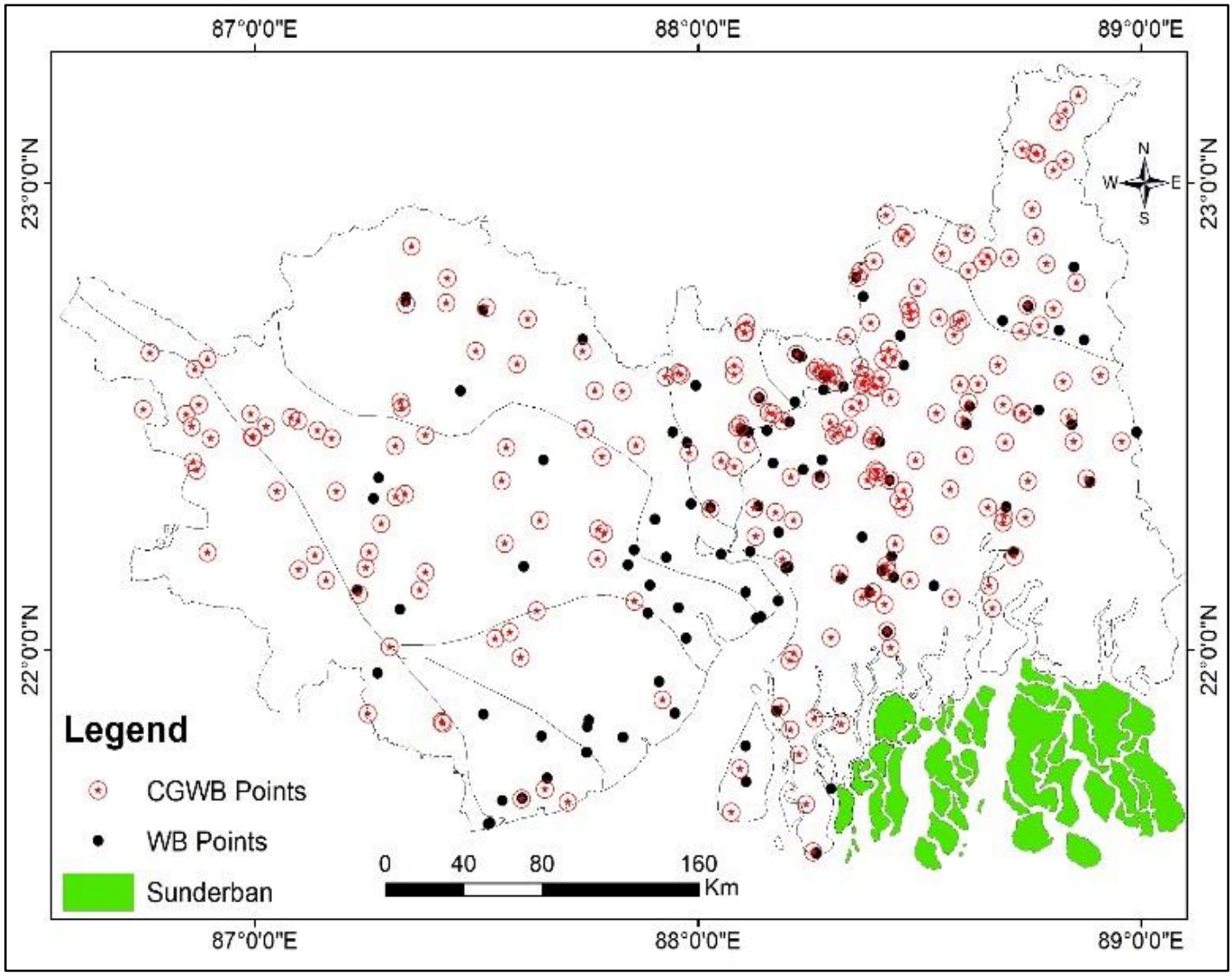

Figure 20. Groundwater sampling for major ion analysis. The locations include (i) Points downloaded from CGWB report and marked as CGWB points (ii) the samples collected by SWID, GoWB in the present study (marked as WB Points). Since, water samples collected in the present study are not sufficiently covering the entire study area, the data set is expanded by adding the data published by CGWB, Government of India. The dotted lines indicate the watershed boundaries.

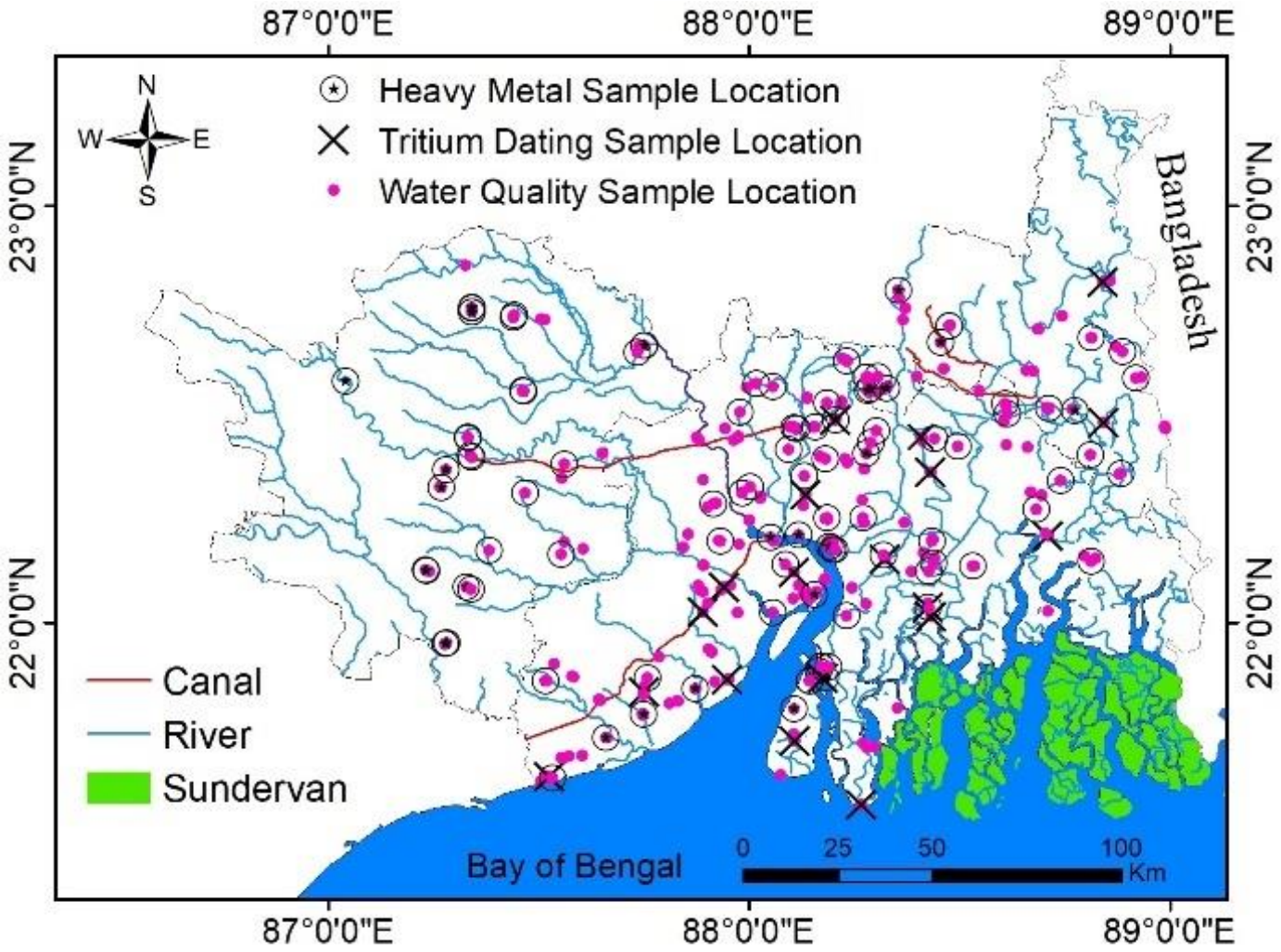

Figure 21: Sampling location and the analysis type: The map marks the water samples collected in the present study and the type of analysis done. The analysis done include analysis of concentration of heavy metal, major ions, stable isotopes and groundwater dating using environmental tritium

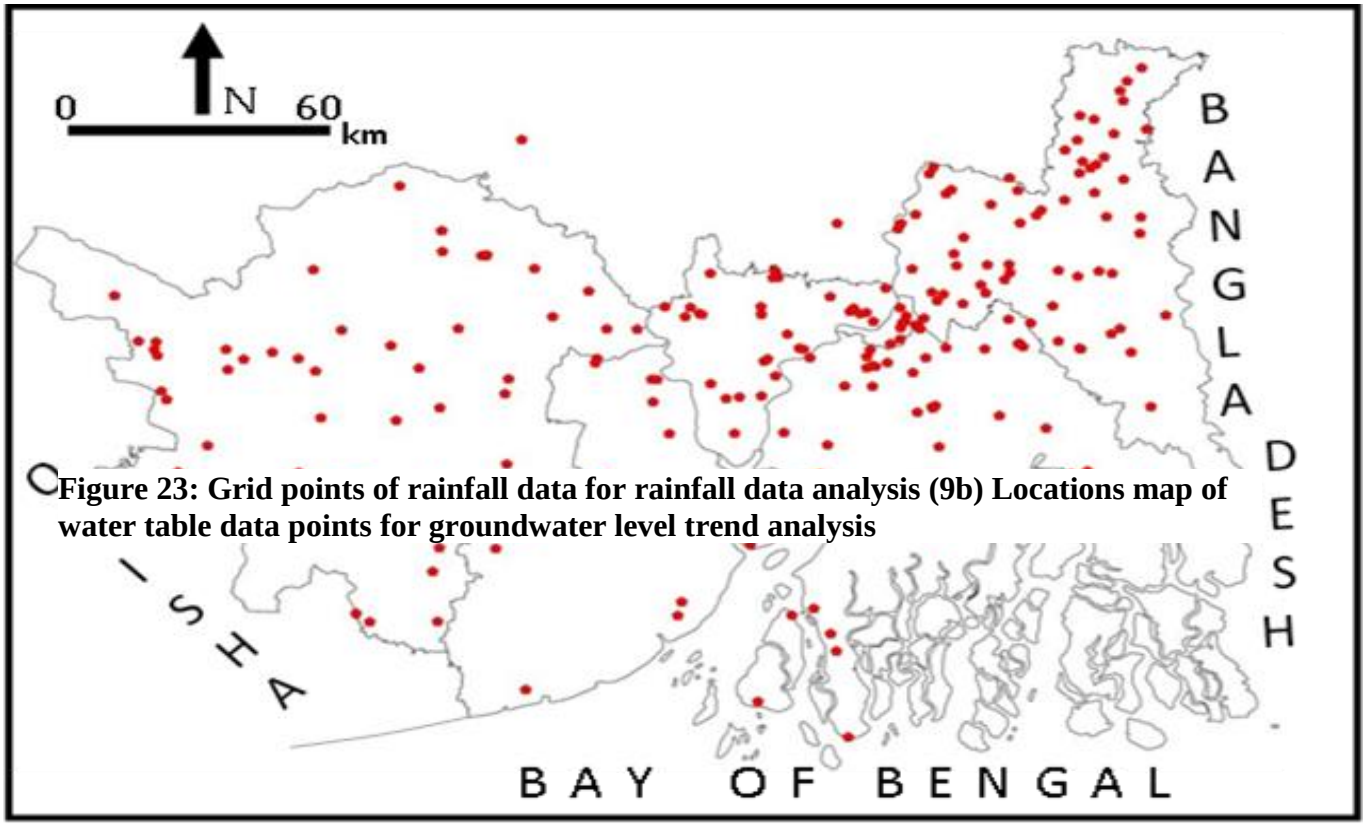

Figure 23: Grid points of rainfall data for rainfall data analysis (9b) Locations map of water table data points for groundwater level trend analysis

Figure 22: District-wise location of groundwater data points used in the present study taken from the report of CGWB, GoI in 2020. The thin polygons marks district boundary.

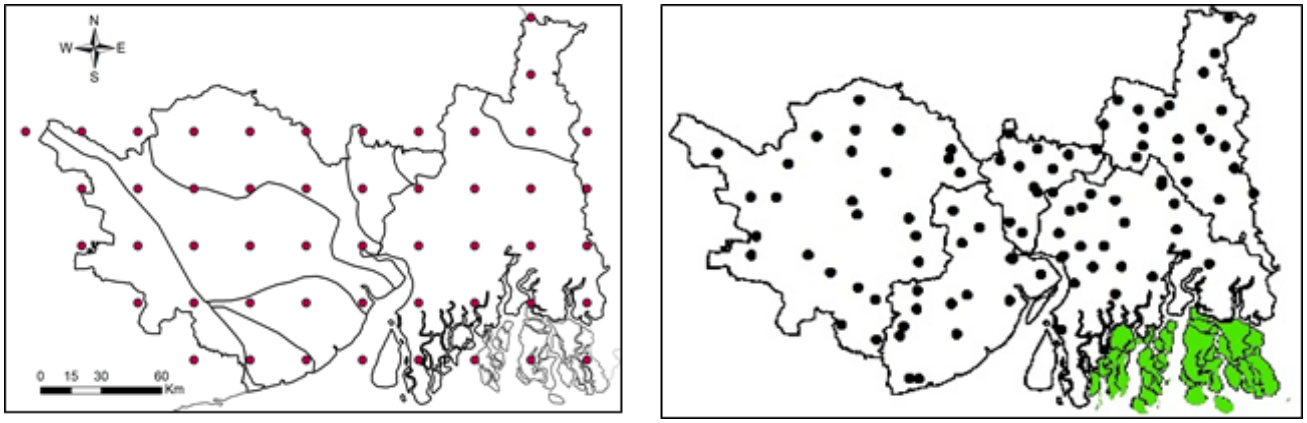

Table 12: Sampling locations of surface and groundwater samples collected from field for the measurement of concentrations of the dissolved major ions, heavy metals, and isotopic analysis in the present study (Depth 0 means surface water sample)

Sample code	Block	Lat	Long	Depth	EC	pH
S1	Rajarhat	22.60806	88.46417	120	820	7.6
S2	Bally Jagacha	22.58761	88.28251	85	1390	7.7
S3	Domjur	22.62652	88.23347	213	640	7.8
S4	Domjur	22.63244	88.22255	228	1200	7.4
S5	Sankrail	22.53093	88.22070	210	750	7.8
S7	Panchla	22.53745	88.13783	30	3000	7.4
S8	Uluberia I	22.46827	88.09755	222	900	7.9
S9	Uluberia II	22.46375	88.11265	220	870	7.8
S10	Haldia	22.09968	88.18017	240	2200	7.7
S12	Haldia	22.06905	88.13240	200	1290	8
S13	Haldia	22.06938	88.14218	210	1340	7.8
S14	Sutahata	22.12075	88.10648	270	1260	7.8
S15	Mahishadal	22.19575	88.05759	300	940	7.8
S17	Tamluk	22.27740	87.90292	300	1020	7.7
S18	Thakurpukur	22.48670	88.20600	256	660	7.8
S20	Budge Budge II	22.39700	88.16800	300	3400	7.5
S21	Bishnupur II	22.38320	88.23407	306	3000	7.5
S22	Bishnupur II	22.36875	88.27310	300	1140	7.8
S23	Bishnupur I	22.40453	88.27998	300	1010	7.9
S26	Barrackpore I	22.79745	88.35699	80	360	8.1
S27	Minakhan	22.51303	88.71377	110	900	7.6
S28	Sandeshkhali II	22.35579	88.88191	300	830	7.7
S30	Hasnabad	22.58880	88.93346	36	1140	7.4
S31	Hingalganj	22.47060	88.98906	192	970	7.9
S32	Shyampur-I	22.29708	88.02709	200	1730	7.3
S33	Shyampur-II	22.31115	87.98427	216	1090	7.5
S35	Bagnan-I	22.46405	87.94241	120	820	8
S36	Howrah	22.58041	88.28072	0	800	7.5
S37	Howrah	22.58400	88.28851	213	1570	7.8
S39	Baduria	22.73524	88.74457	82	750	7.7
S40	Basirhat I	22.66259	88.87132	152	1940	7.1
S42	Deganga	22.70337	88.68784	120	650	7.7
S44	Dmnd Hrbr I	22.17507	88.20363	366	1450	7.8
S45	Magrahat I	22.23957	88.27273	80	1050	8
S46	Dmnd Hrbr II	22.24945	88.18261	274	1760	7.7
S48	Gosaba	22.15316	88.82525	300	5900	7.5
S49	Basanti	22.20703	88.71164	366	990	7.7
S51	Canning I	22.31164	88.66983	182	1030	7.7
S52	Bhangore II	22.51985	88.61227	92	1220	7.6
S53	Bhangore I	22.49931	88.61459	92	160	7.7

S54	Canning II	22.42549	88.61269	60	1005	7.8
S55	Baruipur	22.36103	88.43217	305	520	7.9
S57	Joynagar I	22.19865	88.43723	300	930	7.9
S58	Joynagar II	22.15346	88.44151	300	120	8
S59	Mathurapur II	22.04490	88.42659	300	1050	7.9
S60	Mathurapur II	22.04071	88.42688	360	1070	7.9
S61	Mathurapur I	22.12157	88.38656	300	1470	7.7
S62	Mandirbazar	22.15146	88.32286	336	1140	7.9
S63	Magrahat II	22.23977	88.37060	300	1040	7.9
S65	Shahid Matangini	22.17988	87.84345	200	1060	7.7
S66	Chandipur	22.07380	87.89133	280	1030	7.8
S67	Nandigram I	22.02246	87.97269	300	1030	7.8
S68	Khejuri II	21.86210	87.94822	258	920	9.8
S69	Khejuri I	21.92861	87.91182	246	1000	7.7
S70	Contai I	21.77776	87.74727	60	650	7.9
S71	Contai I	21.77692	87.74993	228	590	7.8
S72	Deshpran	21.81037	87.83032	180	880	7.7
S73	Contai III	21.84009	87.75130	18	2900	7.3
S74	Ramnagar I	21.62641	87.53140	0	12000	7.5
S75	Ramnagar I	21.62395	87.52573	150	580	7.4
S76	Ramnagar I	21.62609	87.53011	210	550	7.5
S77	Ramnagar I	21.67838	87.57269	198	570	7.6
S78	Ramnagar II	21.67977	87.60297	198	1280	7.4
S79	Egra II	21.86986	87.58009	180	450	7.5
S80	Egra I	21.90043	87.53676	30	1400	7.4
S81	Egra II	21.81406	87.64377	174	590	7.5
S82	Sagar	21.71509	88.10843	336	830	8
S83	Sagar	21.72927	88.10496	300	860	8.1
S84	Kakdwip	21.86596	88.18169	360	770	7.9
S86	Patharpratima	21.69901	88.28051	360	940	8
S87	Namkhana	21.56166	88.26757	360	1090	7.6
S88	Howrah	22.55574	88.28274	0	290	8.8
S91	Howrah	22.56215	88.32751	0	290	7.5
S92	Barasat I	22.67112	88.45668	0	570	7.6
S93	Barrackpore I	22.79640	88.35617	0	360	7.6
S95	Haroa	20.60320	88.67707	0	770	7.5
S97	Uluberia I	22.46430	88.11398	0	330	7.9
S98	Kolaghat	22.44347	87.87603	0	260	8.1
S99	Mahishadal	22.19542	88.05860	0	340	7.8
S100	Haldia	22.05678	88.14045	0	1840	7.4
S102	Haldia	22.13677	87.89181	0	840	7.9
S103	Nandigram I	22.02465	87.89050	148	910	7.7
S104	Nandigram II	22.07707	87.93373	214	1310	7.7
S105	Khejuri II	21.83992	87.87356	0	3000	7.5
S106	Contai I	21.72284	87.66387	0	1320	7.4

S107	Dmnd Hrbr I	22.18123	88.19197	0	730	7.4
S108	Dmnd Hrbr II	22.08860	88.11811	0	730	7.6
S109	Sagar	21.85900	88.14444	0	13000	7.5
S110	Sagar	21.88214	88.16428	0	18700	7.3
S111	Debra	22.40566	87.65179	110	620	7.8
S112	Kharagpur-II	22.34471	87.55519	40	780	7.6
S113	Sabang	22.19173	87.56075	44	600	7.6
S114	Narayangarh	22.08482	87.32692	120	280	7
S115	Narayangarh	22.85726	87.32501	60	220	7.4
S116	Datan I	21.94820	87.27696	30	360	7.4
S117	Keshiary	22.12543	87.23120	110	360	7.5
S118	Kharagpur-I	22.36699	87.27871	50	250	7.4
S119	Kharagpur-I	22.32591	87.26479	126	210	7.2
S120	Midnapore Sadar	22.40052	87.33622	0	200	7.8
S121	Binpur-I	22.44343	87.33062	98	40	7.1
S122	Garbeta III	22.75643	87.34070	128	60	6.5
S123	Ghatal	22.66336	87.73881	150	180	7.8
S124	Keshpur	22.55400	87.46270	120	500	7.5
S125	Chandrakona II	22.72878	87.50408	75	330	7.4
S126	Ghatal	22.66460	87.75089	0	600	7.3
S127	Bidhannagar	22.59000	88.40000	0	980	8
S11/2	Haldia	22.07297	88.16063	275	1140	7.8
S116/2	Datan I	21.9467	87.27707	80	210	7.4
S117/1	Keshiary	22.12162	87.24032	70	190	7.3
S122/1	Garbeta III	22.74452	87.33969	40	500	6.4
S124/1	Keshpur	22.55371	87.46416	146	470	6.7
S19/1	Budge Budge I	22.46800	88.15400	210	770	7.7
S23/1	Bishnupur I	22.40481	88.27976	240	880	7.9
S24/1	Barasat I	22.71378	88.47777	180	870	7.5
S25/1	Barrackpore I	22.75478	88.37257	160	650	7.8
S29/2	Sandeshkhali I	22.48035	88.84356	300	980	7.9
S31/1	Hingalganj	22.47098	88.98885	30	1710	7.2
S34/2	Bagnan II	22.43677	87.96296	256	930	7.8
S39/1	Baduria	22.73528	88.74535	232	760	7.7
S41/1	Basirhat-II	22.68333	88.81483	180	690	8
S42/1	Deganga	22.70422	88.68884	220	600	7.6
S43/2	Falta	22.28014	88.13053	270	1380	7.9
S44/1	Dmnd Hrbr I	22.17510	88.20330	216	910	8
S47/1	Dmnd Hrbr II	22.25088	88.18616	256	2400	7.7
S50/2	Basanti	22.30445	88.69598	320	2500	7.7
S6/1	Amta-I	22.56423	87.99487	210	850	7.7
S56/2	Sonarpur	22.43490	88.41372	293	780	7.7
S65/1	Shahid Matangini	22.21112	87.85557	120	1110	7.8
S72/1	Deshpran	21.81037	87.83027	210	940	7.5
S73/1	Contai III	21.83042	87.75026	108	3200	7.6

S81/1	Egra II	21.81406	87.64378	144	620	7.5
S85/2	Kulpi	22.08280	88.24516	282	1050	8.1
S86/1	Patharpratima	21.70909	88.27126	146	870	8.1
S87/1	Namkhana	21.56038	88.26650	363	710	7.5
S88/1	Howrah	22.55574	88.28274	0	310	7.8
S88/2	Howrah	22.55129	88.28571	0	260	7.6
S95/1	Haroa	22.60308	88.67612	320	730	7.7

Table 13: Location of CGWB (CGWB-2020) data points (The prefaced common word 'WB' given before all the sample code is deleted for adjusting the column space. Thus, NT071A is WB NT071A; HA30 is WB HA30 etc.)

Sample code	Block	Lat	Long	Sample code	Block	Lat	Long
NT071A	Amdanga	22.775403	88.495099	HA30	Jagat-ballavpur	22.6788	88.10354
NT124	Amdanga	22.561238	88.402343	HA02		22.698	88.108
HA03B	Amta	22.402988	88.052423	HA01A		22.6775	88.10618
HA22	Amta II	22.583198	87.927089	MP47	Jamboni	22.476	86.85739
HA21A	Amta II	22.588013	87.961009	MP186	Jamboni	22.4006	86.86058
NT018	Baduria	22.728635	88.801864	MP160	Jamboni	22.5129	86.74889
NT114	Baduria	22.825348	88.786616	MP187	Jamboni	22.523	86.87383
NT063	Baduria	22.567954	88.632097	MP198	Jamboni	22.5026	86.84458
NT019	Baduria	22.736884	88.742107	MP185	Jamboni	22.3831	86.86908
NT059	Bagdah	23.130653	88.814161	ST61A	Jaynagar I	22.1664	88.42776
NT136	Bagdah	23.187204	88.858677	ST19A	Jaynagar I	22.2428	88.54664
NT058	Bagdah	23.154683	88.828818	ST150	Jaynagar I	22.1772	88.42558
NT102	Bagdah	22.735749	88.475277	ST139	Jaynagar II	22.1464	88.47843
HA41	Bagnan	22.419975	87.979671	MP193	Jhargram	22.455	86.99649
NT145	Barasat I	22.724497	88.479112	MP206	Jhargram	22.3378	87.04986
NT111A	Barasat I	22.709091	88.543586	MP12	Jhargram	22.4954	87.08178
NT142B	Barasat I	22.572348	88.824539	MP196	Jhargram	22.4763	87.02474
NT057	Barasat II	22.672553	88.578788	ST158A	Kakdwip I	22.024	88.30059
NT056A	Barasat II	22.70572	88.59522	ST0129	Kakdwip I	21.8756	88.1861
NT115	Barasat II	22.707151	88.480986	MP174	Keshiyari	22.1725	87.25093
NT040	Barrackpur I	22.92959	88.424829	MP48	Keshiyari	22.1168	87.2348
NT088A	Barrackpur I	22.88092	88.459379	MP217	Keshiyari	22.2079	87.25844
NT006B	Barrackpur I	22.699188	88.389947	MP173	Keshiyari	22.3684	88.20941
NT005A	Barrackpur II	22.809153	88.367214	MP96A	Keshpur	22.6376	87.49823
NT072	Barrackpur II	22.796172	88.361506	MP164	Kharagpur I	22.326	87.31845
ST04A	Baruipur	22.360868	88.433104	MP33	Kharagpur I	22.2682	87.28537
ST130	Baruipur	22.404338	88.491336	MP162	Kharagpur I	22.3375	87.18373
ST60	Baruipur	22.924201	88.588935	MP166	Kharagpur I	22.3321	87.33866
ST148	Baruipur	22.318438	88.452795	MP202	Khejuri	21.8904	87.92028
ST137	Baruipur	22.838131	88.70293	CT13B	KMC	22.6046	88.36593
ST17	Baruipur	22.342249	88.569161	CT27	KMC	22.5281	88.36571
ST161	Baruipur	22.457812	88.397308	CT25	KMC	22.5629	88.39651
ST125	Baruipur	22.094923	88.420679	CT24	KMC	22.5796	88.41411
ST128	Baruipur	22.361469	88.382037	CT09B	KMC	22.6418	88.43091
ST0165	Basanti	22.197865	88.71402	CT17A	KMC	22.4857	88.29757
ST0173	Basanti	21.850775	88.262015	CT31A	KMC	22.4717	88.34008

ST0170	Basanti	22.087182	88.663895	CT06	KMC	22.517	88.34575
ST0116A	Basanti	22.271202	88.688824	CT35	KMC	22.5846	88.37801
ST085A	Basanti	22.280425	88.7391	CT36	KMC	22.6203	88.41835
ST0115A	Basanti	22.282886	88.690537	CT12C	KMC	22.5732	88.37521
NT048C	Basirhat I	22.523364	88.68813	CT38	KMC	22.5672	88.37068
NT100	Basirhat I	22.58635	88.907893	CT30	KMC	22.4626	88.31517
NT066	Basirhat II	22.680929	88.728222	ST08	KMC	22.4562	88.30674
NT099A	Basirhat II	22.693566	88.770732	ST07	KMC	22.4888	88.19171
HA39	Bauria	22.506449	88.159715	ST135	KMC	22.5377	88.43433
MP156	Bhagwanpur I	21.698246	87.655052	ST002B	Kulpi I	22.1913	88.19088
ST47A	Bhangar	22.504457	88.537583	ST0133	Kulpi I	21.9902	88.21487
ST43	Bhangar	22.10211	87.857439	ST88	Kultali	22.1082	88.57176
ST147	Bhangar	22.414673	88.601891	ST67	Mandir Bazar	22.162	88.31958
ST30	Bhangar	22.567508	88.591322	ST66A	Mathura-pur I	22.1201	88.39431
ST42A	Bhangar	22.527542	88.610571	ST05A		22.0015	88.43463
ST46	Bhangar	22.493145	88.598504	ST127	Mathurapur II	22.0377	88.42685
MP52	Binpur I	22.503651	86.990525	MP98	Mayna	22.2552	87.7755
MP197	Binpur II	22.63449	86.763282	MP99	Mayna	22.2481	87.78768
MP207	Binpur II	22.454017	86.993925	MP209	Medinipur	22.4509	87.17342
MP189	Binpur II	22.598728	86.864586	MP170	Medinipur	22.4687	87.141
ST152	Bishnupur	22.36236	88.277795	MP11A	Medinipur	22.4888	87.09764
ST21	Bishnupur	22.224984	88.445262	MP165	Medinipur	22.4583	87.38466
NT119	Bongaon	23.04655	88.828798	MP208	Medinipur	22.4354	87.31736
NT001	Bongaon	23.062327	88.765025	NT027B	Minakhan	22.5046	88.73464
NT133	Bongaon	23.061616	88.761452	NT026A	Minakhan	22.506	88.73118
NT131	Bongaon	23.026516	88.801765	MP114	Mohanpur	21.8403	87.42523
NT132	Bongaon	23.070966	88.732138	ST099	Namkhana	21.56439	88.26011
ST044	Canning I	22.35928	88.74456	ST0153	Namkhana	21.82631	88.20866
ST176	Canning I	22.302429	88.653496	ST003B	Namkhana	21.77376	88.22808
ST114	Canning II	22.443222	88.693551	ST098	Namkhana	21.66621	88.24354
MP128	Chandrakona I	22.732664	87.522497	MP16B	Narayangarh	22.1256	87.37266
MP10B	Chandrakona II	22.706809	87.6161	MP109	Narayangarh	22.035	87.57549
MP100	Dantan I	21.860549	87.254488	MP218	Narayangarh	22.0047	87.3041
MP215	Daspur I	22.470257	87.744021	HA29	Panchla	22.5406	88.13612
MP129	Daspur II	22.552278	87.828787	MP205	Panskura	22.4117	87.78297
MP130	Daspur II	22.55283	87.767394	MP06	Panskura	22.4365	87.86039
MP103	Debra	22.360168	87.556562	ST159	Pathar Pratima	21.83728	88.32334
MP131	Debra	22.431827	87.567288	MP183	Pingla	22.2753	87.64355
NT146	Deganga I	22.192112	87.773359	MP113	Potash-pur I	22.0809	87.6359
HA16A	Domjur	22.631402	88.222481	MP51		22.0209	87.54227
HA36	Domjur	22.59296	88.296566	MP111	Potashpur II	21.9816	87.59993
HA38	Domjur	22.589234	88.305963	NT038	Rajarhat	22.6217	88.44159
ST84	Falta	22.274695	88.215061	MP177	Ram-nagar II	21.6706	87.70663
ST13	Falta	22.301344	88.127387	MP152		21.6779	87.60227
ST156	Falta	22.292904	88.174922	MP216	Rohini	22.1693	87.099
NT113	Gaighata	22.884013	88.762364	MP102B	Sabang	22.226	87.56345
NT129	Gaighata	22.89069	88.470387	ST091	Sagar	21.7425	88.09472
NT101B	Gaighata	22.943148	88.754231	ST0169	Sagar	21.64963	88.07472
MP08	Garbeta I	22.863204	87.353701	ST090A	Sagar	21.97386	88.20671
MP44	Garbeta II	22.739778	87.340855	MP200	Salboni	22.5161	87.33244
MP167	Garbeta II	22.794744	87.434172	MP41	Salboni	22.5292	87.32863
MP169	Garbeta III	22.741144	87.431772	NT032	Sandesh-khali I	22.3648	88.87703
MP168	Garbeta III	22.831281	88.396804	NT013A		22.4969	88.83658

MP132A	Ghatal	22.638434	87.740153	NT153		22.4444	88.84843
MP97	Ghatal	22.610983	87.591787	HA07	Sankrail	22.5036	88.16915
MP14	Gopiballavpur I	22.205773	86.893171	MP94	Sankrail	22.2001	87.13582
MP92B	Gopiballavpur II	22.621519	86.892713	HA44	Shyampur I	22.5879	88.08249
NT028	Habra I	22.841365	88.653612	HA45	Shyampur I	22.5712	88.31072
NT126A	Habra II	22.829431	88.643032	HA35	Shyampur I	22.2995	88.02762
NT069	Habra II	22.809962	88.610127	ST118	Sonarpur	22.37838	88.40539
NT116	Habra II	22.889298	88.605918	ST32A	Sonarpur	22.38343	88.40065
NT127A	Habra II	22.84745	88.5504	ST57B	Sonarpur	22.1103	88.37062
NT039	Haroa	22.608505	88.676946	ST55A	Sonarpur	22.44745	88.39175
NT160	Hasnabad	22.670735	88.335389	NT065A	Swarupnagar	22.785	88.85434
NT036	Hingalganj	22.603738	88.270351	HA14	Uluberia I	22.3902	88.08248
NT44	Hingalganj	22.44362	88.955745	HA40A	Uluberia I	22.4392	88.11099
HA05A	Howrah	22.5958	88.2636	HA28A	Uluberia I	22.4804	88.09552
HA37	Jagacha	22.590322	88.28425	HA06A	Uluberia I	22.4754	88.08844
HA08B	Jagatballavpur	22.607561	88.081527				

3.10 Water Quality Index

Water is the most vital liquid for sustaining life. Safe drinking water is a fundamental requirement for good health. However, water quality is rapidly deteriorating due to factors such as rapid urbanization, deforestation, land degradation, improper disposal of solid waste, and contamination from sewage, fertilizers, pesticides, organic pollutants, and more. Polluted drinking water can cause numerous diseases, including diarrhea, vomiting, gastroenteritis, dysentery, kidney problems, and other health issues, leading to a significant number of deaths. Water quality parameters provide crucial information about the safety of drinking water, highlighting potential health risks when parameters exceed safe limits. **Table 14** includes water quality parameters, their safety limits as per WHO and Indian Standards, and the associated health effects when these parameters exceed the safe range.

The Water Quality Index (WQI) offers a comprehensive summary of various water quality parameters by comparing them with standard values. It provides a single numerical value that expresses the overall quality of water as excellent, good, poor, etc.

The Water Quality Index (WQI) is calculated by using the weighted arithmetic index method (Tandel et al. 2011). The quality rating scale for each parameter, Qi, was calculated by using the following expression:

$$WQI = \sum_{i=1}^{n} W_i Q_i / \sum_{i=1}^{n} W_i$$

where n = number of variables or parameters, Wi= unit weight for the i^{th} parameter, Qi=quality rating (sub-index) of the i^{th} water quality parameter. The unit weight (Wi) of the various water quality parameters are inversely proportional to the recommended standards for the corresponding parameters.

$$W_i = K / S_n$$

where, Wi=unit weight for the i^{th} parameter, Sn=standard value for i^{th} parameters, K=proportional constant, the value of K has been considered '1′ here and is calculated using the mentioned equation below:

$$K = 1 / \sum (1/ S_n)$$

According to Brown et al. (1972), the value of quality rating or sub-index (Qi) is calculated using the equation as given below:

$$Q_i = 100[(V_o-V_i) / (S_n-V_i)]$$

where V_o = observed value of i^{th} parameter at a given sampling site, Vi = ideal value of i^{th} parameter in pure water, Sn = standard permissible value of i^{th} parameter.

Table 14: Acceptable and Permissible limits (AL & PL) of water quality parameters, source of for dissolved ions and their health effects (W: WHO, I:Indian Standards IS 10500 : 2012; US: USEPA)

Parameters & unit	Limits: AL, PL	Description	Ref
pH	W:6.5-9.2 I:6.5-8.5	Effect of low pH (acidic water): At low pH, water becomes corrosive. Consumption of acidic water leads to neurological effects, gastrointestinal issues, and reproductive problems. Acidic water can also cause acid reflux, heartburn, digestive issues, can dissolve tooth enamel, etc Alkaline water rich in bicarbonate helps improving bone resorption by replacing old bone cells with new ones pH increases with mineralization and GW age	1
EC (μS/cm) TDS mg/l	W:500 W_{max}:1400 I: 500, 2000	EC increases with mineralization (increase in dissolved salt concentration and inorganic chemicals in water) and GW age	
TH TH as $CaCO_3$ (mg/l)	W: 500 I: 200, 600	Total hardness occurs mainly due to calcite, dolomite, and aragonite dissolution Excess hardness causes grayish white scale on surfaces, piping, and equipment, presence of calcium	2,3

		and magnesium prevents detergent from foaming or when foam is formed, it is less stable	
Ca^{2+} (mg/l)	W: 100 I: 75, 200	Ca^{2+} minerals: Calcite, dolomite, gypsum Ca^{2+} is essential for bone development Health effects: Excess Ca^{2+} leads to kidney stones, bone calcification, sclerosis of kidneys and blood vessels, prostate cancer, Mg-depleting effect	
Mg^{2+} (mg/l)	W: 150 I:30,100	**Mg^{2+} source Minerals:** Dolomite, magnesite, brucite, carnallite, olivine etc Effect of Mg2+ deficiency in drinking water: calcification disorders, effect on brain, headache, suicidal ideation, anxiety, irritability, insomnia, short-term memory loss and general depression **Effect of Excess Mg^{2+}**: Decreases crop yield. Excess in drinking water leads to hypotension, nausea, vomiting, facial flushing, retention of urine, ileus, depression, and lethargy	4, 5
Na^{+} (mg/l)	W: 6.5 200mg/l	**Sources:** Halite and plagioclase feldspars Above 200 mg/l: nephropathy and blood circulatory problems. **Effect due to excess Na^{+}**: Excess Na^{+} in soil impede plants' uptake of water and cause plant tissues to become dry and discolored. Excess Na^{+} in drinking water leads to high BP, cardiovascular disease, heart disease, kidney problem, etc	6,7
Carbonate and bicarbonate (mg/l) Total Alkalinity as calcium carbonate	HCO_3^- W: 1000 I: 200,600	**Source:** Dissolution of atmospheric CO_2, soil CO_2, dissolution of mineral carbonates in soils, aragonite, calcite, dolomite, etc At high pH values carbonate mainly contribute to the alkalinity **Health effect:** Excess calcium present in hard water may cause kidneys work harder to filter, stomach upset, nausea and constipation, whereas magnesium carbonate may cause diarrhea.	8
Chloride (mg/l)	W :500 I: 250, 1000	Cl is a conservative ion, High Cl reduces pH. High Cl gives salty taste. Excess Cl in water reduces plants ability to take up water, increases water corrosive to pipes, pumps and plumbing fixtures, an increase in chloride concentration causes a salty taste in the water	
Sulphate (mg/l)	W: 250 I: 200, 400	**Source:** Fertilizers, domestic and industrial wastes, human and animal waste Sulfates are corrosive to metallic materials due to conversion from sulfates to sulphides by anaerobic reducing bacteria **Health effect:** Excess intake of sulphate may cause diarrhea and dehydration	
Fluoride (mg/l)	W: 1.5 I: 1.0, 1.5	**Anthropogenic sources:** fertilizers or aluminum smelting	9

		Natural sources: fluorite, biotite, topaz, and their corresponding host rocks such as granite, basalt, syenite, and shale, **Health effect:** Excess fluoride causes dental and skeletal fluorosis, skeletal fluorosis, arthritis, bone damage, osteoporosis, abdominal pain; excessive saliva; nausea and vomiting; seizures and muscle spasms	
Nitrate (mg/l)	45 mg/l I:45, 45	**Source:** fertilizers, pit latrines **Risk from excess nitrate**: methemoglobinemia or 'blue baby syndrome' in humans, stomach cancer, denitrification processes contribute to the emission of greenhouse gases	10
Arsenic	W: 0.01 I: 0.01, 0.05	**Toxicity:** $As^{3+}>As^{5+}>As^{0}$, As^{3-} **Natural Sources:** arsenopyrite, realgar, orpiment **Industrial use of arsenic:** glass industries, textile industries, paper industries, mining industries, metallurgical, semiconductor industries, in metal adhesives, ammunition, in wood preservatives, herbicides, etc. **Co-existence:** DOM and ferrihydrite, and Mn decreases arsenic mobility, As adsorbs on finer particles, and the adsorption is more in the acidic to neutral conditions **Health effects**: cancers of the skin, bladder and lungs; anemia, leukopenia, and thrombocytopenia, stomach pain, vomiting, diarrhea and impaired nerve function	11, 12, 13
Fe	US:0.3 I: 0.3, 0.3	**Natural Sources:** , pyrite, pyroxenes, amphiboles, biotite, magnetite, marcasite, siderite, organic waste, plant debris Solubility of Fe is high below pH 7 **Health Importance:** It is essential for making hemoglobin, variety of metabolic processes, gastrointestinal processes, preserves many vital functions in the body Deficiency leads to anemia **Health effect:** Excess Fe causes cirrhosis or hemochromatosis, β-thalasemia, diabetes, congestive heart failure, irregular heart rhythms, chest pain, palpitations, and dizziness	14, 15, 16
Zn (mg/l)	W:5 I:5,15	**Natural sources:** zincite, zinc sulphide and zinc, smitsonite **Anthropogenic sources:** smelters, fly-ash, fertilizers, wood preservatives, galvanized metals etc. **Health Effect:** Excessive intake of zinc may cause anemia, stomach cramps, nausea, vomiting, decrease levels of HDL cholesterol headache, fever etc	17, 18

Pb (mg/l)	W:0.01 I: 0.01, 0.01	**Natural sources:** galena, anglesite, cerussite, mimetesite, and pyromophite. **Anthropogenic sources:** Mining, smelting, cumbstion of coal and oil, vehicle emissions, fertilizers, power plants, industrial emissions, paints, batteries, waste incineration, etc. **Health effect due to excess Pb intake**: Increases risk of high blood pressure, cardiovascular problems, kidney damage, miscarriage, stillbirth, premature birth, low birth weight, slowed growth, hearing problems, anemia, decreased kidney function, joint and muscle pain, difficulties with memory or concentration, nausea, numbness, headache, depression/mood changes, behavioral problems, learning disabilities, to seizures and death	19
Mn (mg/l)	W:0.1 I: 0.1, 0.3	**Natural sources:** pyrolusite, romanechite, manganite, hausmannite, and rhodochrosite **Anthropogenic sources**: mining and mineral processing, emissions from alloy, steel, and iron production, combustion of fossil fuels **Health concern:** Mn is useful to for tissues, bone formation, blood clotting, in carbohydrate metabolism, cholesterol and glucose formation; decreases arsenic mobility Excess intake of Mn leads to trembling, stiffness, severe depression, anxiety, hostility, damage to lungs, liver, and kidneys, neurological damage etc.,	19, 20

References: 1: Dengan et al., 2020; 2: Selvakumar et al., 2017; 3: Maskooni et al., 2022; 4:Faryadi., 2012; 5: Chakraborty et al., 2022; 6: Khan 2023, 7: Talukdar et al., 2016; 8: Singh et al. 2021; 9: Saxena & Shakeel, 2001; 10: Elgood et al, 2010; 11: Xiao, et al., 2023; 12: Youru et al., 2024; 13: Kien et al., 2022; 14: Abbaspur et al., 2014; 15: Clara, 2019; 16: Pierry and Czop 2020; 17: Plum et al., 2010, 18: atsdr.cdc.gov; 19: Williams et al., 2012; 20: epa.gov, who.int.

3.11 Stable Isotope Hydrology

Stable isotopes are variants of elements that have the same number of protons but differ in the number of neutrons. Stable isotope ratios, like those of hydrogen (H) and oxygen (O) in water molecules, provide valuable information about the origin and history of water sources. Delta notation is a common way to express stable isotope ratios, typically denoted as $\delta^{18}O$ and $\delta^{2}H$, representing deviations from a standard reference. These ratios serve as unique "fingerprints" of water sources, as different processes, such as evaporation, precipitation, and

groundwater recharge, leave distinct signatures. By analyzing stable isotopes, water movement in the hydrological cycle and its interaction in various hydrological compartments can be traced, aiding in water resource management, environmental studies, and climate research.

The isotope ratio is given by

$$R = \frac{^{18}O}{^{16}O} \quad \text{Or} \quad R = \frac{^{2}H}{^{2}H}$$

The isotope ratio can be used to calculate δ. It can be defined as follows: -

$$\delta^{18}O = \left(\frac{R_{sample}}{R_{sample} - R_{standard}}\right) x\ 1000\ ‰$$

The values of $\delta^{18}O$, and $\delta^{2}H$ is reported in per mill or per mil (‰).

In the present study, stable isotopes (^{2}H or D and ^{18}O) in water were analyzed using GV-Isoprime Dual Inlet Isotope Ratio Mass Spectrometer. The measured values are reported as delta (δ) values (Gehre et al., 2004). The precision of measurement for $\delta\ ^{2}H$ is ± 1‰ and that for $\delta\ ^{18}O$ is ± 0.1‰.

4 RESULTS & DISCUSSION

4.1 RAINFALL ANALYSIS

For the rainfall analysis, annual average rainfall data from fifty locations in the study area, covering a 26-year period (1993 to 2018), were collected. The rainfall variation over this period is shown in **Figure 24.** The average rainfall fluctuated around a mean value of 1728±293 mm, ranging from 1435 mm to 2022 mm. The rainfall data, when arranged in ascending order, reveal **Figure 25: Rainfall range in the study area. Annual average rainfall for various years are shown in an ascending order. Value 1728mm indicate average rainfall for all the 26 data points whereas, 1786 mm indicates value averaged after excluding the 1st two extreme low rainfall data.** two extreme droughts between 2010 and 2012. Excluding these two drought years, the long-term annual average rainfall for the study area is estimated at 1786.2 ± 216.08 mm.

To support the average graph (**Figure 25**), rainfall at a few locations during the drought and extreme wet years is shown in **Table 15**. It can be seen from Table 4.1 that in North 24 Parganas district (see Sl. No. 1, 2, and 7), the rainfall in 2012 ranged from 377 mm to 387.1 mm, whereas in 2014 (see Sl. No. 10), it was 2338 mm. Similarly, in South 24 Parganas, the rainfall in 2012 ranged (see Sl. No. 3, 5, 12, 13) from 385 mm to 641.7 mm, while in 2014 (see Sl. No. 2, 4, 5, 6, 8, 9, 13) it ranged from 2467.6 mm to 2303.6 mm. At Manasakhali, during 2012 (see Sl. No. 12), the rainfall was 602 mm, whereas in 2014 (see Sl. No. 13) it was 2303.6 mm. These extreme rainfall values indicate that the North 24 Parganas and South 24 Parganas districts are highly vulnerable to rainfall extremes.

The spatial distribution pattern of rainfall during 2012 and 2014 is shown in Figure 4.2. It depicts that during 2012, almost the entire eastern half of the study area received less than 800 mm of rainfall, whereas the same area received more than 2000 mm of rainfall in 2014.

To understand the changing rainfall pattern, the 26-year period (1993-2018) was subdivided into 5-year intervals, and the spatial distribution pattern of 5-year average rainfall data was inter-compared (**Figure 26**). Figure 26 broadly depicts high rainfall near the coast, with decreasing rainfall towards the northeast and northwest directions, except for 1998-2002, when the northeast region also received a significant amount of rainfall.

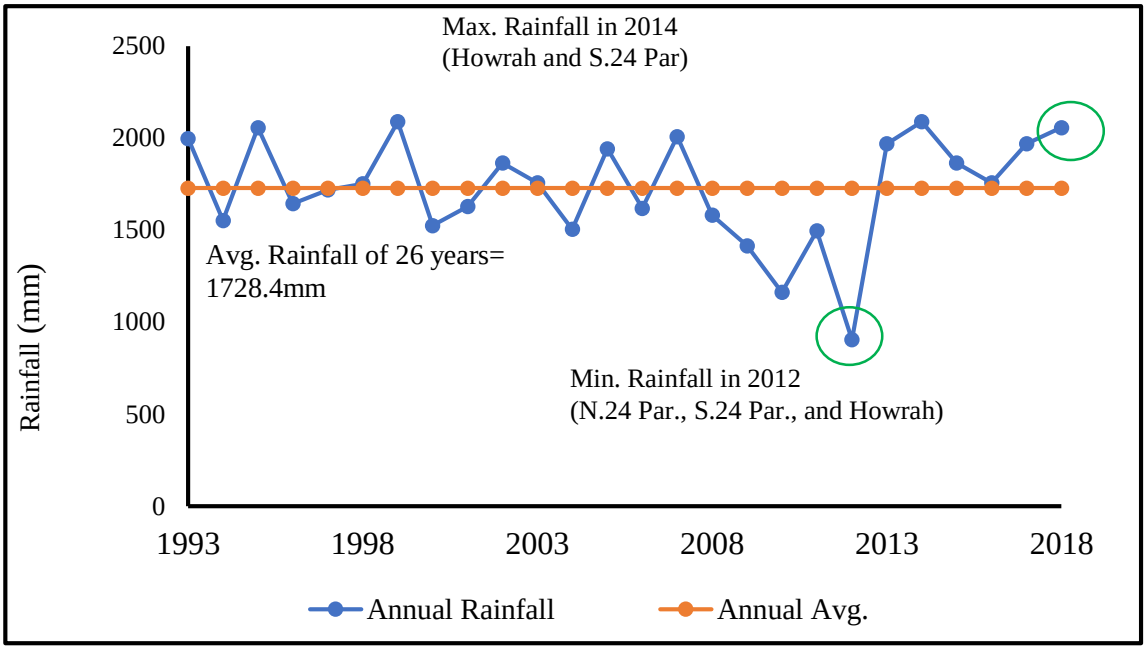

Figure 24: Variation of annual rainfall (1993 to 2020)

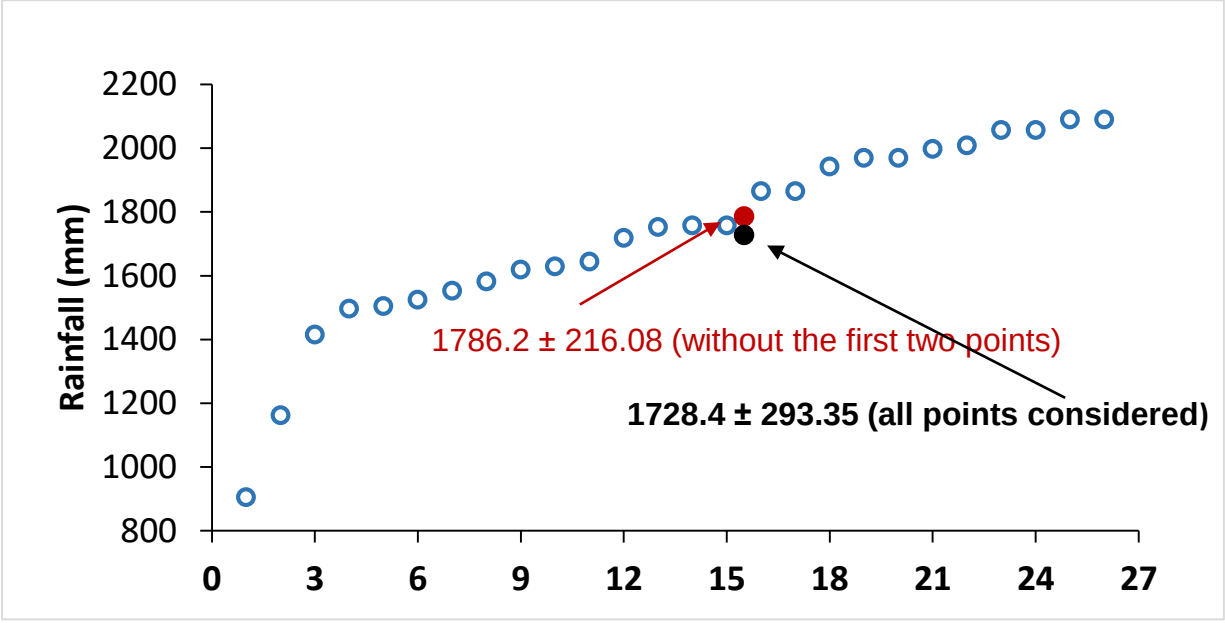

Figure 25: Rainfall range in the study area. Annual average rainfall for various years are shown in an ascending order. Value 1728mm indicate average rainfall for all the 26 data points whereas, 1786 mm indicates value averaged after excluding the 1st two extreme low rainfall data.

The eastern part of East Medinipur district, being near the coast, consistently received higher rainfall than the northwestern parts of West Medinipur district.

Table 15: Rainfall at a few locations during extreme rainfall year 2014 and drought year 2012

Sl No	Rainfall During the Drought Year 2012			Extreme rainfall year 2014		
	Place, District	Lat, long	Rainfall (mm)	Place	Lat, long	Rainfall (mm)
1	Bangaon (N.24 Par.)	23.25, 88.75 23.0, 88.75	377.0 381.6	Natibpur (Hooghly)	22.5, 88.0	2568.6
2	Bamangachi, Barasat (N.24 Par.)	22.75, 88.5	382.5	South Gosaba (S.24 Par)	21.75, 88.75	2467.6
3	Maheshtala (S.24 Par.)	22.5, 88.25	385	Sunderban (S.24 Par)	21.75, 89.0	2460.2
4	Jadurhati (N.24 Par.)	22.75, 88.75	385.1	Rakhalpur (S.24 Par)	21.75, 88.5	2445
5	Tardaha Kapashati (S.24 Par.)	22.5, 88.5	385.8	Namkhana (S.24 Par)	21.75, 88.25	2433.3
6	Dholbaria, Satkhira (B.Desh.)	22.75, 89.0	386.9	Hamilton Island (S. 24 Parg)	22.0, 89.0	2371.2
7	Baligari (N.24 Par.)	22.5, 88.75	387.1	Dobanki Camp (Sundarbans)	22.0, 88.75	2359.4
8	Baruipara, Tisa (Hoghly)	22.75, 88.25	400.0	Sagar Island (S. 24 Parganas)	21.75, 88.0	2347.4
9	Rahimpur (Hooghly)	22.75, 88.0	495.4	Nakali (S. 24 Parg)	22.0, 88.25	2342.1
10	Nalta Mobarak Nagar Satkhira, Khulna (B. Desh)	22.5, 89.0	496.0	Malekhan Gumti (N. 24 Parg)	22.25, 89.0	2338.9
11	Natibpur (Hooghly)	22.5, 88.0	519.3	Sonatikari (S. 24 Parg)	22.0, 88.5	2324.8
12	Manasakhali (S. 24 Parg)	22.25, 88.75	602.0	Nalta Mobarak Nagar Satkhira, Khulna (B. Desh)	22.5, 89.0	2318.6
13	Ramrudrapur (S. 24 Parg)	22.25, 88.5	641.7	Manasakhali (S. 24 Parg)	22.25, 88.75	2303.6

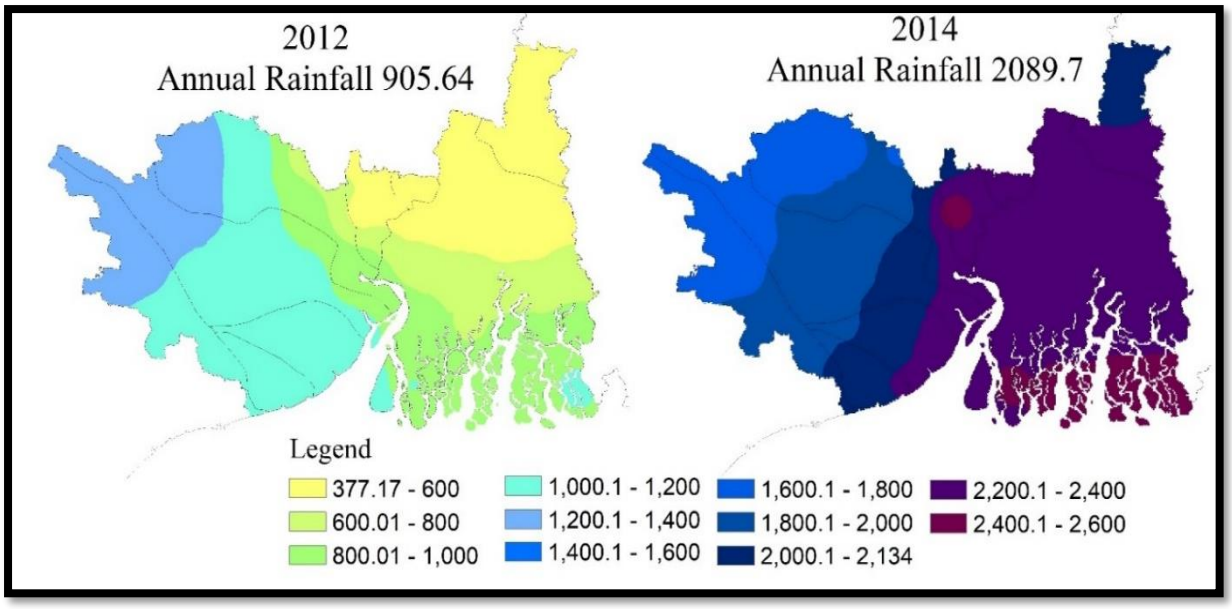

Figure 26: Spatial distribution of annual Min. (2012) & Max. (2014) rainfall

The five-year average rainfall distribution pattern showed decreasing rainfall along the north direction during 1993-1997 and 2002-2007; along the north-northeast direction during 2008-2012; along the northwest direction in the western parts and along the north direction in the eastern parts during 2013-2018; and along the northwest direction during 1998-2002. These variations suggest complexities in the spatio-temporal patterns of rainfall distribution, making forecasting challenging.

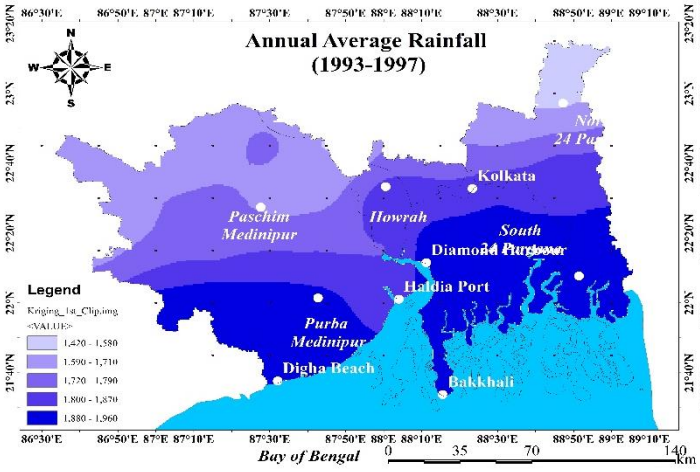

(a)

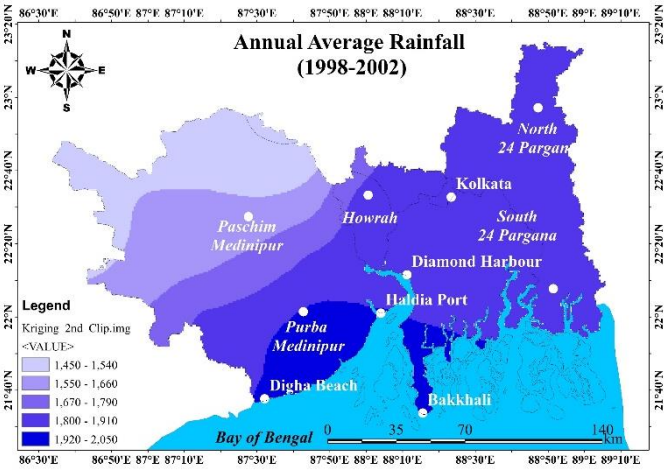

(b)

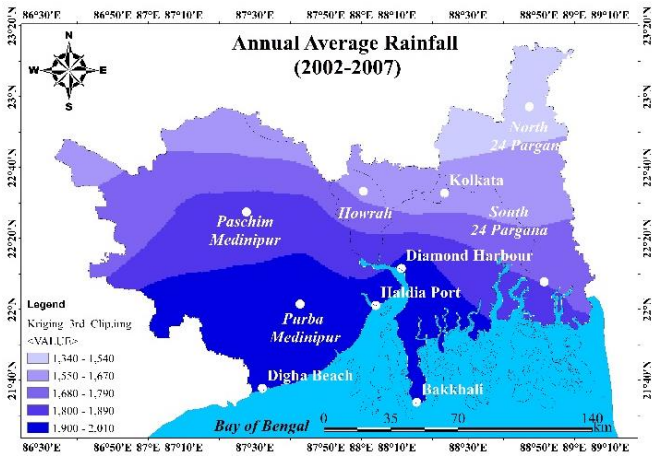

(c)

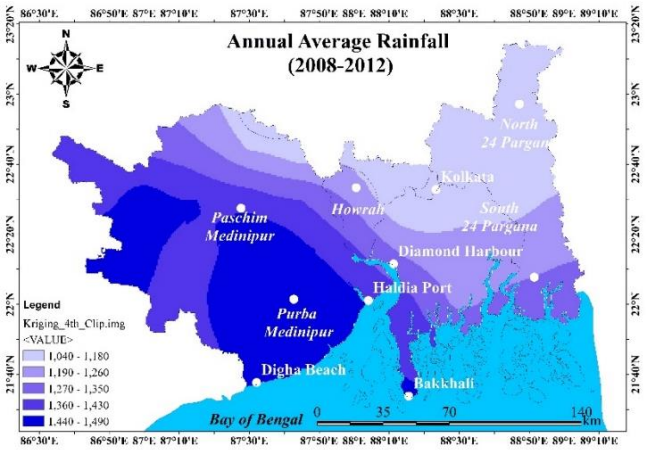

(d)

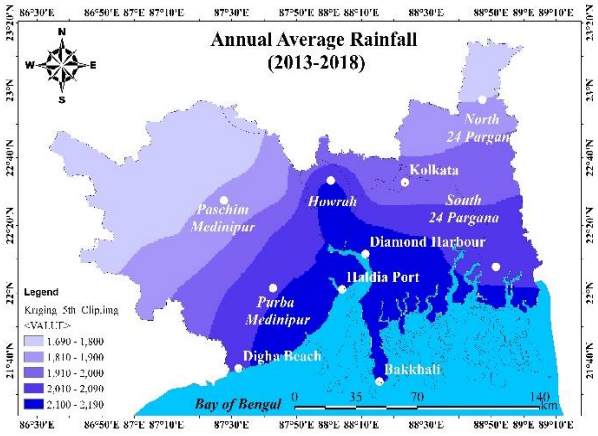

(e)

Figure 27: Annual Average Rainfall of 5 years from (1997-1997,1998-2002,1998-2002,2002-2007,2008-2012,2013-2018)

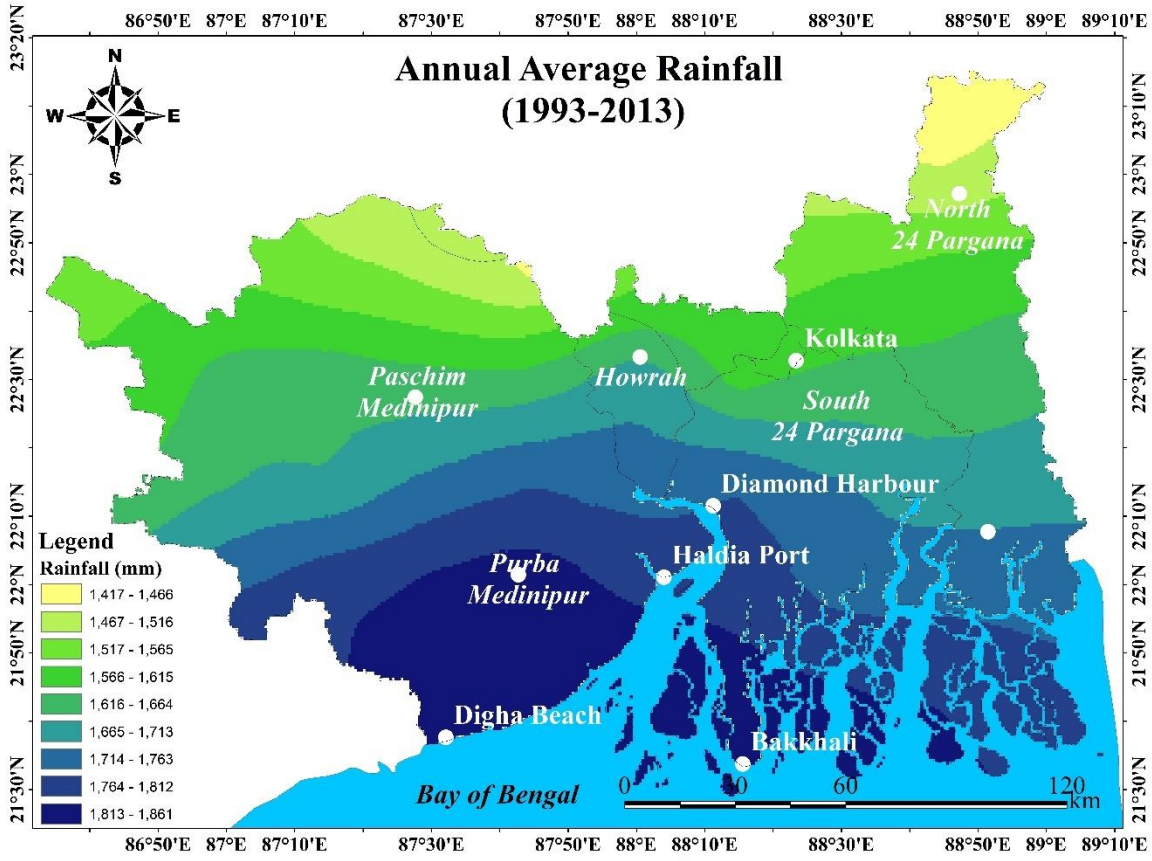

Figure 28:Annual Average Rainfall 1993 to 2013

4.2 ESTIMATION OF SURFACE RUNOFF

The SCS runoff curve number for West Bengal has been estimated for the river watersheds namely; Ichhamati Damodar, Rasulpur, Pichhabani, Subarnarekha, Kasai Haldi, Rupnarayan, Saraswati and Tidal Streams in a GIS environment through integration of land use land cover maps (**Figure 29).** Obtained from remote sensing images of Sentinel data and hydrologic soil data **(Figure 32).** The estimated curve number is then validated using rainfall-runoff data. The daily rainfall database has been incorporated in the analysis to estimate the surface runoff. Based on this study, the following conclusions are drawn.

In this study, the land use/cover classes of coastal area of West Bengal were delineated using remote sensing imageries of SENITEL-2 sensor. These land use/cover classes were integrated with the hydrologic soil groups of the basin in a GIS package viz. ARC/INFO. Subsequently, the runoff curve numbers of coastal area of West Bengal were estimated.

Sub-watershed wise runoff varies from 28.83% to 52.53%. Maximum runoff (52.53%) noticed in the Damodar River watershed followed by Rupnarayan River watershed (47.03%), Kasai-Haldi watershed (44.57%), Subarnarekha River watershed (43.47%), Jamuna-Ichhamati River watershed (35.72%), Tidal Stream (31.8%), Pichhabani River watershed (30.64%) and Rasulpur River Watershed (28.83%).

(i) The SCS runoff curve number method has its obvious advantages viz. simplicity, predictability, stability, responsiveness to major runoff producing watershed properties and reliance on only one parameter namely, the curve number. The SCS runoff curve number for AMC II (average conditions) of the study area is estimated at 75.

(ii) The use of remote sensing technique for determination of land use/cover not only saves time but is less expensive as compared to conventional methods like ground surveys. Further, the satellite based remote sensing has advantages like large area coverage, synoptic view and capability to provide information over all accessible and inaccessible regions. However, the success of remote sensing technique depends on the accurate interpretation of the false colour composites.

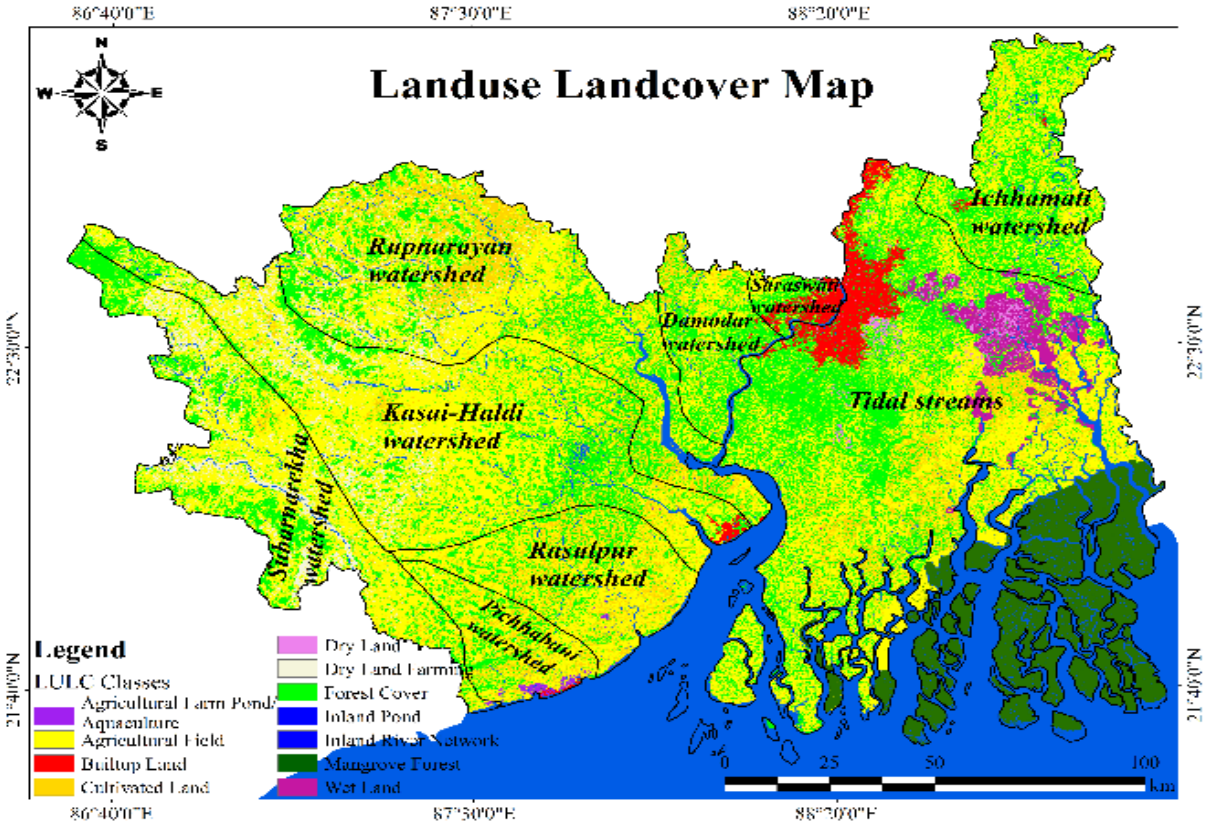

Figure 29: Land use land cover map

Table 16: Area covered under different LULC classes (colour code is as per the Fig. 29)

Sr. No.	LULC Classes	Color code	Area (sq.km)	Area %
1	Agricultural Field		11463.3	43.5
2	Forest Cover		7149.45	27.13
3	Cultivated Land		2491.82	9.46
4	Mangrove Forest		1875.23	7.12
5	Inland River		1181.76	4.48
6	Open Land		940.38	3.57
7	Builtup Land		559.62	2.12
8	Wet Land		479.42	1.82
9	Dry Land		177.4	0.67
10	Agr.Farm Pond/Aquaculture		29.28	0.11
11	Inland Pond		2.96	0.01
Total			26350.6	100

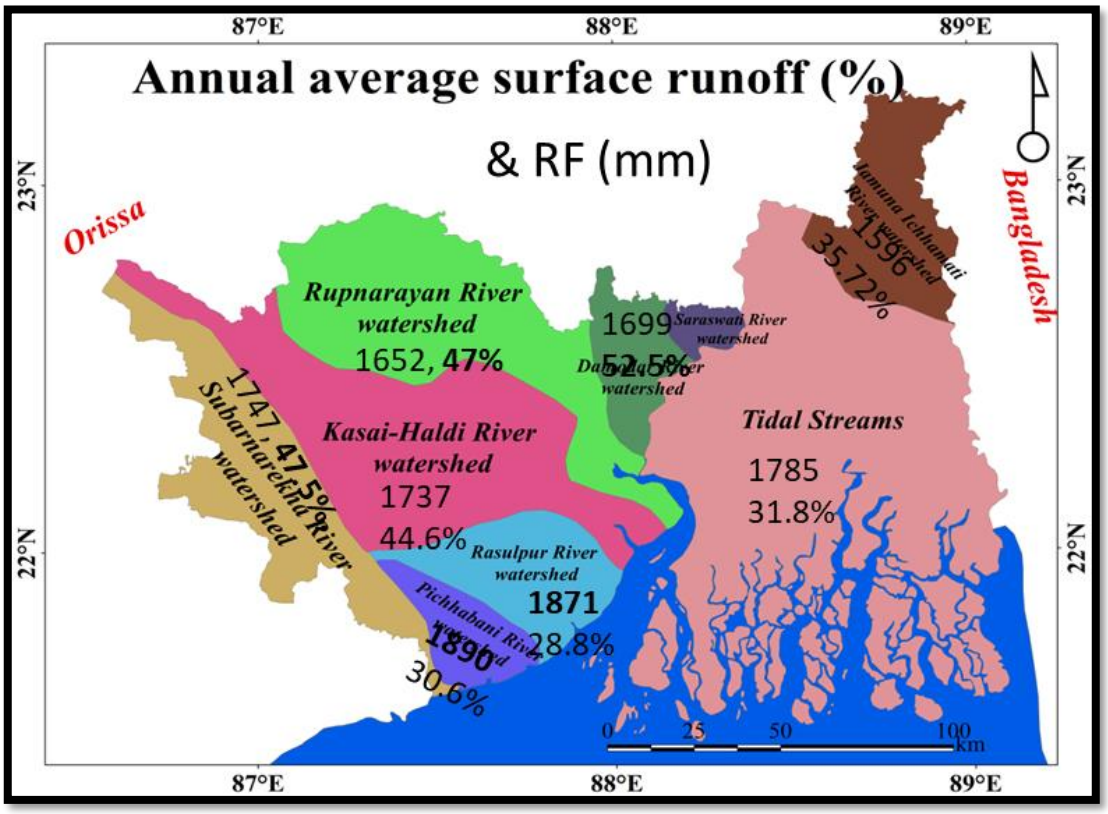

Figure 30: Annual average surface runoff (%) and Rainfall (mm)

Table 17: Rainfall-Runoff characteristic of watersheds in the study area. Colour code is same as shown in the Fig. 32

Colour code	Total runoff (Mm^3)	Districts	Watersheds	Annual Average Rainfall (mm)	Annual Average Surface Runoff (%)
	802.27	Howrah	Damodar	1699.28	52.53
	1002.03	N 24 Parganas	Jamuna Ichhamati	1595.75	35.72
	5552.35	N & S 24 Parganas	Tidal Streams	1785.31	31.8
	3592.19	East and West Medinipur	Kasai-Haldi	1737.72	44.57
	476.535		Pichhabani	1890.24	30.64
	843.13		Rasulpur	1871.29	28.83
	3041.01		Rupnarayan	1651.94	47.03
	2040.93		Subarnarekha	1747.43	43.47

(iii) The land use/cover classes interpreted from satellite remote sensing data are more generalised in comparison to ground survey. Therefore, it is necessary to develop more generalised land use classes suitable for remote sensing data in curve number method.

(iv) GIS serves as a powerful tool for integration of land use/cover data and hydrologic soil data for computation of areas under different categories. It not only saves time but makes the computations accurate as well.

(v) Sub-watershed wise runoff varies from 28.83% to 52.53%. Maximum runoff (52.53%) noticed in the Damodar River watershed followed by Rupnarayan River watershed (47.03%), Kasai-Haldi watershed (44.57%), Subarnarekha River watershed (43.47%), Jamuna-Ichhamati River watershed (35.72%), Tidal Stream (31.8%), Pichhabani River watershed (30.64%) and Rasulpur River Watershed (28.83%).

(vi) The results of this work can be applied especially in the areas of flood risk management, urban or landscape planning. The presented results can be also useful for identifying suitable locations for polders or small retention areas using geo-information technologies so as to reduce the high surface runoff and avoid floods in the study area. However, the main importance of the paper can be seen in the methods used which can be replicable in other similar small basins.

4.3 GROUNDWATER POTENTIAL ZONE

Background Data

GIS tools were employed to create a composite map using various data sources to assess the groundwater potential zones. Satellite data, Survey of India (SOI) topo-sheets at a scale of 1:50,000. and Geological Survey of India (GSI) data were utilized to gather precise information. Soil maps were prepared by digitizing maps from the National Bureau of Soil Survey and Land Use Planning, which were updated to include urban land use based on the 2017 SENTINEL-2B dataset. The geomorphology and geology-themed layers were created using ArcGIS 10, incorporating both existing maps and supplemental data. High-resolution satellite data, particularly from the SENTINEL-2B dataset, were used to map land use/land cover (LULC) and surface water bodies. Topographic elevation was determined using 1:25,000 topo-sheets with 5-meter contour intervals, and hydrogeology maps were prepared based on the GSI report published in 2000 at a scale of 1: 250,000.

Methodology for Groundwater Potential Zone Assessment:

To evaluate the factors determining groundwater potential zones, several key characteristics were considered: geology, slope, drainage density, geomorphic units, and lineament density. These factors are crucial for understanding the potential for groundwater recharge in different areas. The thematic maps generated using remote sensing (RS) and conventional data helped in assessing the groundwater potential in the study area. The maps were then updated with additional data and satellite information to improve their accuracy.

Methodological Approach:

In ArcGIS, the various factors influencing groundwater potential were combined using a weighted overlay technique. Each characteristic was assigned an appropriate ranking, and weight factors were allocated to different geomorphic units based on their capacity to hold groundwater. This technique was applied to each layer, and the resulting layers were classified into four groundwater potential zones: very high, high, moderate, and low. The Cumulative Score Index (CSI) was used for this classification. The groundwater potential zone map thus obtained was categorized into these four classes. The study revealed that about 29.52% of the river basin is covered under moderate groundwater potential zones. Low and high groundwater potential zones were observed in 0.22% and 53.48% respectively, with 16.78% in very high potential zones **().**

Topography:

Generally, locations with level or gently inclined topography facilitate infiltration and groundwater recharge, whereas steeply sloped terrain leads to runoff with little to no infiltration. Therefore, flat and gradually sloping landscapes are predicted to have higher groundwater potential. The topography of the study area was generated using ASTER (Advanced Spaceborne Thermal Emission and Reflection Radiometer) data, which has a resolution of 30 meters. The Digital Elevation Model (DEM) was used as an input for delineating watersheds and determining the topographic elevation of the study area, as shown in **Figure 31**.

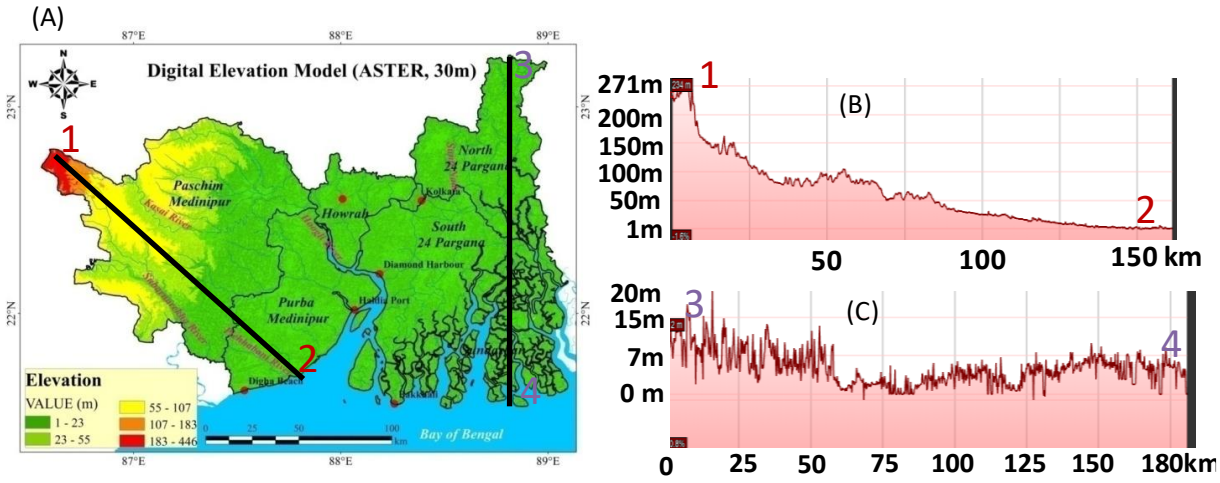

Figure 31: Topographic elevation. (A): Digital Elevation Model, (B) & (C) Elevation profile along the cross sections 1-2 and 3-4 as marked in the figure (A).

Table 18: Study area within different elevation range

Elevation Range	Area (Percentage)
1-23m	76.59 %
24-55m	7.13 %
56-107m	6.18 %
108-183m	5.16 %
184-446m	5.09 %
Total	100 %

Soils:

The entire coastal area, consisting of 59 blocks (29 blocks in South 24 Parganas, 5 blocks in North 24 Parganas, 9 blocks in Howrah, and 16 blocks in Purba Medinipur), is under confined conditions. Kolkata is also under confined conditions. The soil in the study area is broadly classified into six types: clay skeletal, clayey, loamy, loamy skeletal, and sandy soil, with the majority of the area covered by loam soil (**Figure 32**).

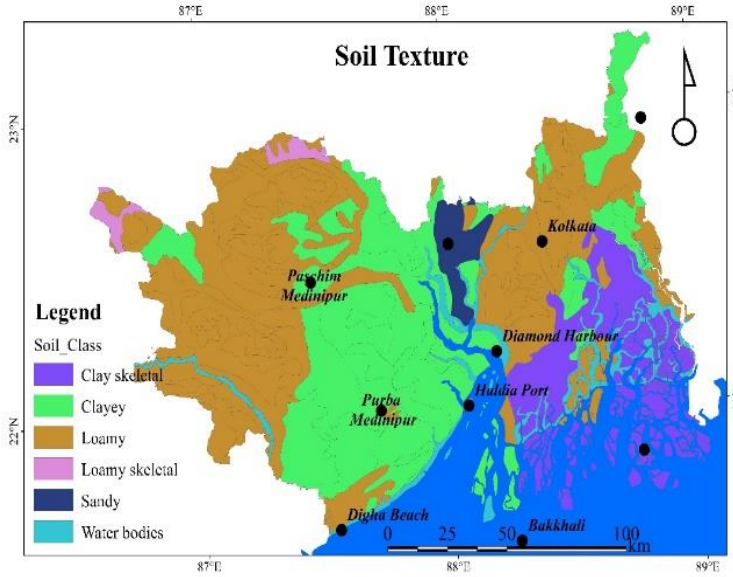

Soil Class	Color code	Area (%)
Loamy		44.82
Clayey		34.48
Clay skeletal		12.18
Water bodies		4.82
Sandy		2.38
Loamy skeletal		1.29

Figure 32: Topographic soil texture of the study area, and the area covered under different soil texture

Land Use Land Cover:

The major dominant land use and land cover (LULC) types in this sub-watershed include Agricultural Field (11,463.31 sq. km), Forest Cover (7,149.45 sq. km), Cultivated Land (2,491.82 sq. km), Mangrove Forest (1,875.23 sq. km), Inland River (1,181.76 sq. km), Open Land (940.38 sq. km), Built-up Land (559.62 sq. km), Wetland (479.42 sq. km), Dry Land (177.4 sq. km), Agricultural Farm Pond/Aquaculture (29.28 sq. km), and Inland Pond (2.96 sq. km). The major crops were found rice, maize, pulses, oil seeds, and wheat etc. **(Figure 29).**

Drainage Characteristics:

The coastal areas of the study region receive significant river water from several large river systems, including the Rupnarayan River, Kasai-Haldi Subarnarekha River, Jamuna-Ichhamati River, Tidal Stream (31.8%), Pichhabani River, and Rasulpur River (**Figure 33**). The study area exhibits wide variations in drainage characteristics, with drainage congestion being a

common issue in coastal plains with flat slopes. In these low-lying coastal areas, the disposal of surface runoff takes considerable time, leading to acute surface drainage problems that impact crop production.

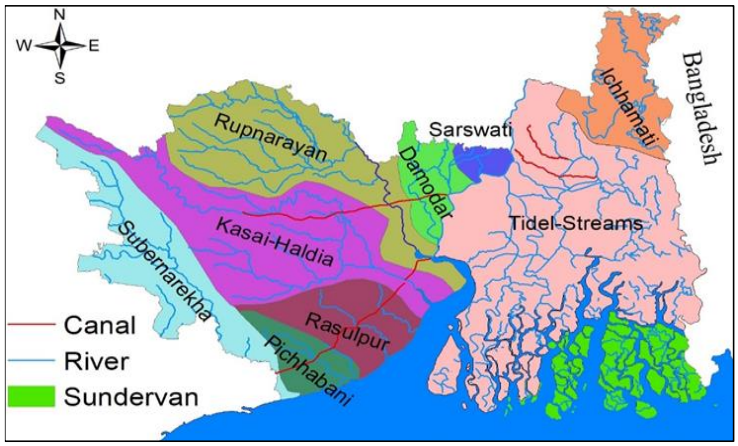

Color code	Watershed	Area (sq.km)	Avg. slope (%)
	Tidal Streams	9779.93	0.005
	Kasai Haldi	4638.06	0.122
	Rupnarayan	3914.25	0.08
	Subarnarekha	2686.82	0.14
	Ichhamati	1757.94	0.009
	Rasulpur	1562.82	0.18
	Damodar	898.77	0.16
	Pichhabai	822.79	0.03
	Saraswati	280.82	0.06

Figure 33: Watersheds and drainage map; and the table showing area under different watersheds, and the average slope of the watersheds. The colour code given in the table is same as that shown in the figure.

Delineation of Groundwater Potential (GWP) Zones:

Groundwater availability in the study area primarily depends on factors such as geology, geomorphology, soil, lineament density, drainage density, rainfall, and land use. The relative importance of various thematic layers and their corresponding classes was used to generate the groundwater potential zone map. Based on the rank and weightage of individual layers, the study area was classified into low, moderate, high, and very high groundwater potential zones.

Very high and high groundwater potential zones are characterized by geologic units such as quartz gravel, conglomerate, sandstone, sand, and sandy clay; geomorphological units such as alluvial plain, deltaic plain, and low drainage density; and areas with high mean annual rainfall. The moderate potential zone is dominated by geologic units of laterite and geomorphic units such as pediments, pediplains, and medium drainage density. Low potential zones are primarily found in the denudational hills. The upper portion of the north-western part of the study area has moderate groundwater potential, whereas the coastal areas exhibit very high groundwater potential.

The groundwater potential area was prepared by delineating the study area, into four classes: very high, high, moderate and low. The Cumulative Score Index (CSI) was used for this classification. The groundwater potential zone map thus obtained was categorized into four classes-**very high, high, moderate, and low**. The study reveals that about **29.52%** of the river basin is covered under moderate groundwater potential zone. The low and high groundwater potential zones are observed in **0.22%** and **53.48%** respectively and **16.78%** is observed very high potential zone **().**

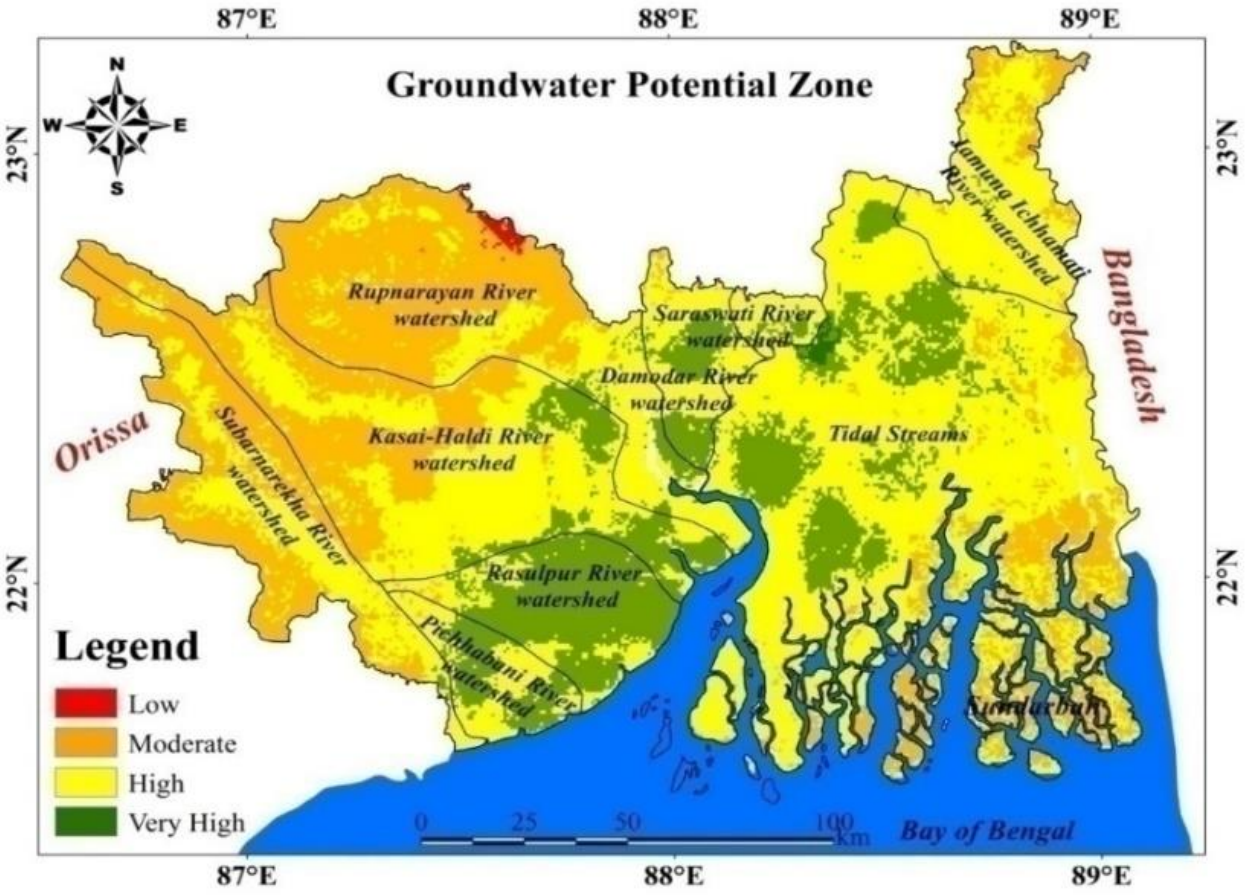

Category of GW potential zone	Range	Area (%)
Low	<1.8	0.22
Moderate	1.8-2.6	29.52
High	2.6-3.4	53.48
Very high	>3.4	16.78

Figure 34. Groundwater potential zone

Results and Conclusions:

This study was carried out to map the groundwater potential zones in the coastal areas of West Bengal, India, where groundwater is being over-exploited to meet the demand from agriculture, industry, and domestic users. Based on this study, the following conclusions are drawn:

1. Weighted overlay analysis was adopted to prepare a map of groundwater potential zones using seven thematic layers: geology, geomorphology, soil, drainage density, rainfall, and land use.

2. The delineated zones within this region were classified as very high, high, moderate, and low groundwater potential zones. Further, it was identified that the recharge zones are located in regions with high groundwater potential zones. These observations validate the map prepared in this study.

3. The study revealed that about 29.52% of the river basin is covered under moderate groundwater potential zones. Low and high groundwater potential zones were observed in 0.22% and 53.48% respectively, with 16.78% in very high potential zones.

4. The saltpans and saline water intrusion are likely due to the over-extraction of groundwater, which affects the quality of the groundwater along the coastal region. To meet the increasing demand and to prevent seawater intrusion, new well fields may be formed in other high groundwater potential zones.

This study demonstrates the application of remote sensing and GIS techniques for integrating surface and subsurface information in a rapid and cost-effective manner, which may assist in locating sites for the development of groundwater in the future.

4.4 GROUND WATER FLOW REGIME

Groundwater generally flows from areas of high hydraulic head (water table elevation) to areas of low hydraulic head due to gravity. The direction of groundwater flow is often influenced by surface topography, as groundwater typically follows the gradient of the land surface. As a result, the flow patterns of surface water bodies can provide valuable insights into the direction and rate of underlying groundwater movement.

Factors that alter the storage or recharge of groundwater can cause fluctuations in groundwater levels over time. Local groundwater withdrawals through pumping create "cones

of depression" on the water table, lowering levels in the immediate vicinity. Conversely, groundwater recharge from precipitation, surface water bodies, or other sources can lead to rising water table elevations.

Seasonal fluctuations in the water table often reflect variations in precipitation and recharge patterns throughout the year. Longer-term water table variations may indicate the impacts of droughts, wet periods, climate change, increased pumping, land-use changes, or even geologic events like earthquakes.

In coastal areas, small-scale diurnal (daily) fluctuations in groundwater levels can occur due to factors like tidal influences or daily patterns of domestic water use. Increased hydrostatic pressure during high tides can cause the water table to rise, while low tides can lead to decreased pressure and falling water levels.

It's important to note that not all areas are equally conducive to groundwater recharge. While precipitation is typically the primary source of groundwater replenishment, surface water bodies like streams, rivers, and lakes can also contribute to recharge in some settings. Understanding the specific hydrogeologic characteristics of a region is key to evaluating its groundwater recharge potential.

Overall, a careful analysis of groundwater flow patterns and water table fluctuations can provide valuable insights into the dynamics of groundwater systems and inform sustainable management strategies. Monitoring groundwater levels helps assess the resource, its recharge and discharge areas, identify groundwater mining zones, potential groundwater zones, groundwater-surface water interaction regions, causes of decreasing groundwater levels, causes of coastal groundwater salinization, and areas of submarine groundwater discharge. This analysis is crucial for sustainable groundwater utilization, ecosystem impact assessment, and maintaining socio-economic growth. Therefore, monitoring seasonal and long-term groundwater levels is essential for planners and policymakers to make informed decisions for sustainable groundwater use.

To analyze groundwater flow patterns, changes in these patterns, and potential depletion and recharge areas, groundwater contour maps were prepared for the pre-monsoon and post-monsoon periods. These maps were averaged over four five-year intervals from 2001 to 2019: 2001-2005, 2006-2010, 2011-2015, and 2016-2019. Averaging the data over five-year periods was done to minimize the effects of minor variations in rainfall and groundwater abstraction,

providing a clearer view of the average flow patterns. By comparing these maps, the aim was to identify any significant changes in the overall groundwater flow or levels over time.

The **Figure 35** shows that the overall groundwater flow is in the direction from northwest to southeast in the Medinipur districts, and along a north-south direction in North 24 Parganas. However, there is no clear flow direction in Howrah district and its southern areas, as well as in the South 24 Parganas. The absence of a clear flow direction in the South 24 Parganas is attributed to the flat topography near sea level, and the landscape with a dense criss-cross network of streams.

The change in groundwater fluctuation and flow patterns between 2001-2005 and 2016-2019 is highlighted in **Fig.35** (A, B, C, and D). Figures 2A and 2B show that in the northwest parts of the region, the groundwater contour interval of 30-45 meters during 2001-2005 (Figure 2A) increased to 30-60 meters during 2016-2019 (Figure 2B). Additionally, the contour interval of 45-60 meters in 2001-2005 (Figure 2A) increased to 60-75 meters during 2016-2019 (Figure 2B), indicating a rise in groundwater depth by nearly 15 meters over 15 years.

In the central part, near Howrah district, the groundwater flow pattern during 2001-2005 shows an outward flow direction from Howrah district towards nearby rivers (Figure 2C). However, during 2016-2019, a minor reversal in the flow pattern is observed (Figure 2D), indicating an increased effect of concentrated groundwater withdrawal in the Howrah urban region. Since these rivers carry tidally induced seawater, there is a strong possibility of groundwater contamination from seawater intrusion due to the induced flow.

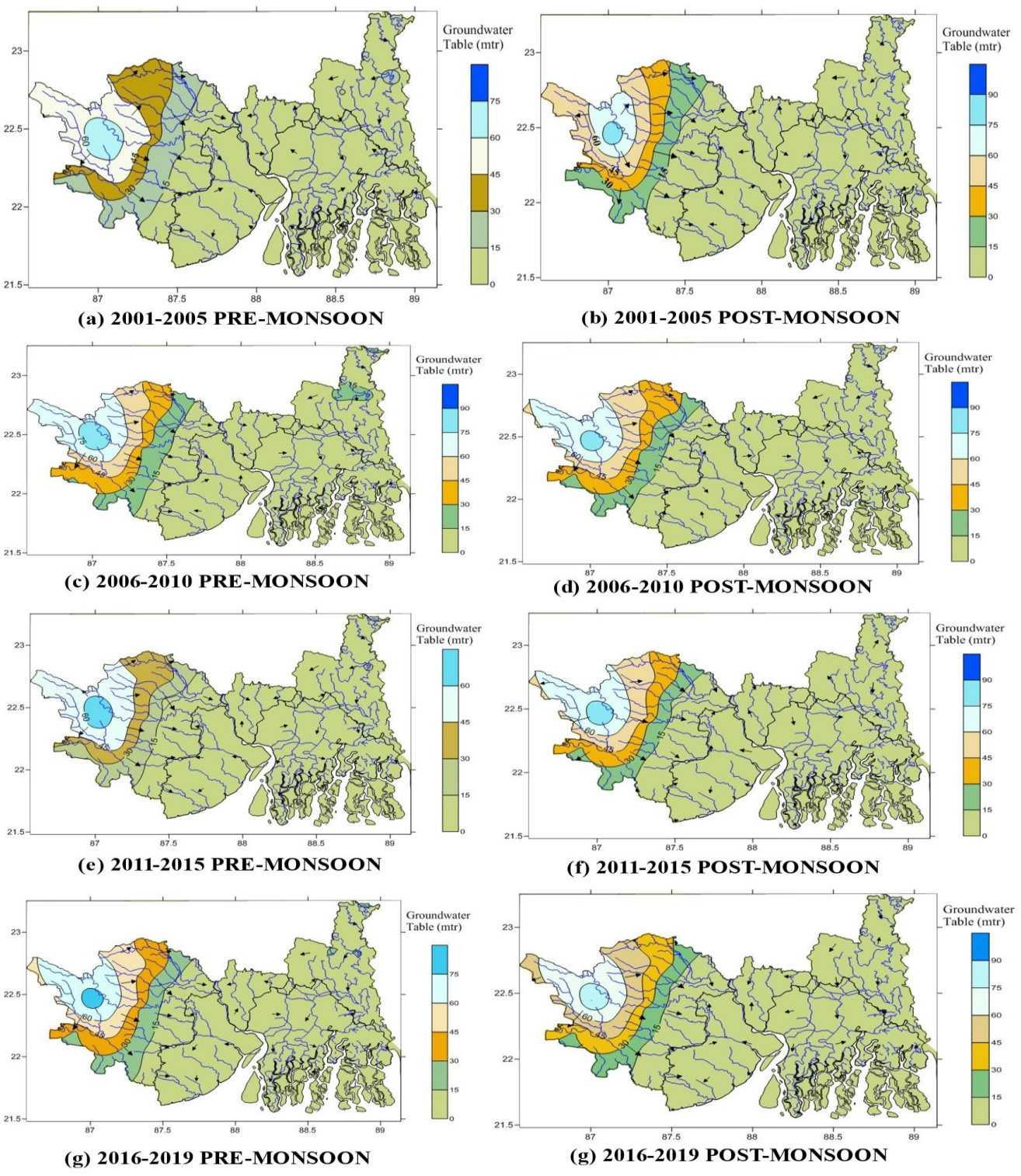

Figure 35: Ground Water Level Variations in 5 years average periods from 2001 to 2019

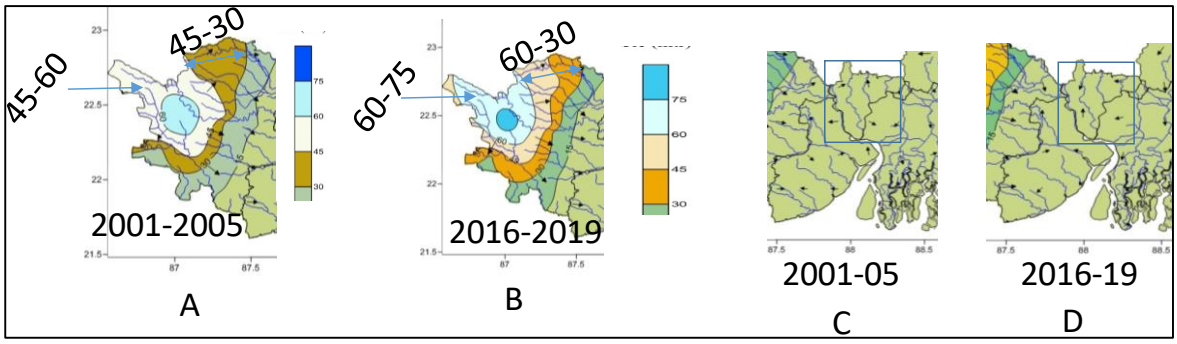

Figure 36: Comparison of pre-monsoon groundwater level during the periods 2001-05 and 2016-19. An and B: Comparison in the NW parts of the study area. C & D: Comparison near Howrah district

Groundwater depletion occurs due to natural outflow during the post-monsoon (non-recharge) period and from anthropogenic withdrawals, while levels are replenished through groundwater recharge during the monsoon from precipitation and from nearby water bodies like lakes, rivers, and canals, when the water levels in these bodies are higher than the groundwater levels, and there is an interconnection between these water bodies and the local groundwater. The difference in groundwater levels between the pre-monsoon and post-monsoon periods (calculated as pre-monsoon minus post-monsoon) generally reflects the extent to which groundwater levels are replenished post-monsoon, compared to the levels at the end of the pre-monsoon period. More negative values indicate greater depletion during the pre-monsoon period.

In areas with steep topographic slopes, the higher groundwater flow velocities typically result in elevated pre-monsoon water levels, leading to a more negative difference between pre-monsoon and post-monsoon levels. Conversely, in coastal areas where topographic slopes are very low, seawater acts as a barrier, preventing groundwater from discharging into the sea. As a result, the natural discharge rate of groundwater is low, and the difference between pre-monsoon and post-monsoon levels is minimal. These coastal areas are often discharge zones for continental groundwater. Depending on the flow paths and the time it takes for groundwater to reach these discharge zones, water levels tend to remain relatively stable with minimal fluctuations. Although groundwater withdrawals near the coastline may cause depletion, this can induce seawater intrusion, which in turn helps to maintain groundwater levels, although intrusion may lead to increase in groundwater salinity.

Groundwater fluctuation (calculated as pre-monsoon minus post-monsoon) averaged over the period 2016-2019 for the study area is shown in Figure 35. Significant groundwater fluctuations (-5m to -14m) are observed in the East and West Medinipur districts due to steep topography. In contrast, generally low fluctuations (0m to -3m) are observed in the North 24 Parganas and Howrah districts. In some areas of South 24 Parganas and on Sagar Island, a rise in the water table can also be observed.

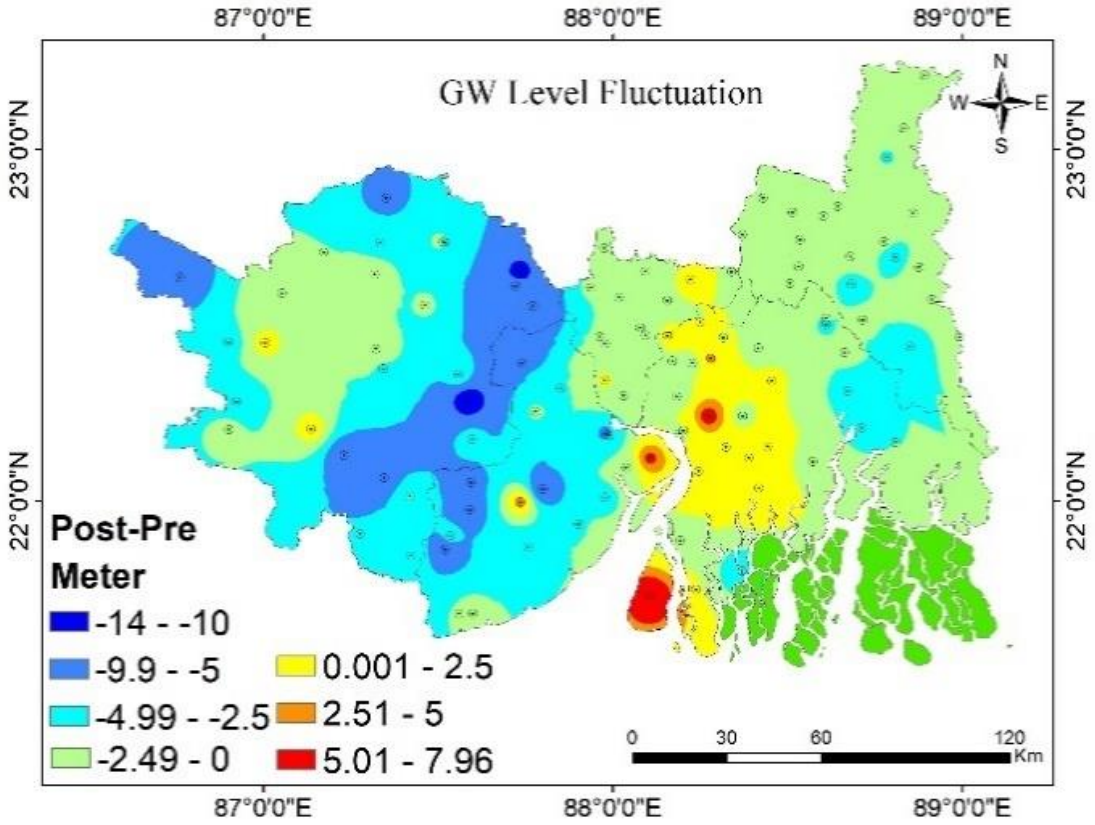

Figure 37: Ground water fluctuation [(Pre-monsoon) – (post-monsoon)]. The water levels data is averaged over 2016 to 2019 prior to fluctuation analysis

To determine whether groundwater depletion is primarily due to natural factors, such as a decreasing rainfall trend, or due to increasing groundwater withdrawals, a comparison was made between the long-term rainfall trend (1995-2018) and the groundwater level trend (1995-2018), as shown in **Figure 37** The average rainfall and groundwater levels remained almost constant from 1996 to 2006. After 2006, rainfall decreased until 2012, then sharply increased, eventually surpassing the pre-2006 levels slightly. Groundwater levels, however, continued to

decline until 2013 and, although they rose thereafter, they did not return to pre-2006 levels. Post-2016, groundwater levels began to fall again.

When the average rainfall during 1996-2006 was approximately 1750 mm, the groundwater level was 8 meters below ground level (bgl). In contrast, during 2013-2018, with the same average rainfall of 1750 mm, the groundwater level had dropped to 15 meters bgl. This statistic indicates a continuous decrease in groundwater levels since 2006, suggesting that the decline is not primarily due to rainfall but likely due to increased anthropogenic withdrawals. The substantial increase in groundwater withdrawals post-2006, compared to earlier years, is likely causing unsustainable groundwater use and could induce seawater intrusion if negative hydraulic gradients develop near the coastline.

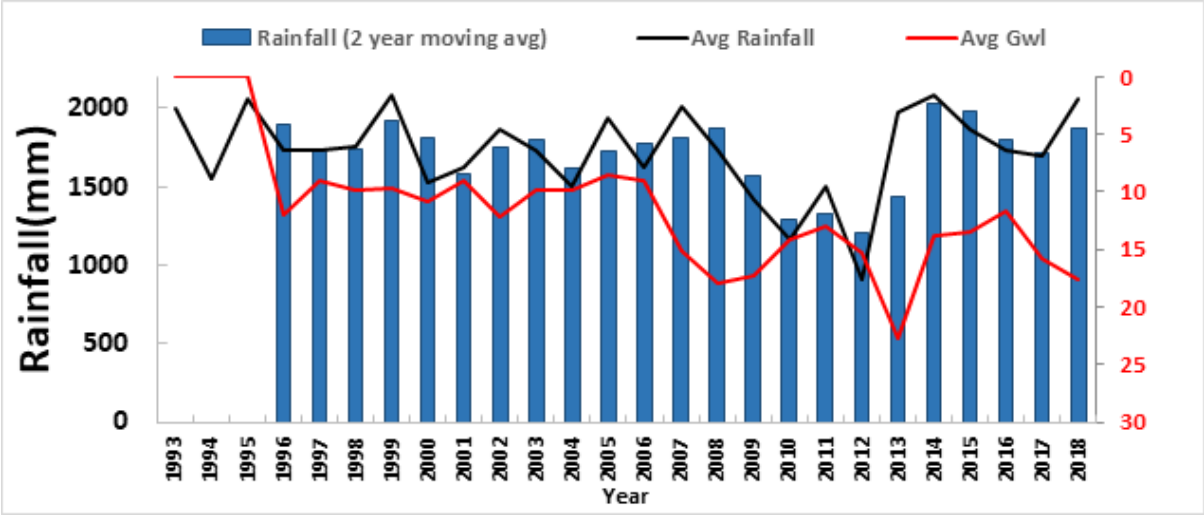

Figure 38: Comparison of rainfall (primary Y axis) and groundwater level (secondary Y-axis, units in meters below ground surface)) trend in the study area.

4.5 RIVER WATER QUALITY

4.5.1 Surface water quality evaluation

The study area is characterized by large coastal rivers and tidal channels. As discussed in the previous section, groundwater levels in the study area are depleting due to extensive extraction. In such a scenario, groundwater salinization is likely to develop if surface channels recharge local groundwater through surface water-groundwater interaction, leading to a reduction in fresh groundwater resources in the region. If these channels carry freshwater, the recharged groundwater is expected to become fresher. However, if these interacting rivers discharge saline water, the salinity of the groundwater is expected to increase.

To assess this, surface water quality data from 11 different river locations were collected for a 10-year period (2010-2022) from the State Pollution Control Board. The temporal variation of electrical conductivity (EC) and chloride concentration was examined. The locations of the river water sampling points are shown in Figure? 31, and Table? 4.5 provides the location details. The range of observed EC and chloride concentrations is given in **Table 20**, and the observed variation in EC and chloride concentration are shown in **Figure 40** as high saline stream water and low saline stream water locations.

Table 19: - Monitoring stations of surface water quality analysis (in the Figure 39).

Location of monitoring stations of river water analysis			
Districts	Station code, station, and River	Lat	Long
Medinipur (W)	01) Midnapore, Kansbati River	22.395734	87.320136
	Ghatal, Silabati River	22.661477	87.731655
Medinipur (E)	02) Kolaghat, Rupnarayan River	22.447738	87.878373
	03) Geonkhali, Rupnarayan River	22.201099	88.046354
	Durgachak, Ganga River	22.056688	88.148718
24-S Parganas	04) Diamond Harbour, Hooghly River	22.185972	88.177137
Howrah	05) Uluberia, Hooghly River	22.46703	88.118789
	Howrah-Shivpur, Hooghly River	22.562777	88.330718
24-N Parg.	06) Haroa Bridge, Bidyadhari river	22.602822	88.675831
	07) Malancha Burningh Ghat, Bidyadhari river	22.503357	88.768
	Palta, Ganga River	22.792936	88.349718
Kolkata	N-C) Noai Canal, Near Airport	22.67237	88.455692

Figure 39: Stations of long-term surface water quality monitoring stations, monitored by SPCB, GoWB

Figure? 37 depicts that EC variation follows exactly in according to chloride concentration indicating major source for EC due to chloride salts such as NaCl. The seasonality of variation of EC and Cl from 2010 to 2020 shows that during the pre-monsoon period (March to May), river water quality at locations 02, 03, 04, 06, and 07 is highly saline, with electrical conductivity (EC) values (in µS/cm) ranging from several thousand at sites 02, 04, and 06 to nearly 10,000 µS/cm at location 03 and around 20,000 µS/cm at location 07. However, during the post-monsoon period, the EC at all these sites decreases to less than 1,000 µS/cm, and at site 02, it drops to below 500 µS/cm. This indicates that these rivers carry freshwater discharge during the monsoon, whereas during the non-monsoon lean period, seawater intrusion into these channels increases the river water salinity.

Long-term data show a decrease in pre-monsoon river water salinity at locations 04, 06, and 07 after 2016. For example, at location 07, the pre-monsoon chloride concentration in 2016 was about 11,000 mg/l, which reduced to 3,000 mg/l by the pre-monsoon of 2020. Similarly, at location 06, the chloride concentration during the pre-monsoon of 2015 was 3,648 mg/l, which decreased to 600 mg/l in 2020. The sharp decline in salinity after 2016 indicates a rapid freshening of these river channels in the study area.

However, no significant change in pre-monsoon river water salinity was observed at locations 02 and 03. The river at these locations borders the southern and western boundaries of Howrah district. Since there is no decrease in the salinity of this river, any interaction between this river and groundwater in the Howrah district is likely to increase groundwater salinity in the vicinity. Conversely, at other locations where river water freshening began in 2016, areas with river-groundwater interaction are also expected to experience groundwater freshening.

Table 20: River water quality analysis

Location	EC (µs /cm)			Chloride (mg/l)Series		
	Min	Avg.	Max	Min	Avg.	Max
North 24 Parganas (Malancha Buning ghat) Bidyadhari River	679	6956.7	29900	95.97	3090.2	11826.1
North 24 Parganas (Haroa Bridge) Bidyadhari River	303.7	2055.4	6335	69.97	841.3	4434.8
North 24 Parganas (Ganga at Palta) Shitalatala River	175	305.3	471.4	3.57	11.31	23.48
East Medinipur (R. Rupnarayan before confluence)	220	1819.6	12200	8.39	456.3	4431.5
North 24 Parganas (Noal- Canal)	316	1133.9	2170	11.9	162.2	471

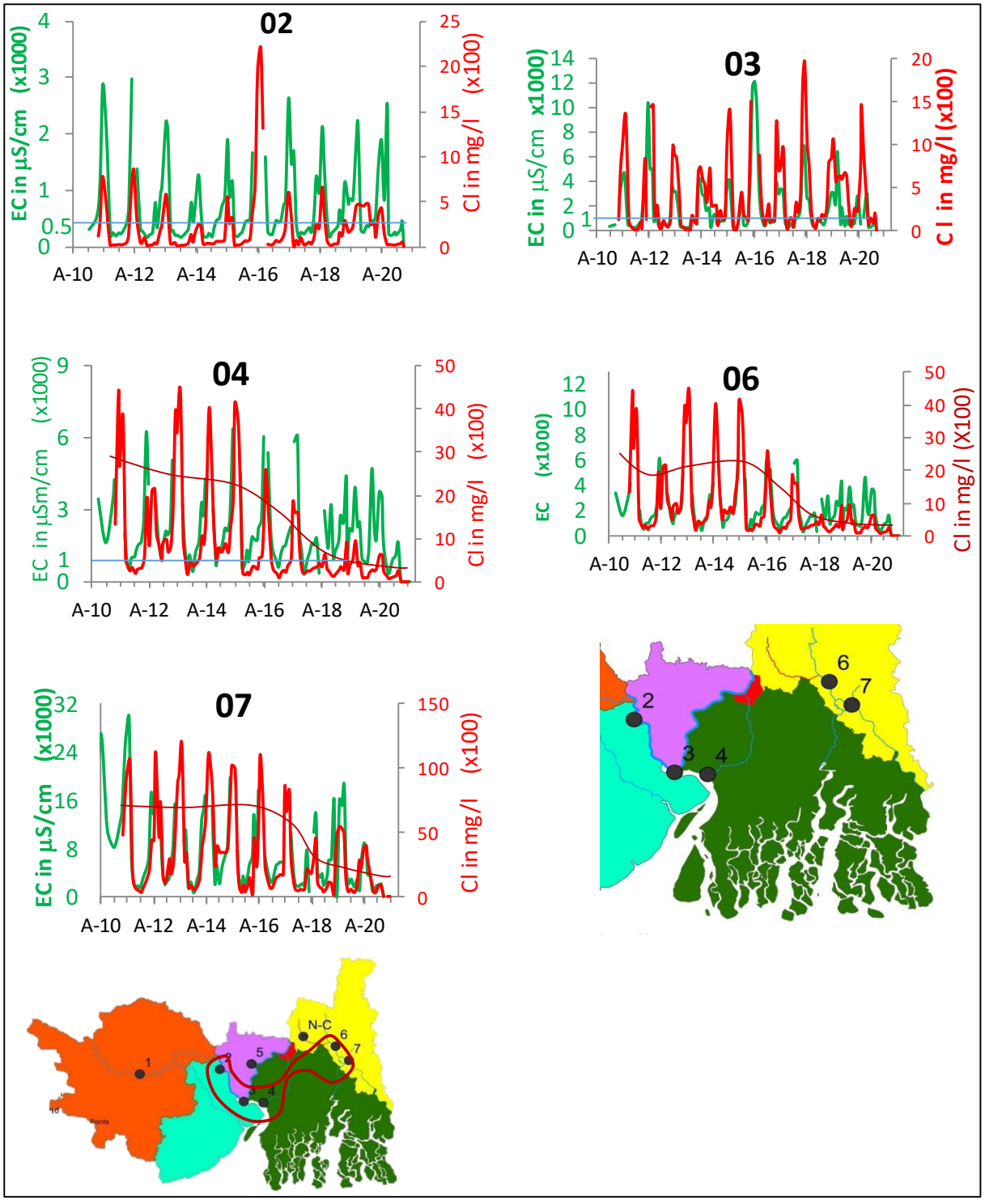

Figure 40: Variation in EC and chloride concentration in river waters (of high salinity) in the study area over the period 2010-2020. X-axis is in years. 'A-10' means April 2010, 'A-20' means April 2020. Location point (02, 03,, 04, 06, and 07) shown in the individual graphs are also marked in the study area figure. Red graph is for the chloride concentration and green for EC.

Locations 1, 5, and N-C are situated in the upper regions of the study area. Location 1 is on the Kasai River in West Medinipur district, location 5 is in Howrah district, and N-C is in North 24 Parganas. The EC at these sites varies between the post-monsoon and pre-monsoon periods, with the following ranges:

- Location 1: 84-360 µS/cm
- Location 5: 216-700 µS/cm
- Location N-C: 350-1900 µS/cm

Stream water quality at locations 1 and 5 is nearly fresh, as more than 80% of the time their EC is less than 500 µS/cm. In contrast, N-C is moderately saline, with water quality in the range of 1000-1900 µS/cm about 50% of the time. It is noteworthy that locations 6 and 7 are just downstream of N-C. At location 6, the EC during the pre-monsoon period ranges from 4000-6000 µS/cm, while at location 7 it ranges from 10,000 to 29,000 µS/cm. Even during the monsoon, the salinity at location 7 remains above 1700 µS/cm, indicating that seawater inflows reach up to this point. Above N-C, however, river water is consistently fresh.

Similarly, comparing the pre-monsoon EC of river water at locations 3 and 5, location 3 has an EC ranging from 3000-5500 µS/cm, while at location 5 it remains between 300-550 µS/cm. This suggests that seawater inflow through the river stops between locations 3 and 5. Therefore, the saline river channels are confined downstream, below points N-C and 2. Notably, the stretches between locations 2 and 3 are important as they are saline and border Howrah district, which is highly populous.

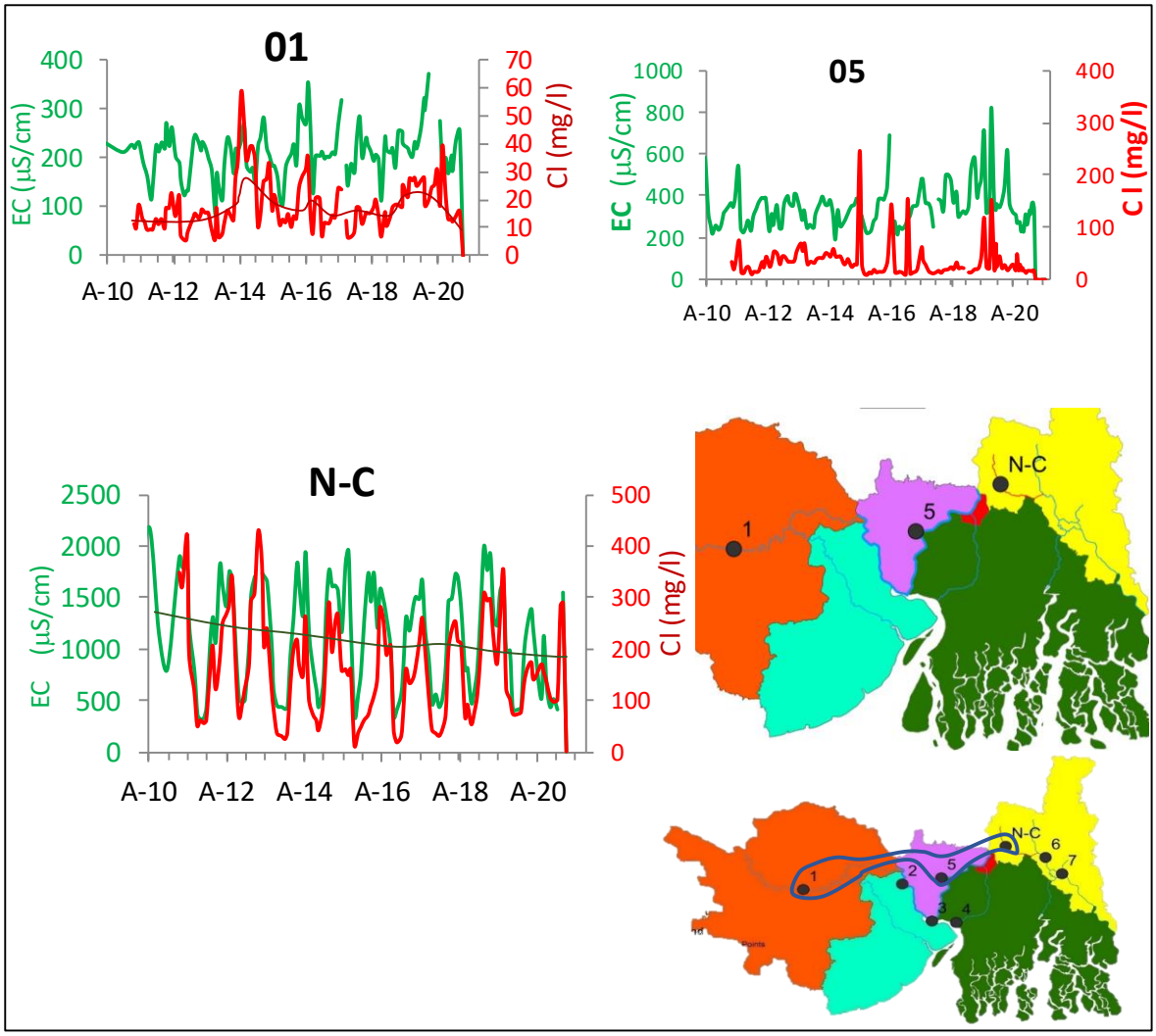

Figure 41: Variation in EC and chloride concentration in river waters (of low salinity) in the study area over the period 2010-2020. X-axis is in years. 'A-10' means April 2010, 'A-20' means April 2020. Location point (02, 03,, 04, 06, and 07) shown in the individual graphs are also marked in the study area figure. Red graph is for the chloride concentration and green for EC.

In order to investigate the marine water fraction in the river channels in the Hooghly estuarine zone, published river water salinity and seawater salinity data is collected (Mitra et al., 2011) and has been interpreted for estimating the seawater fraction in the river channels. For the calculation, seawater salinity (dissolved salts per liter) is assumed as 33g/l The location points of the data is shown in the Fig and the estimated seawater fraction is shown in the Table are graphically shown in the figures 9-12. The data confirms the results of the present study observed for the river water quality at Diamond Harbour.

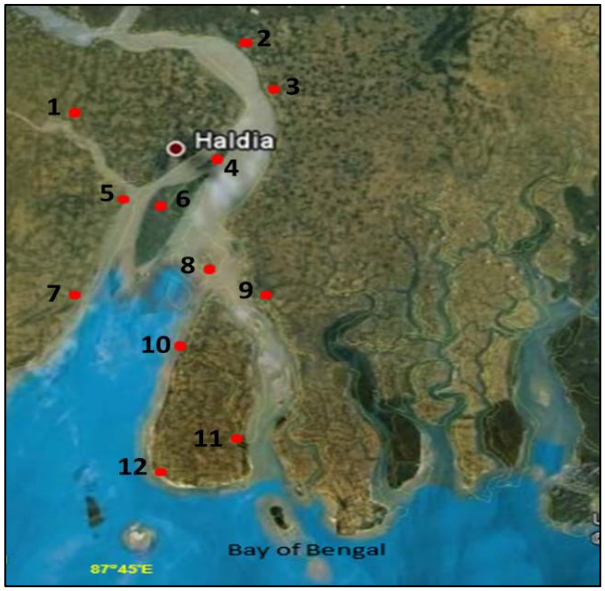

Site No.	Site Name
1	Raichak
2	Diamond Harbour
3	Kulpi
4	Balari
5	Haldi River Mouth
6	Nayachar
7	Khejuri RF
8	Ghoramara
9	Harwood Point
10	Harinbari
11	Chemaguri
12	Sagar South

Figure 42: Surface water sites, and the table for location name for the corresponding site number. The published data from the sites are used for calculating the fraction of seawater in the river channel during high-tide and low-tide (Source for Raw data: Mitra et al., 2011)

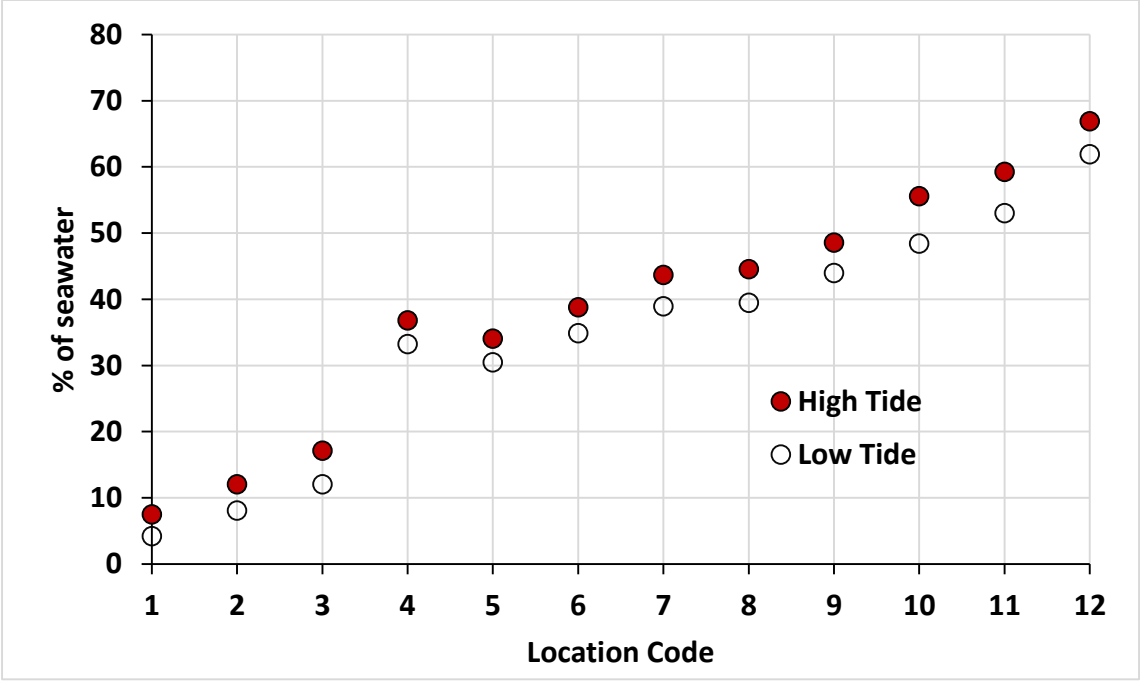

Figure 43: Estimated seawater fraction in the river channel water during high tide and low tide. See Fig for site location corresponding to the location code.

Impact of Tides and Sea-Level Changes on Coastal River Hydrology and Salinity Intrusion

In coastal river systems, tidal waves can induce seawater intrusion into river channels, leading to salinization. The extent and impact of this intrusion are influenced by several factors, including the geometry of the river mouth, local geology, topography, wind patterns, sea-surface temperature, tidal amplitude, and the overall slope of the river channel.

As tidal surges progress upstream, seawater mixes with freshwater in the river channel, forming a saline-freshwater mixing zone. This mixing zone creates a salinity gradient that extends a certain distance inland from the coast and diminishes rapidly beyond the saline-freshwater interface. Beyond this mixing layer, tidal energy can continue to propagate upstream.

The landward penetration of tidal energy creates a "pushing" or backwater effect on freshwater discharge. This effect, driven by the kinetic energy of the tidal surge, can extend beyond the saline-freshwater mixing zone, leading to a slowdown or temporary halt in freshwater outflow.

The distance over which this tidal energy effect is observed depends on factors such as tidal amplitude, resistance to flow within the river channel, and the elevation of the riverbed. Generally, larger tidal amplitudes, lower flow resistance within the channel, and lower topographic slopes allow the tidal energy effect to penetrate further upstream.

In the present study, the tidal impacts on river channels were investigated by identifying tidal marks on toposheets and superimposing them on a Digital Elevation Model (DEM) on a drainage network base map. This process was used to determine the inland extent of tidal influence and its relation to topographic elevation. Daily tidal amplitude data were collected over three years at three different coastal locations; Digha, Canning Town and Haldia. These data were used to create tidal amplitude graphs, which were then analyzed to determine variations in low and high tide levels at these points. The relationship between tidal amplitude and the landward extent of tidal impact was examined. Additionally, historical sea-level records over the past 50 years were analyzed at two locations to investigate long-term sea-level changes.

The map combining DEM, drainage map and the high salinity river channels is shown in the Fig 96. The figure shows that the tidal waves landward travelling distance is confined by the 10m elevation contour and this is far beyond the saline-freshwater interface region. The 10m elevation contour covers entire districts of Howrah, N-24 Parganas, and S-24 Parganas, and East Medinipur. However, much before reaching the 10m elevation, salinity in all the river

channels reach to the minimum background salinity level (freshwater). Therefore, at heights above 10m, groundwater is getting recharged from freshwater channels (and not from saline water). At elevation less than 10m mean sea level, where water channels are saline and the groundwater is getting recharged from the overlying saline river channels, lining of channels may help in creating barrier for avoiding any salinization of fresh groundwater resource.

The map combining the DEM, drainage network, and high salinity river channels (shown in Fig. 96) illustrates that the landward extent of tidal influence is limited by the 10-meter elevation contour. This 10-meter elevation line lies significantly beyond the saline-freshwater mixing zone in the river channels.

The 10-meter elevation contour encompasses the entire districts of Howrah, North 24 Parganas, South 24 Parganas, and East Medinipur. However, well before reaching the 10-meter elevation, the salinity in all the river channels decreases to the minimum background salinity level, indicating a transition to freshwater conditions.

This suggests that at elevations above 10 meters, the groundwater is being recharged by freshwater channels, not saline water. In contrast, at elevations below 10 meters above mean sea level, where the river channels remain saline, the groundwater recharge occurs from these overlying saline channels.

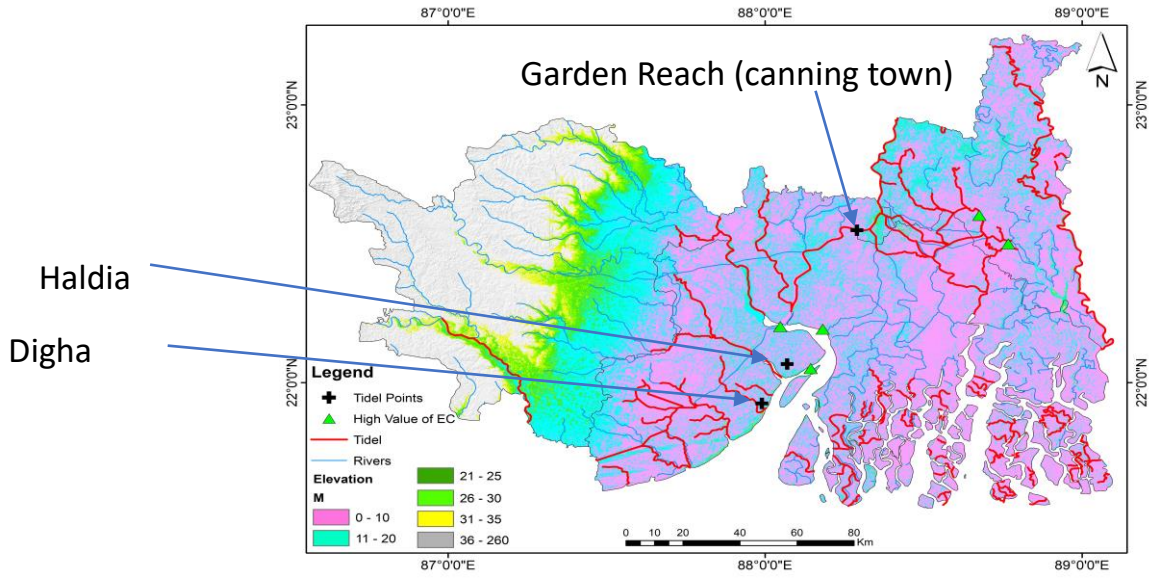

Figure 44: Map showing tidal points, rivers, and elevation with high values of electrical conductivity (EC)

In areas where the groundwater is at risk of salinization due to the hydraulic connection with saline river channels, lining the river channels may be a beneficial mitigation measure. Such lining could act as a barrier, preventing the seawater from intruding into the freshwater groundwater resources in the low-lying coastal regions. Similarly, by installing barrier gates on the surface channels near the interface region, contamination of freshwater from the surge of saline water can be prevented, and discharge of freshwater can also be regulated.

Tides bring seawater inland through tidal creeks and streams, leading to the salinization of groundwater through stream-aquifer interaction. Daily tidal data was collected from three sites: Digha, Canning Town, and Haldia. Analysis of the tidal data shows that the tidal waves fluctuate within a range of ±2.5 meters relative to the average sea level. The tidal pattern is diurnal, with tides occurring twice within 24 hours, and it follows the cycle of the lunar phases.

It is noteworthy that although Canning Port is approximately 38 km from the open sea, the tidal amplitude at Canning is the same as that at Digha, which is located on the coastline. During the monsoon season, the tidal amplitudes are 1.46 meters for low tide and 5.45 meters for high tide. In contrast, during the summer, the amplitudes are 1.99 meters for low tide and 3.8 meters for high tide. The tidal surge carries seawater through the Hooghly River, bringing saline water as far as Kolkata. Beyond Geonkhali, where the Hooghly River branches, the saline water surge enters the Roopnarayan River and extends up to Kolaghat.

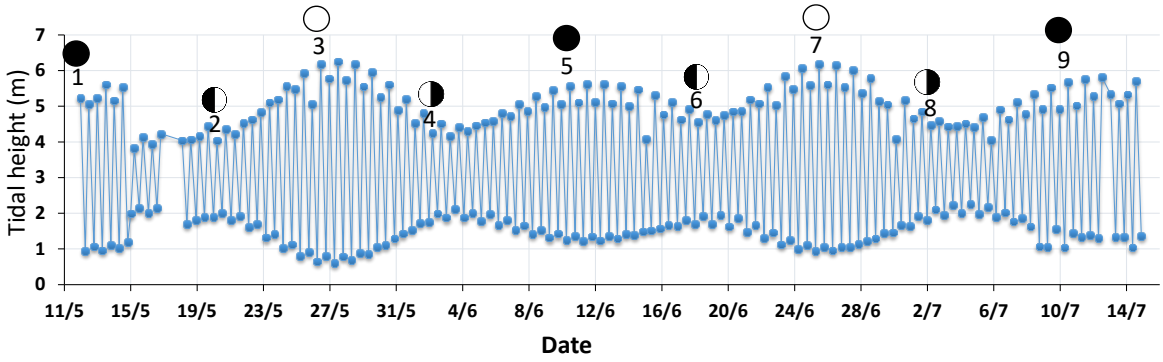

New Moon		First Quarter		Full Moon		Third Quarter	
1) 12/5	11:56	2) 20/5	06:05	3) 26/5	23:55	4) 2/6	6:05
5) 10/6	11:26	6) 18/6	09:24	7) 25/6	00:10	8) 2/7	05:40
9) 10/7	11:52						

Figure 45: Tidal amplitude at Halida port during May-July, 2021. Also shown in the graph the moon's phases to interrelate with moons' phases. The dates of moon's phases are detailed in the table.

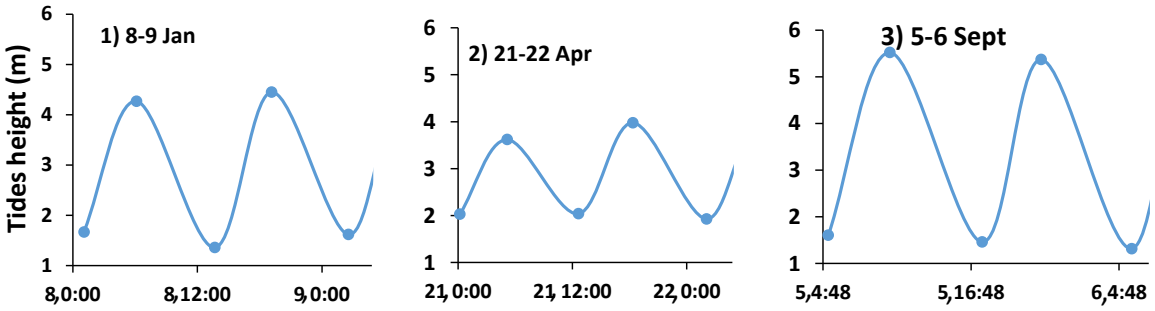

Figure 46: Seasonal variation in semi-diurnal tides at Haldia, during 2021. Tidal variation graphs show 2 high tides and 2 low tides of approximately equal magnitudes in 24 hours characterizing the semidiurnal type of tides in the region. The period of semidiurnal tides are shown for the periods 8th Jan to 9th Jan; 21st Apr to 22nd Apr, and for 5th Sept to 6th Sept.

Mean sea level data from the Bay of Bengal was collected at four sites: Haldia, Garden Reach, Sagar, and Hiron (Bangladesh). The annual sea level changes at Haldia from 1915 to 2021, downloaded from the PMSL (Permanent Service for Mean Sea Level) site are depicted in **Figure 47**. A comparison of sea level changes at these four sites, along with global sea level data from 1970 to 2021, is presented in **Figure 48**. **Figure 49** shows that the data trend for Garden Reach deviates from the other sites and also from the global data. **Figure 49**b, the data has been re-drawn, excluding the Garden Reach data. The sea level data from Haldia, Sagar, and Hiron demonstrate good internal consistency and align well with the global data. The rate of sea level rise at Haldia is 2.7 mm/year, which closely matches the global sea level rise rate of 2.8 ± 0.8 mm/year observed from in-situ data (Hauer et al., 2020). With rising sea levels, seawater is expected to penetrate further inland through tidal channels and could potentially submerge low-lying coastal areas, such as the Sundarbans and other low-lying islands, permanently. Additionally, there is an increased risk of coastal inundation and forced displacement of coastal communities.

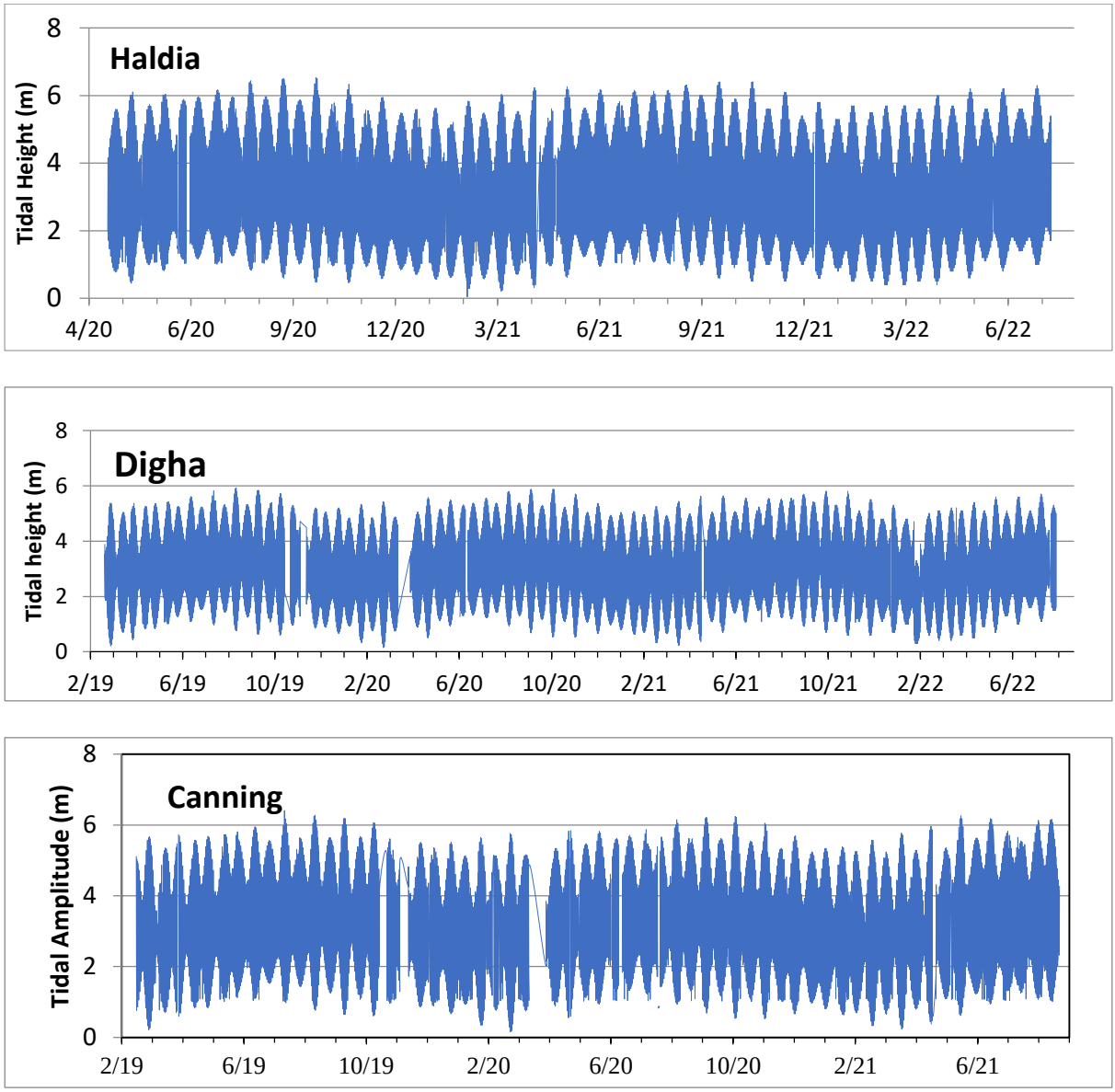

Figure 47: Variation of daily tidal amplitude at Haldia, Digha and Caaning ports during 2019-2022. Blanks indicate missing data. Approximate areal distance of sites from open sea: (i) Haldia:38km, (ii) Digha: 0km (iii) Canning :38km

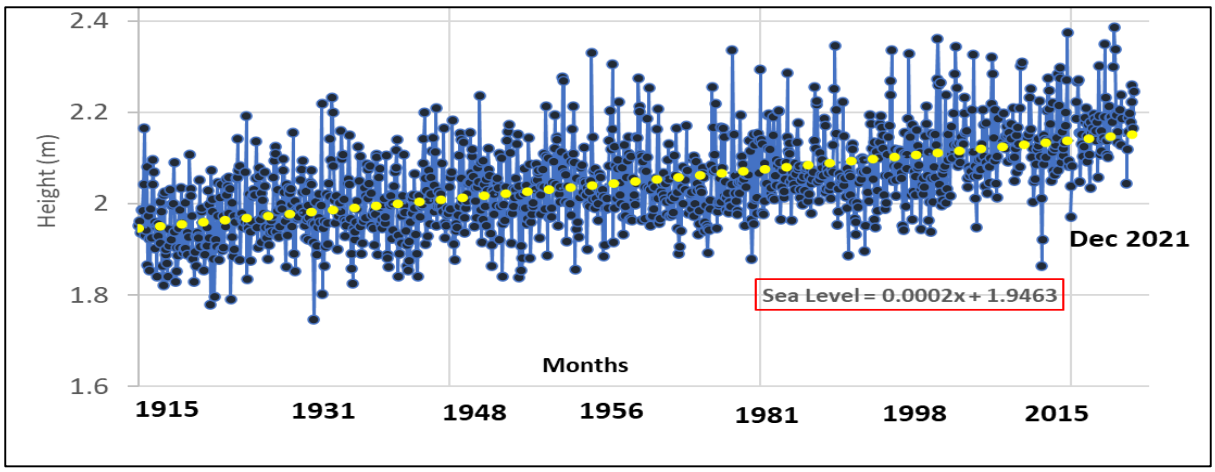

Figure 48: Time spectrum of sea level change at Haldia during Jan 2015 to Dec 2021

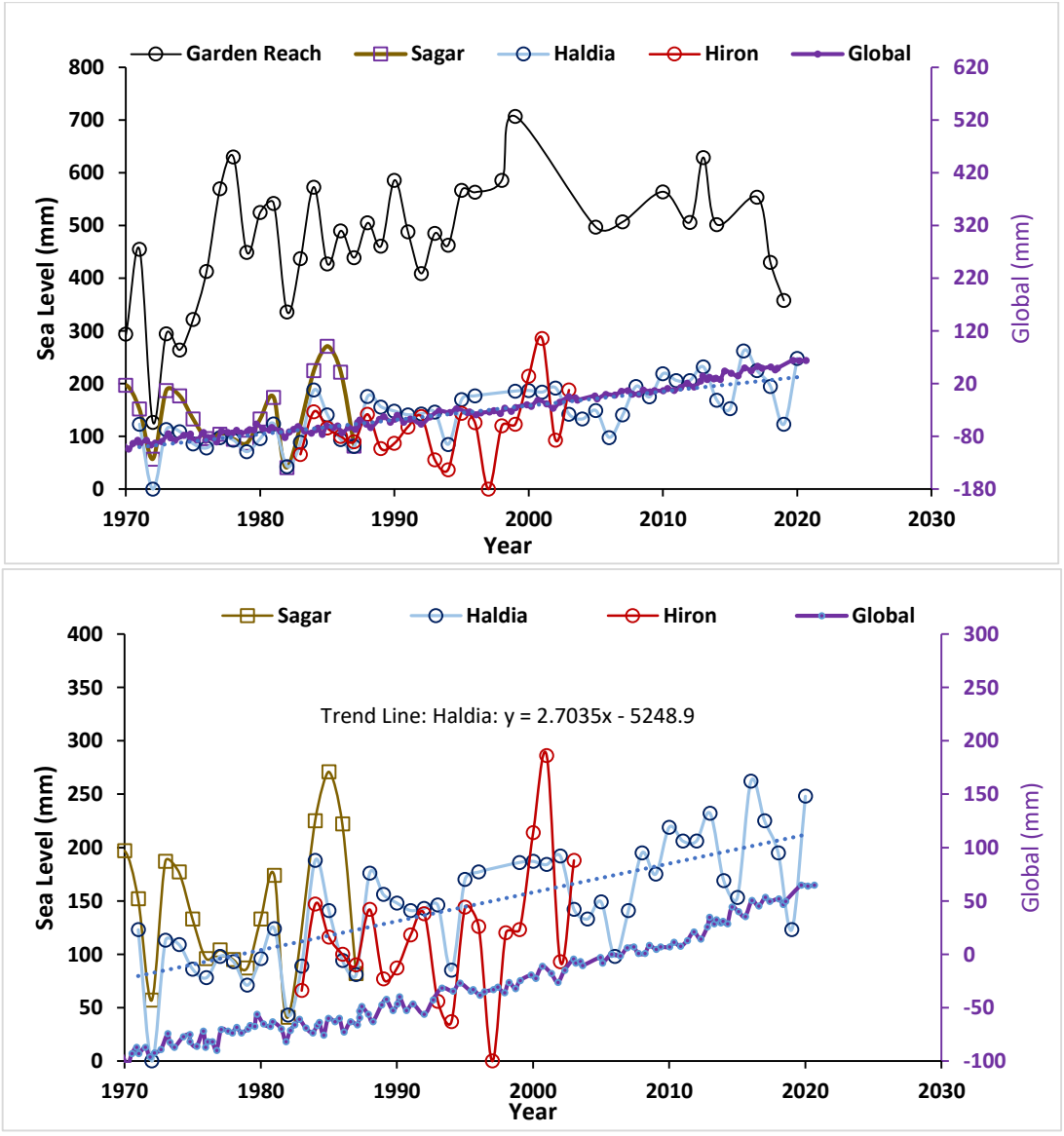

Figure 49. Change of sea level observed in Bay of Bengal at sites Sagar, Haldia, Hiron (Bangladesh). For comparison, the mean global sea level trend is also shown

4.5.2 Ground Water Quality

4.5.2.1 Sub-division of the study area- Coastal West Bengal

The study area, located within the West Bengal coastal zone, exhibits a diverse range of topography, geomorphology, and groundwater salinity. Given its coastal location, groundwater salinity is a critical parameter to consider. Accordingly, the data was segregated and mapped based on electrical conductivity and spatial distribution (**Figure 50**). The map identifies five distinct regions: (i) 60–750 µS/cm (freshwater), (ii) 750–1450 µS/cm (fresh to mildly saline), (iii) 1450–5000 µS/cm (brackish), (iv) 5000–6500 µS/cm (saline), and (v) 1450–3000 µS/cm (brackish groundwater near the island zone). Additionally, a broad variation in major ion concentrations (meq/liter) within each of these five units was analyzed using a Box and Whisker plot (Fig. 51).

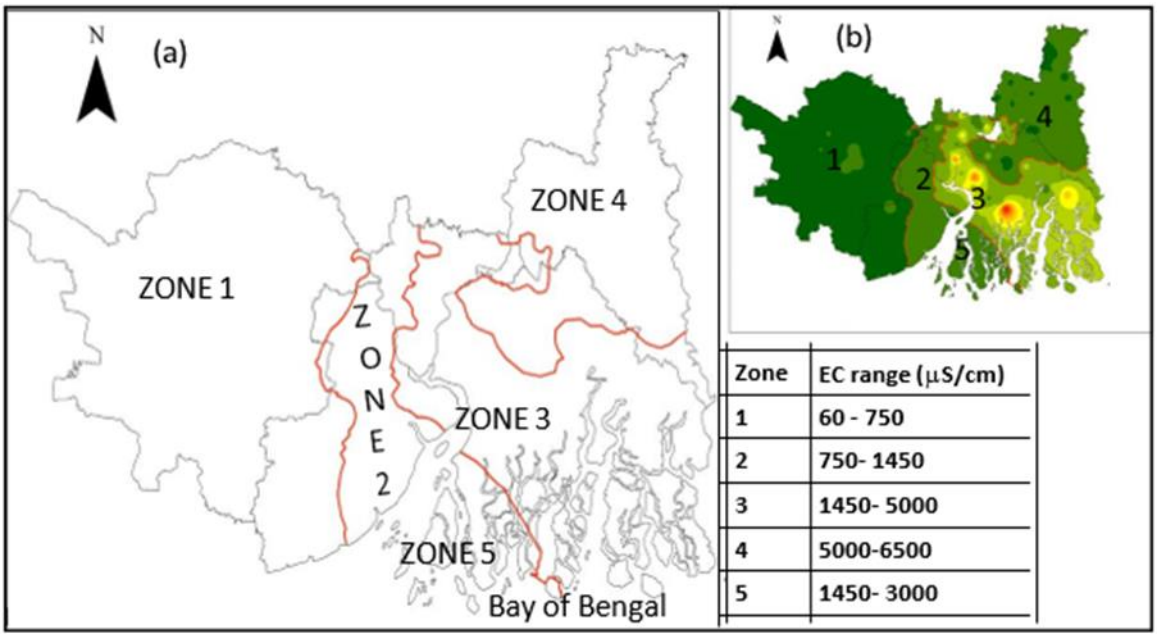

Figure 50: Sub-divisions of the study area in the coastal zone, West Bengal (Source: NIH, 2023)

The Box and Whisker plots and the Table 51 reveals the following insights about the major ion concentrations in the groundwater of the coastal zone:

I. The highest ionic concentrations (in meq/L) are observed in Zone 3, while Zone 1 has the lowest overall ionic concentrations.

II. Sulfate (SO_4) shows the lowest concentration across the entire study area, indicating a limited influence of sulfate-bearing minerals in the groundwater system.

III. Calcium (Ca) concentration is relatively low in Zones 2, 3, 4, and 5 compared to Zone 1, suggesting a lower influence of calcium-bearing minerals in these zones.

IV. Sodium plus potassium (Na+K) and bicarbonate (HCO3) concentrations are highest in Zone 2, indicating a hydrochemical environment dominated by rock weathering processes controlled by (Na+K) interactions such as feldspars and micas, as well as the dissolution of carbonate minerals.

V. The median statistics for Zone 1 suggest almost equal concentrations of calcium (Ca), magnesium (Mg), and sodium plus potassium (Na+K), pointing to dolomite and alkaline rock weathering as the dominant hydrogeochemical processes.

VI. In Zones 4 and 5, the median statistics reveal nearly equal concentrations of sodium plus potassium (Na+K) and magnesium (Mg), suggesting a potential influence of magnesium-bearing minerals in these zones.

4.5.2.2 Box Plot of West Bengal

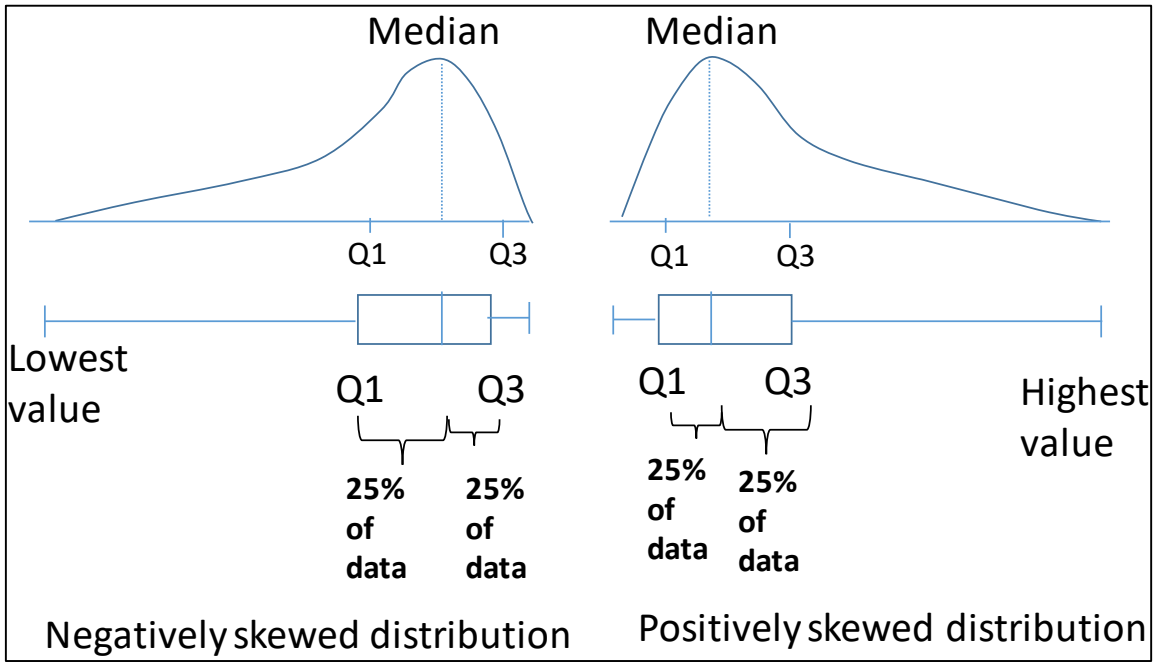

Figure 51: Statistical summary of water quality data across five zones using Box and Whisker plots, with an illustration for interpreting the plot.

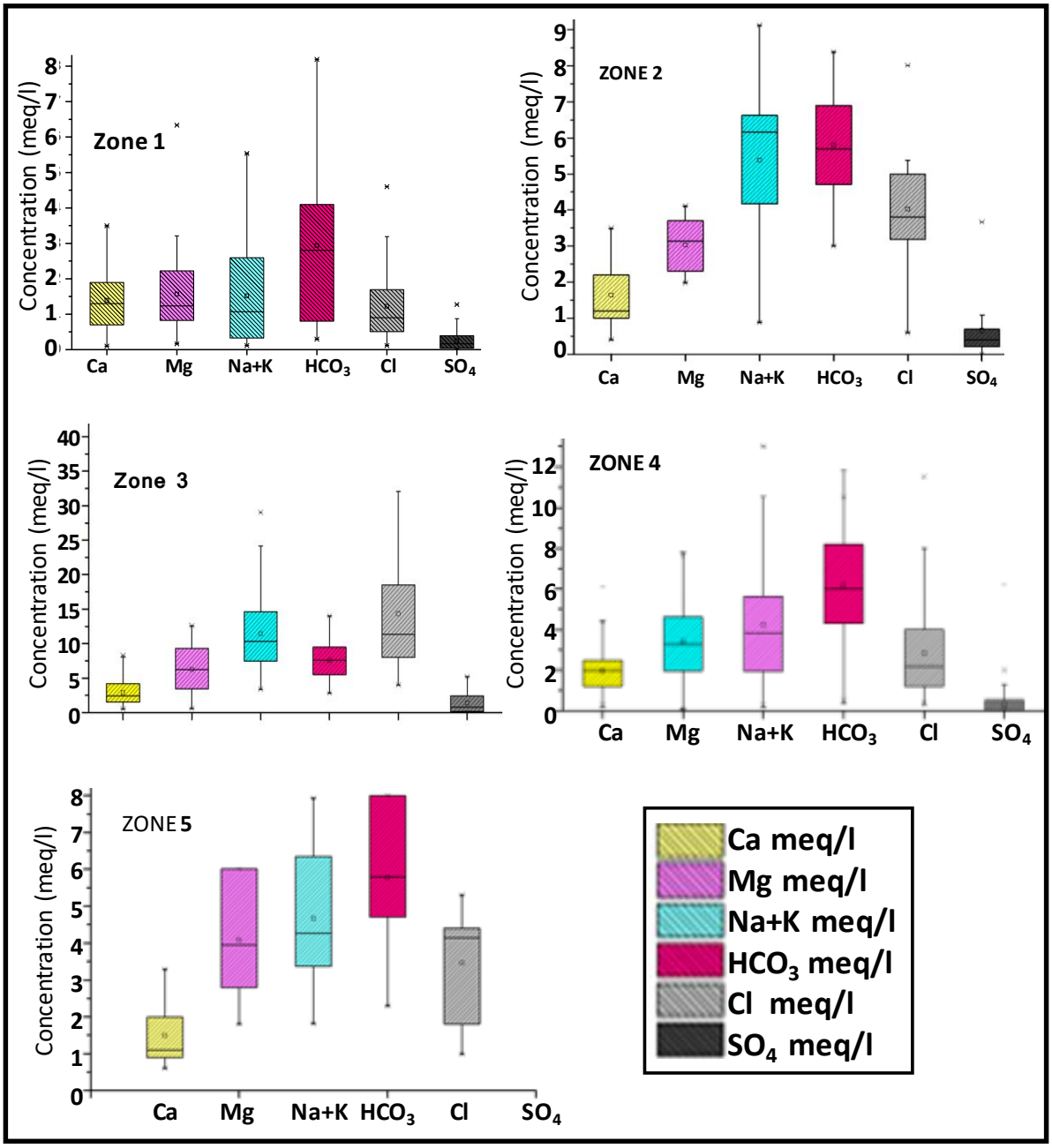

Figure 52: Box & Whisker plot of groundwater water quality

Table 21: Statistical summary of water quality data. Green highlights indicate minimum values, and pink highlights indicate maximum values in the series.

Zone	Parameters	EC	pH	Ca	Mg	Na	K	HCO_3	Cl	SO_4	Ca	Mg	Na+K	HCO_3	Cl	SO_4	TH
		(µS/cm)		(mg/l)				(mg/l)			(meq/l)			(meq/l)			(mg/l)
Zone 1 (n=169)	Average	429.0	7.4	28.0	19.0	31.3	6.0	179.2	43.5	12.2	1.4	1.6	1.5	2.9	1.2	0.2	148.1
	1st Quartile	242.0	7.3	14.0	10.0	7.0	1.0	49.0	18.0	2.0	0.7	0.8	0.3	0.8	0.5	0.0	96.1
	Median	467.0	7.4	26.0	15.0	23.0	1.0	171.0	32.0	8.5	1.3	1.2	1.1	2.8	0.9	0.2	145.2
	3rd Quartile	603.0	7.5	38.0	27.0	51.0	3.0	250.0	60.0	19.0	1.9	2.2	2.6	4.1	1.7	0.4	200.7
	Std Deviation	228.0	0.2	17.0	15.2	28.4	16.9	126.6	32.4	12.9	0.8	1.2	1.4	2.1	0.9	0.3	82.8
Zone 2 (n=12)	Average	1050.3	7.6	34.0	37.9	116.9	7.7	360.0	147.8	34.5	1.7	3.1	5.3	5.9	4.2	0.7	240.4
	1st Quartile	849.0	7.5	21.5	28.0	85.8	3.0	287.0	119.0	10.0	1.1	2.3	4.0	4.7	3.4	0.2	176.1
	Median	1018.5	7.5	25.0	39.0	135.5	3.5	351.0	147.5	21.0	1.2	3.2	6.0	5.8	4.2	0.4	219.3
	3rd Quartile	1222.0	7.7	46.5	45.3	150.3	4.3	433.3	178.8	36.5	2.3	3.7	6.7	7.1	5.0	0.8	297.9
	Std Deviation	227.0	0.4	18.7	9.2	55.5	10.3	106.5	64.8	47.5	0.9	0.8	2.4	1.7	1.8	1.0	75.8
Zone 3 (n=43)	Average	2475.7	7.5	57.8	76.0	247.7	25.4	461.5	508.0	66.2	2.9	6.3	11.4	7.6	14.3	1.4	457.4
	1st Quartile	1663.0	7.1	30.0	43.0	151.5	5.0	351.0	284.0	9.5	1.5	3.5	7.5	5.8	8.0	0.2	320.2
	Median	2028.0	7.5	48.0	76.0	227.0	11.0	464.0	401.0	38.0	2.4	6.3	10.3	7.6	11.3	0.8	448.9
	3rd Quartile	2796.0	7.8	84.0	103.0	319.5	30.0	576.5	656.0	110.5	4.2	8.5	14.6	9.4	18.5	2.3	568.6
	Std Deviation	1187.2	0.5	37.2	41.3	134.5	31.5	157.7	348.3	64.1	1.9	3.4	0.5	37.2	41.3	134.5	199.5
Zone 4 (n=115)	Average	902.5	7.6	39.5	41.5	92.2	9.6	376.5	101.1	14.7	2.0	3.4	4.3	6.2	2.9	0.3	269.5
	1st Quartile	739.0	7.2	25.0	24.5	41.0	3.0	265.0	43.0	0.0	1.2	2.0	1.9	4.3	1.2	0.0	201.7
	Median	845.0	7.5	40.0	40.0	85.0	4.0	366.0	78.0	1.0	2.0	3.3	3.8	6.0	2.2	0.0	277.9
	3rd Quartile	1014.5	7.9	49.0	55.5	117.5	6.0	494.0	140.0	23.5	2.4	4.6	5.6	8.1	3.9	0.5	330.8
	Std Deviation	318.6	0.5	19.3	21.2	64.2	16.2	136.4	87.0	33.4	1.0	1.7	2.8	2.2	2.5	0.7	99.9
Zone 5 (n=6)	Average	949.0	7.6	30.0	49.7	103.7	6.2	351.8	122.8	0.2	1.5	4.1	4.7	5.8	3.5	0.0	279.4
	1st Quartile	811.5	7.2	18.5	35.8	74.8	3.3	302.3	84.3	0.0	0.9	2.9	3.6	5.0	2.4	0.0	184.7
	Median	849.5	7.6	22.0	48.0	95.5	4.5	354.0	147.0	0.0	1.1	3.9	4.3	5.8	4.1	0.0	289.7
	3rd Quartile	1085.5	7.8	36.0	68.5	131.3	5.8	456.0	154.3	0.0	1.8	5.6	5.8	7.5	4.4	0.0	381.1
	Std Deviation	216.2	0.6	20.0	21.0	50.7	5.0	131.3	59.5	0.4	1.0	1.7	2.2	2.2	1.7	0.0	116.2

4.5.2.3 Parsons Plot of West Bengal

The Parson's plot for groundwater in the West Bengal coastal zone without any difference distinction between the zones, indicates 35% of the data points fall within the Na-Cl zone and 65% in the Ca-Mg-Cl zone.

Na-Cl zone: The points in this zone indicate a dominance of Na and Cl, suggesting the potential influence of seawater intrusion or the presence of chloride-rich minerals in the aquifer. The points distributed along the y-axis [along [Na/(Ca+Mg)] show that larger data points with low Na concentrations could be due to the reverse ion exchange process replacing Na by Ca and Mg ions.Na by Ca and Mg ions.

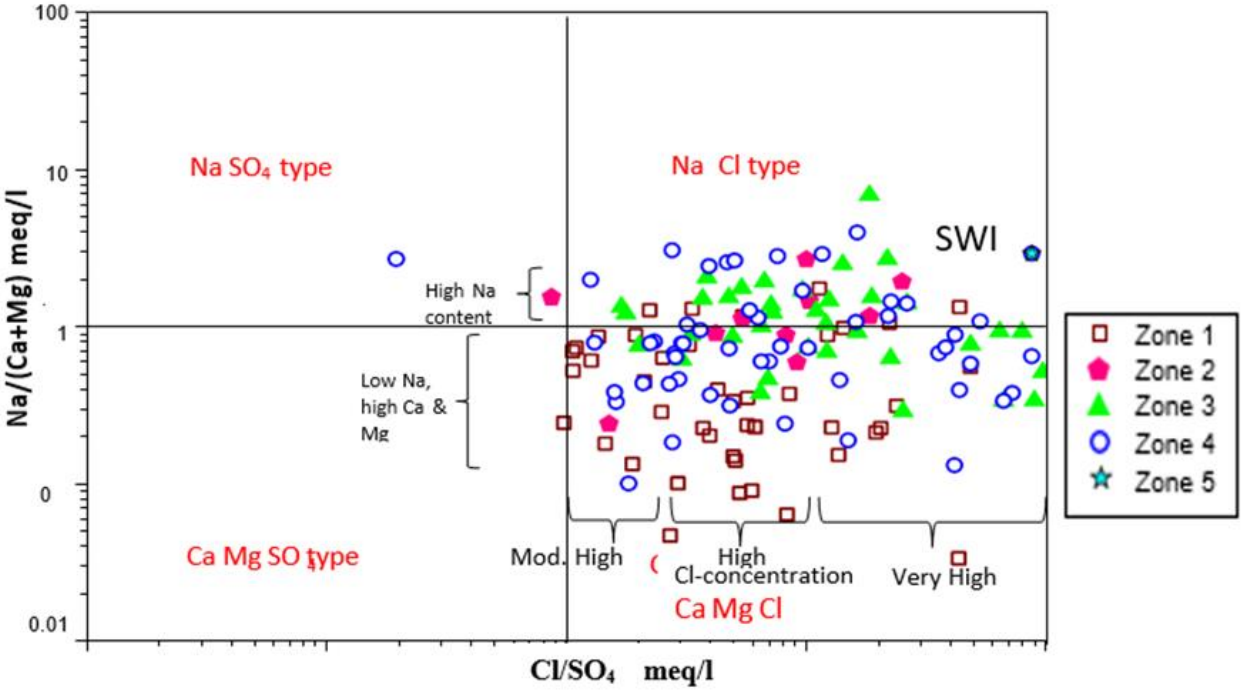

Figure 53: Water type classification using Parsons Diagram for West Bengal Region

Similarly, the distribution of data points along the X-axis (Cl/SO4 ratio) indicates a large number of data points with high to very high chloride ion concentrations relative to sulfate ions in the groundwater. This may be attributed to the presence of chloride-rich minerals or seawater intrusion. Thus, the Parsons plot shows the dominance of Ca-Mg-Cl and Na-Cl types of water, the influence of rock-water interactions, seawater intrusion, and reverse ion exchange processes. However, comprehensive investigations are necessary to fully understand the hydrochemical evolution and sources of the observed groundwater composition.

4.5.2.4 TDS vs TH plot of West Bengal

The interpretation of the TH-TDS plot for the coastal zone of West Bengal shown in the Fig.15 provides insights into the groundwater quality and mineral content in the area.

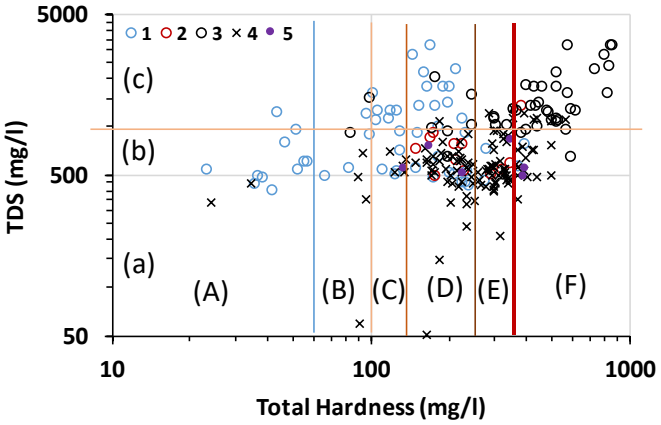

TH	Hardness	TDS	Water type
(A) <50	Soft	(a) <500	Drinking water
(B) 50-100	Moderately soft	(b) <1000	Fresh water
(C) 100-150	Slightly Hard	(c) 1000- 5000	Mildly Brackish water
(D) 150-250	Moderately Hard	5000-15,000	Moderately brackish water
(E) 250-350	Hard	15,000-35,000	Heavily brackish water
(F) >350	Excessively Hard	>35,000	Seawater

Figure 54: Groundwater classification based on Total Dissolved Solids (TDS) and Total Hardness (TH). Numerals 1, 2, 3, and 4 indicate different groundwater sampling zones. Panels (a), (b), and (c) show water classification units according to TDS, while panels (A), (B), (C), (D), (E), and (F) show water classification units according to Total Hardness. In the study area, all TDS values are below 5000 mg/L; thus, class values exceeding 5000 mg/L are shown in gray text in the table.

The plot reveals that approximately 65% of the samples had a TDS (Total Dissolved Solids) value below 1000 mg/l, indicating relatively low mineral content in the groundwater. This suggests that the majority of the samples have a lower concentration of dissolved solids.

35% of the samples fell within the TDS range of 1000-4500 mg/l, indicating a higher concentration of dissolved solids that is elevated mineral content and thereby affecting the groundwater taste and its quality.

Among the samples with TH, approximately 8% are soft, 4% moderately soft, 10% slightly hard, 32% moderately hard, 15% hard and 31%. As per the sample data distribution, 50% of groundwater of West Medinipur are soft to moderately soft fresh drinking water type whereas, 50% groundwater samples of South 24 Parganas are excessively hard and mild-brackish type. The Total Hardness is primarily influenced by the presence of divalent cations such as calcium

and magnesium in the water. The significant presence of these divalent cations contributes to the hardness of the water, which can have implications for its suitability for various uses, such as domestic consumption and industrial processes.

Furthermore, Pearson's plot provides additional information about the hydrochemical composition of the groundwater in the study area. The plot indicates that the groundwater is categorized as Ca-Mg-Cl type water, which signifies the influence of calcium, magnesium, and chloride ions in the water chemistry. This observation aligns with the presence of elevated hardness in the groundwater due to the abundance of calcium and magnesium.

4.5.2.5 Gibbs Plot of West Bengal.

The Gibbs diagram broadly classifies groundwater hydrochemistry based on TDS (Total Dissolved Solids) as follows: TDS < 100 mg/L indicates a precipitation-dominated origin, 100 mg/L to 1000 mg/L is typically due to rock-water interaction, and TDS levels above 1000 mg/L suggest (TDS in excess of rock-water interaction as due to) evaporation-driven enrichment. In the present study, 70% of the groundwater samples show TDS primarily arising from rock-water interactions, while the remaining 30% of samples indicate TDS enrichment due to evaporation. Specifically, 20% of groundwater samples in Zone 1 and 60% in Zone 3 exhibit evaporation-dominated processes.

According to the concentration ratios [$Cl/(Cl + HCO_3)$] and [$(Na + K)/(Na + K + Ca)$], 60% of groundwater samples have higher carbonate (HCO_3) concentrations than chloride (Cl), indicating that the water chemistry is influenced by the dissolution of carbonate minerals. Similarly, in 60% of the samples, the (Na + K) concentration exceeds (Na + K + Ca), suggesting that the chemistry is predominantly controlled by the dissolution of sodium (or Na + K) minerals. This implies that 60% of the groundwater chemistry is governed by the dissolution of sodium (or Na + K) bicarbonate type of minerals.

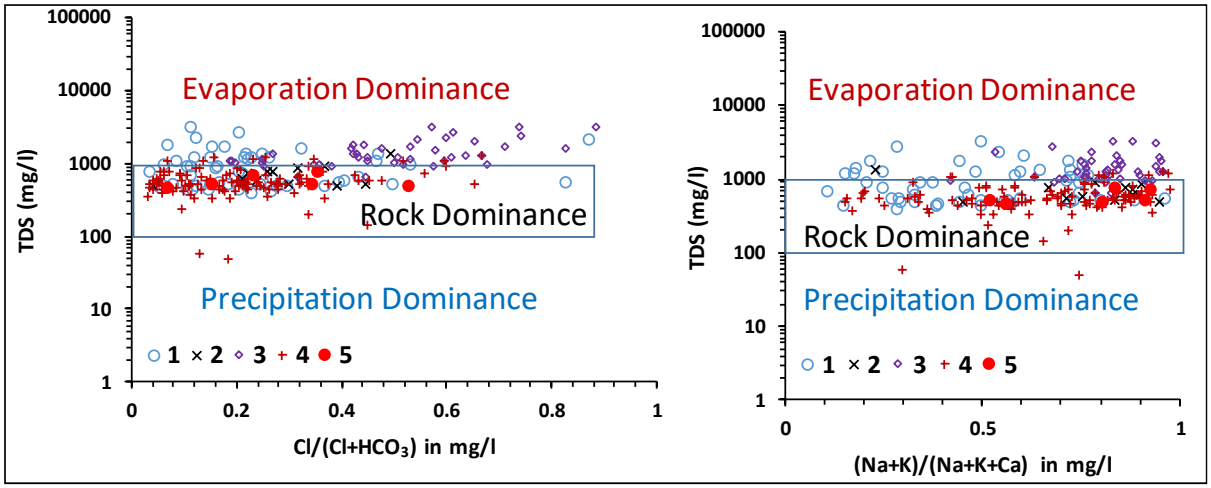

Figure 55: Interpretation of TDS in groundwater using Gibbs plot

4.5.2.6 Piper Diagram of West Bengal

The Piper diagram for the West Bengal samples is shown in Fig.23. From the figure, the following observations can be drawn:

In the cation triangle of the Piper Diagram, the data reveals that 60% of the groundwater composition is attributed to the dissolution of minerals rich in sodium and potassium, such as albite and orthoclase. These minerals contribute to the elevated levels of sodium and potassium ions observed in the groundwater. Additionally, 15% of the data points indicate the influence of magnesium-rich minerals, such as dolomite or magnesite, suggesting the dissolution of these minerals and the release of magnesium ions into the groundwater. The remaining data points in the cation triangle represent a mixed type, indicating the involvement of diverse sources and hydrogeochemical processes.

Turning to the anion triangle of the Piper Diagram, the majority of the data, accounting for 90%, indicates the dominant role of carbonate mineral dissolution. This suggests the dissolution of carbonate minerals, such as calcite or dolomite, releasing carbonate ions and contributing to the bicarbonate-type water chemistry. Furthermore, 5% of the data points represent the chloride type, implying the presence of chloride-rich minerals or sources, potentially arising from the dissolution of minerals like halite or sylvite. The remaining data points in the anion triangle reflect a mixed type, indicating the involvement of various anionic species and their sources.

Within the diamond zone of the Piper Diagram, 65% of the data points are associated with magnesium bicarbonate-type water chemistry. This type can be attributed to the dissolution

of minerals like dolomite, which contains both magnesium and carbonate ions. The 10% contribution of calcium bicarbonate-type water chemistry suggests the dissolution of minerals rich in calcium and carbonate, such as calcite. These minerals contribute to the presence of calcium and bicarbonate ions in the groundwater. The remaining data points in the diamond zone are indicative of diverse sources and hydrogeochemical processes.

The observed discrepancies between the cation triangle and the diamond zone in terms of magnesium dissolution can be explained by the complex interplay of mineral dissolution, precipitation, reverse ion exchange, and ion exchange processes. While the cation triangle suggests a significant contribution from sodium and potassium-type minerals, the diamond zone reveals a higher proportion of magnesium bicarbonate type water chemistry, indicating the dissolution of magnesium-rich minerals like dolomite. These variations may arise from variations in aquifer mineralogy, hydrological conditions, and the interaction between groundwater and different rock formations.

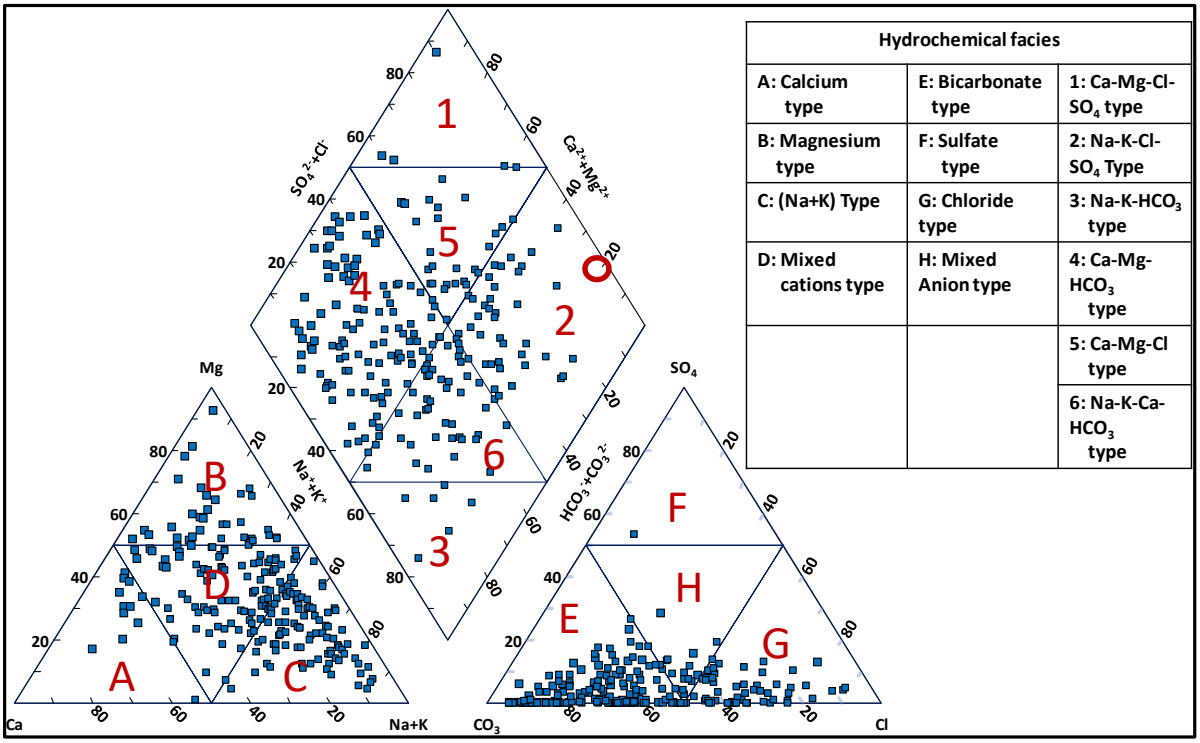

Figure 56: Piper diagram of groundwater in the study area, showing hydrochemical classifications (HFC) based on cation-anion ternary diagrams (A to D for cations, E to H for anions) and the HFCs within the central diamond shape (1 to 6). The attached table provides details of these HFCs. The red circle in Zone 2 marks the HFC for global average seawater.

Overall, the Piper Diagram provides valuable insights into the hydro geochemistry of the study area, highlighting the types of mineral dissolution (such as albite, orthoclase, dolomite, and calcite) and the ion-exchange processes. Additionally, the presence of diverse sources and hydro geochemical processes further underscores the complexity of the groundwater system in West Bengal.

The spatial distribution of molar fraction and the spatial distribution of the Diamond zones of the Piper Diagram provide the following details of the study area:

Spatial Distribution of the Molar Fraction:

A.) Eastern and Western Howrah Districts:

Na^+-type groundwater: The groundwater in these districts, excluding the southwestern part of South 24 Parganas district, the upper half of East Medinipur district, and the eastern half of West Medinipur district, shows a molar fraction range of Na+ distribution from 0.65 to 0.8. This indicates a relatively high concentration of sodium in the groundwater samples from these districts.

B.) South 24 Parganas District:

Bicarbonate-type groundwater: The majority of the study area, about 80%, is covered with bicarbonate type water. Specifically, in the southern part of South 24 Parganas district (forming the coastal boundary line), the molar fraction of bicarbonate type water exceeds 0.78, indicating a significant prevalence of carbonate mineral dissolution in the groundwater.

Chloride signatures: The eastern half of the district shows chloride signatures greater than 0.66, suggesting the presence of chloride-rich minerals or sources.

C.) North 24 Parganas District:

High-Calcium: A small zone confined to the northeastern part of the district exhibits a high molar fraction of calcium (>0.58), indicating the influence of calcium-rich minerals in that area.

Chloride signatures: Approximately 50% of the district shows chloride signatures, implying the presence of chloride-rich minerals or sources.

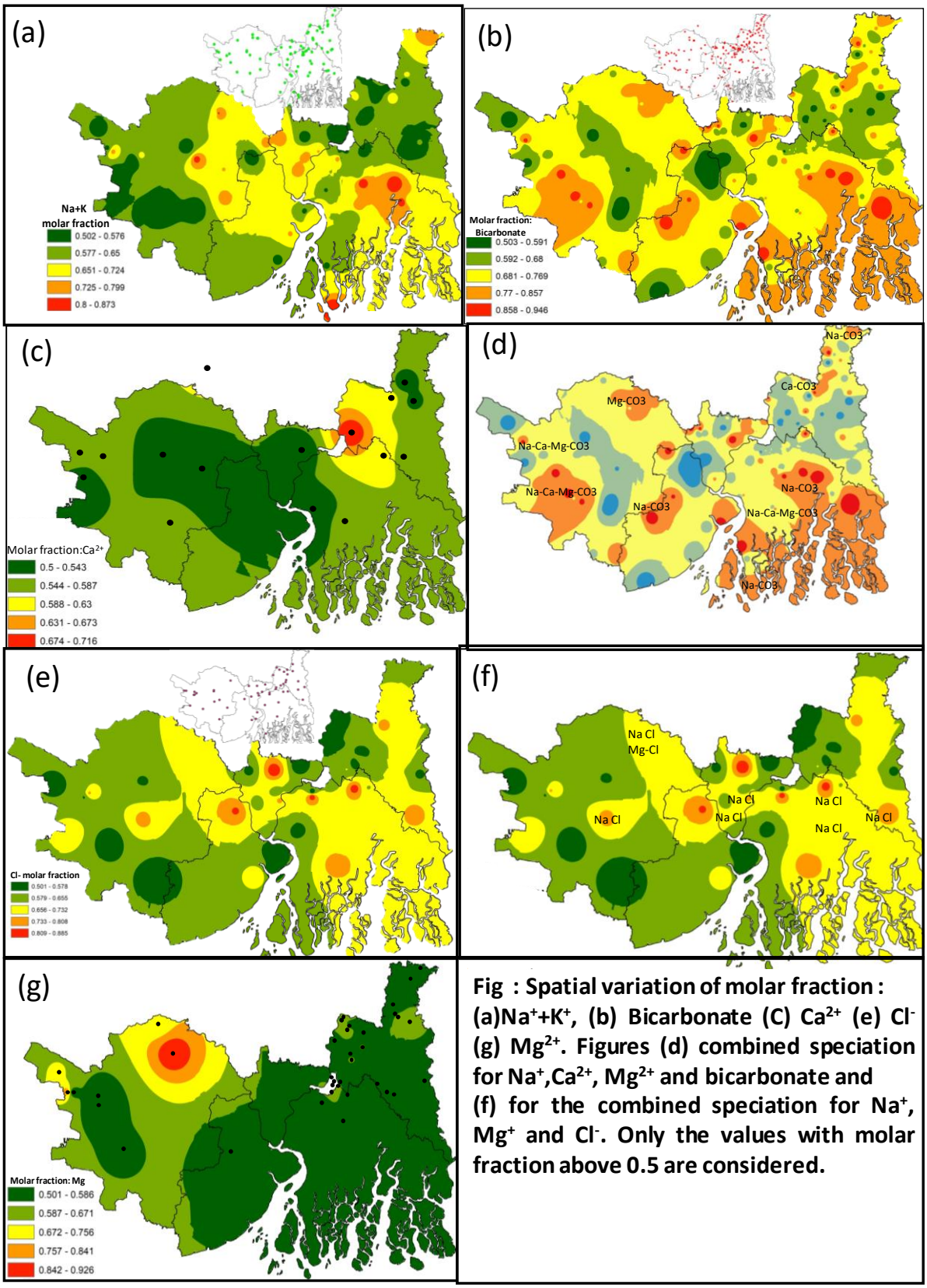

Fig : Spatial variation of molar fraction : (a)Na^++K^+, (b) Bicarbonate (C) Ca^{2+} (e) Cl^- (g) Mg^{2+}. Figures (d) combined speciation for Na^+,Ca^{2+}, Mg^{2+} and bicarbonate and (f) for the combined speciation for Na^+, Mg^+ and Cl^-. Only the values with molar fraction above 0.5 are considered.

Figure 57: Spatial Variation of Molar Fraction and the Spatial Variation of points in Diamond zone of the Piper Diagram.

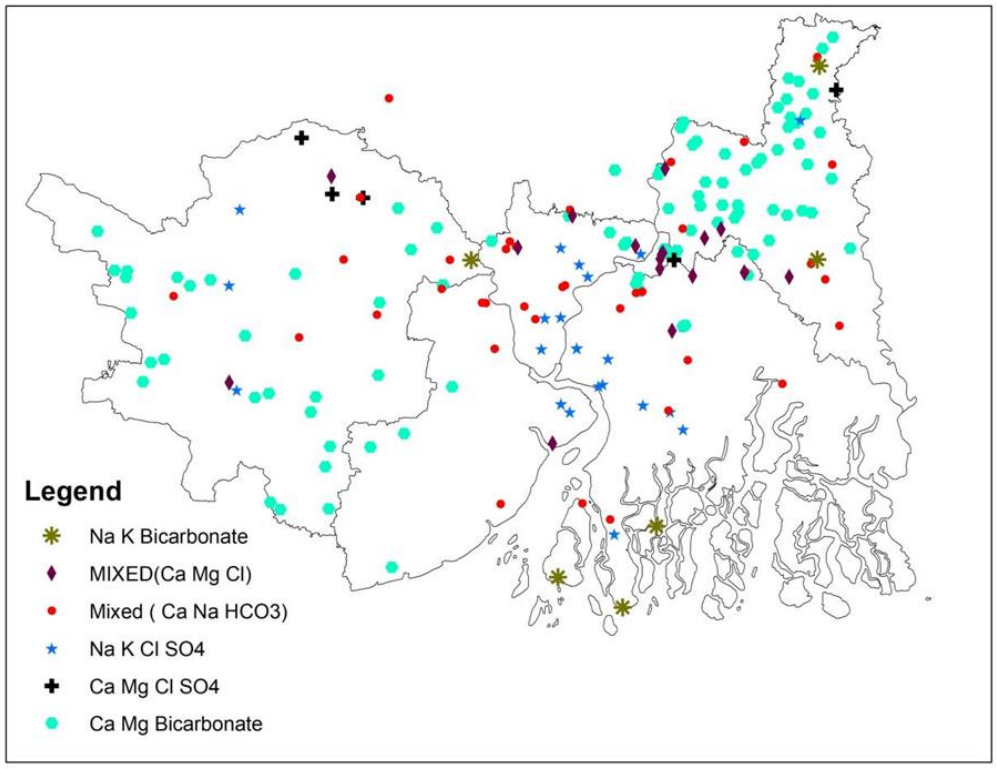

Figure 58: Distribution of Piper Diagram Diamond in West Bengal

D. West Medinipur District:

High-Magnesium: A small zone located in the northern part of the district exhibits high magnesium (molar fraction >0.7), suggesting the influence of magnesium-rich minerals in that area.

Chloride signatures: The central part of the district shows chloride signatures, indicating the presence of chloride-rich minerals or sources.

(2) Spatial Distribution pattern of the points in the Diamond Zones of Piper Diagram:

Overall, the central zone of the study area shows more variations in groundwater types, while the northeastern and western parts predominantly exhibit Ca Mg Bicarbonate type water chemistry. The spatial distribution maps provide valuable insights into the hydrochemical and geochemical characteristics of different districts, highlighting the prevalence of specific ions and water types in each region. District-wise, water types are discussed below:

A) District North 24 Parganas:

Ca Mg Bicarbonate type: About 70% of the district is covered by Ca Mg Bicarbonate type water, indicating the dissolution of minerals rich in calcium and magnesium.

Mixed water: The southern part of the district shows mixed water types, including Ca-Na-HCO_3 type and Ca-Na-HCO_3 type, as well as Na K Bicarbonate type.

B) District South 24 Parganas:

Na-K-Bicarbonate type: Along the southern coastline of the district, groundwater exhibits Na K Bicarbonate type water chemistry.

Na-K-Cl-SO_4 type: In the central area of the district, groundwater is characterized by Na K Cl SO4 type water chemistry.

Mixed water: In the northern parts of the district, there is a mixture of Ca Mg Bicarbonate type water and mixed water types, including Ca Mg Cl and Ca Na HCO3 types.

Haldi River: Along the southern portion of the Haldi River, the water type is Na K Cl SO4 type, and there is also a presence of mixed water (Ca Mg Cl) type.

C) District Howrah:

Na-K-Cl-SO_4 type: Groundwater in the eastern part of the district exhibits Na K Cl SO4 type water chemistry.

Mixed water: The western part of the district shows mixed water type, specifically Ca Na HCO_3 type.

Mixed water: In the northwestern portion of the district, groundwater is characterized by Ca Mg Bicarbonate type water with occasional mixed water (Ca Mg Cl type).

D)West Medinipur District:

Ca Mg Bicarbonate type: In most parts of the district, groundwater is dominated by Ca Mg Bicarbonate type water chemistry, indicating the dissolution of minerals rich in calcium and magnesium.

Mixed water: Occasional locations in the district exhibit mixed water type, specifically Ca Na HCO_3 type.

Ca Mg Cl SO4 type: In the northern part of the district, groundwater shows Ca Mg Cl SO4 type water chemistry, suggesting the presence of dolomite type minerals or rocks.

E) East Medinipur District:

Ca-Mg-Bicarbonate type: Groundwater in the western boundary of the district exhibits Ca Mg Bicarbonate type water chemistry.

Mixed-water: The northern part of the district shows mixed water types, including Ca Na HCO3 type.

Mixed-water and Na-K-Cl-SO_4 type: The eastern part of the district contains mixed waters (Ca Na HCO3, Ca Mg Cl) as well as Na K Cl SO4 type water chemistry.

Ca-Mg-Bicarbonate type: The southern boundary of the district, forming the coastline, exhibits Ca Mg Bicarbonate type water chemistry.

In summary, carbonate mineral dissolution plays a dominant role in the overall water chemistry, TDS and TH of water because, bicarbonate type water observed in most part of the study area.

The presence of Na^+ distribution in certain districts, particularly in the eastern and western parts of Howrah district, suggests potential influence from seawater intrusion. The Na K Cl SO4 type water chemistry observed in various districts, along with the distribution of chloride signatures, further indicates the potential influence of seawater or chloride-rich minerals in the aquifers.

4.5.2.7 Chadha Plot of West Bengal

Data distribution in Chadha diagram shows:

37% data : Ca-HCO3, indicating recharging area water type

11% data: NaHCO3, indicating groundwater undergone base-ion exchange

10.5% data: Na-Cl, indicating sea water contaminated groundwater

6.4% data: Ca-Mg-SO4-Cl type indicating groundwater that has undergone reverse ion exchange

8% data: Na+K type; 8% data : bicarbonate type; 6.8% data : (Ca+Mg) type; and 4.9% data : (Cl+SO4) type water.

This is very similar to that observed from the Piper Diagram

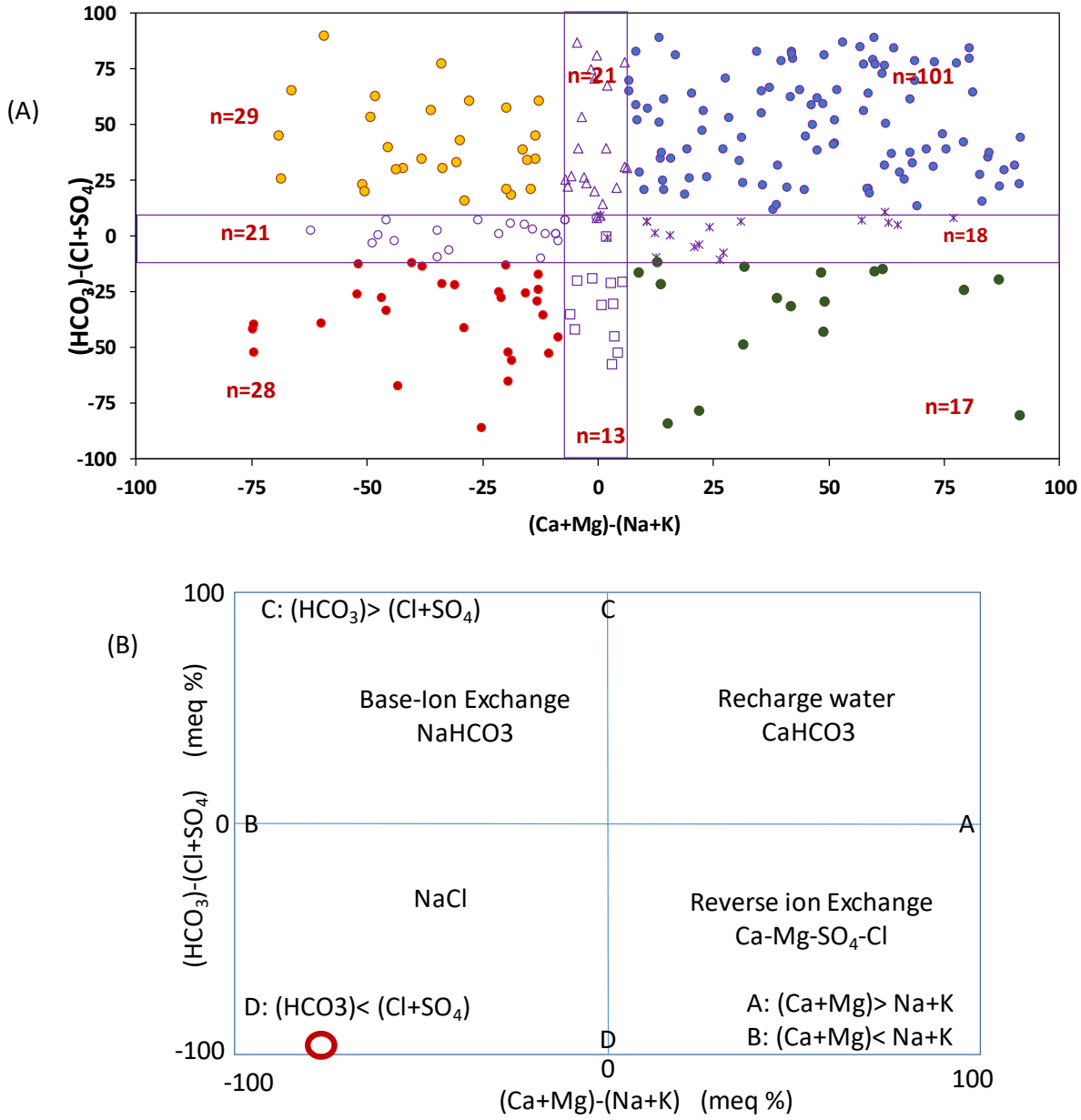

Figure 59: Chadha Diagram. (A) Chadha diagram for groundwater in the study area. (B) Schematic of the Chadha diagram for data interpretation. Red circle indicates average seawater composition.

4.6 Spatial and Depth Dependent Variation in major ion concentration

After rainfall, the quality of infiltrating water changes due to various hydro geochemical reactions from water-rock interactions and anthropogenic effects. Along the coastline, the mixing with seawater in areas affected by seawater intrusion further modifies groundwater quality. Consequently, depending on the geospatial variation of groundwater, its quality falls between the extremes of infiltrating rainwater and seawater.

Table 22: Principal constituents of seawater (at salinity equal to 34.7 psu or parts per thousand (Ref: modified from https://www.britannica.com/science/seawater)

Ionic Constituent	g/kg of seawater	ppm	Concentration in %	meq/l	Ratio in meq/l (R)
Cl	19.162	19162	55.14	540.56	R(Na/Cl) =0.859 R(Ca/Mg)=0.194
Na	10.679	10679	30.73	464.54	
Mg	1.278	1278	3.68	105.17	
SO_4	2.680	2680	7.7	55.80	
Ca	0.4096	409.6	1.18	20.44	
K	0.3953	395.3	1.14	10.11	
HCO_3	0.150	150	0.43	2.46	

Table 23: Principal constituents of rainwater (at salinity equal to 34.7 psu or parts per thousand (Ref: modified from https://www.britannica.com/science/seawater)

Place	Unit	Water quality parameters							
		Cl	**HCO_3**	**SO_4**	**Na**	**K**	**Mg**	**NO3**	**Ca**
Dhaka	ppm % µeq/l	0.67 11.35 18.9		0.6018 10.19 12.53	0.4697 7.95 20.43	0.249 4.21 6.36	0.1159 1.96 9.54	2.5 42.69 40.64	1.2765 21.63 63.7
Tirupati	ppm % µeq/l	1.202 7.7 33.9		6.148 39.40 128.0	0.761 4.87 33.1	1.325 8.49 33.9	0.614 3.93 50.5	2.53 16.21 40.8	3.026 19.39 151.0
Goa	ppm % µeq/l	4.786 44.55 135		1.537 14.308 32.0	2.644 24.61 115.0	0.117 1.1 3.0	0.365 3.39 30.0	0.372 3.46 6	0.922 8.58 46.0
Thumba	ppm % µeq/l	8.083 53.47 228		0.672 4.448 14.0	4.759 31.48 207.0	0.219 1.45 5.6	0.462 3.05 38.0	0 0 0	0.922 6.1 46.0
Colaba	ppm % µeq/l	6.062 32.17 171		2.498 13.26 52.0	4.115 21.84 179.0	0.235 1.25 6.0	0.717 3.80 59.0	2.108 11.19 34	3.106 16.49 155.0
Calcutta	ppm % µeq/l	2.87 14.09 80.96	7.5 36.81 122.9	3.73 18.31 77.66	1.17 5.74 50.89	0.43 2.11 11.0	0.58 2.85 47.73	0.26 1.28 4.19	3.83 18.80 191.12

Table 24: Ionic ratio (Na/Cl) and (Ca/Mg) in rainwater in the units μeq/l (Source: Handa, 1969; Krishnaswami & Singh, 2005; Ullah et al., 2022)

Places	Dhaka	Tirupati	Goa	Thumba	Colaba	Calcutta
Na/Cl	1.08	0.976	0.85	0.91	1.05	0.63
Ca/Mg	6.68	2.99	1.53	1.21	2.6	4.0

Tables 22, 23 and 24 demonstrate significant differences in the hydrochemical quality of seawater and rainwater, both in the absolute concentrations of major ions and in ionic ratios, such as Ca/Mg. These variations make ionic ratios a valuable parameter for identifying seawater intrusion in coastal groundwater systems.

The hydrochemical evolution of groundwater systems in coastal regions is complex, influenced by factors such as hydrochemical reactions in inland recharge areas, anthropogenic contamination, seawater intrusion, coastal climate conditions, and the diverse mineral composition of aquifers within the multi-aquifer system of the coastal zone.

The spatial variation of major ion concentrations and ionic ratios in groundwater at different depths (shallow, intermediate, and deep) offers valuable insights into ionic concentration, hydrogeochemical processes, and the evolution of groundwater quality within this multi-aquifer system. For example, the (Na/Cl) ratio (in meq/l) can indicate the origin of salinity in groundwater—whether it is due to halite dissolution (if the ratio is ~1) or other processes like cation exchange, mineral weathering, or mixing with seawater. Similarly, the (Cl/HCO_3) ratio can help distinguish groundwater influenced by marine sources (higher Cl/HCO_3) from those affected by carbonate rock weathering (lower Cl/HCO_3). The (Ca/Mg) ratio provides information about the relative presence of calcite or dolomite minerals in the aquifer. Additionally, the (SO_4/Cl) ratio can help identify the sources of sulfate in groundwater, such as the oxidation of sulfide minerals, dissolution of evaporites, or seawater intrusion.

The spatial distribution of hydrochemical quality of groundwater at three depths: D1 (<60m), D2 (60m to 200m), and D3 (>200m); is presented in the figures. The extent of groundwater contamination by seawater, as indicated by specific water quality parameters, is summarized in the table. According to the table, no part of the study area exhibits Ca/Mg ratios (in meq/l) that align with those of seawater. For other parameters like EC, Na, and Cl, the shallow groundwater (D1) shows contamination across 5% to 20% of the area, D2 shows contamination in 0% to 5% of the area, and D3 shows contamination in 2% to 5% of the area. Since all seawater characteristics must be met, it can be concluded that 5% of the area at D1 depth is contaminated, 0% at D2, and 2% at D3 by seawater. Since the contaminated area does not show a systematic increase or decrease with depth (with D2 being uncontaminated), it can be inferred that these layers are hydrochemically distinct and likely function as separate aquifers.

Table 25: Percentage of study area contaminated by seawater intrusion (≥3% Contamination) based on groundwater quality analysis

Parameter value	**Area covered at depths (D1, D2, and D3)**			**3% of the characteristic seawater value**
	D1	D2	D3	
EC >1500µS/cm	20%	5%	5%	1500 µS/cm
Na >320 ppm	10%	**Nil**	**2%**	320 ppm
Cl >574 ppm	**5%**	2%	3%	574 ppm
$(Ca/Mg)_{[meq/l]}$=194	0%	0%	0%	For seawater $(Ca/Mg)_{[meq/l]}$=194
Minimum area based on EC, Na and Cl values	5%	0%	2%	

From these figures the following points may also be noted:

i) The concentrations of Na, Cl, Mg, HCO_3, and salinity (EC) are observed to be low in the western parts (West Medinipur district), low to moderate in the northern parts, moderate in the eastern parts, and high in the central parts along the Haldi River.

ii) Regarding the extent of area covered by saline groundwater (EC > 1500 µS/cm), the covered area extent is lowest at middle depths (D2), moderately high at deeper depths (D3), and highest at shallow depths. The spatial distribution of high-salinity (EC > 1500 µS/cm) groundwater pockets at these three depths also does not exactly match. This means that where high-salinity groundwater occurs in the shallow aquifer, it does not appear in the middle aquifer, and where it occurs at middle aquifer, it does not appear at deeper depths. This suggests a probable difference in the mechanisms of salinity concentration at different depths.

iii) The spatial variation of high salinity (EC > 1500 µS/cm) in groundwater shows a strong correlation with pockets of high Na (Na > 251 mg/l) and Cl concentrations (Cl > 251 mg/l) in groundwater, indicating that high salinity (EC) is linked to NaCl concentration. High Mg concentrations (Mg > 50 mg/l) are observed only in the shallow aquifer, predominantly in the central region along the Haldi River.

iv) Bicarbonate (HCO3) concentrations in the shallow aquifer are moderate (250-500 mg/l) over 70% of the study area, with higher concentrations near the central region along the Haldi River. In the middle-depth aquifers, bicarbonate concentration is below 250 mg/l throughout. In deep aquifers, it is marginally above 250 mg/l in 10% of the area, while in the remaining area, it is below 250 mg/l. This further confirms that these aquifers are chemically distinct and have very limited interaction.

v) Excess sodium ions in groundwater may arise from silicate weathering as per the following chemical reaction:

$NaAlSi_3O_8$(Albite) + $2H_2CO_3$ + $9H_2O$ → $Al_2Si_2O_5(OH)_4$(Kaolinite) + $2Na^+$ + $4H_4SiO_4$ + $2HCO_3$

Similarly, the cation exchange process can result in the exchange of Ca^{2+} or Mg^{2+} with Na^+ or K^+ ions, as shown in the following reaction, leading to an increase in Na^+ or K^+ ions in groundwater:

$Ca^{2+}_{(aq)}$ or $Mg^{2+}_{(aq)}$+ 2Na-X or 2K-X → $2Na^+_{(aq)}$ or $2K^+_{(aq)}$ + Ca-X_2 or Mg-X_2

Due to the additional Na^+ ions, the Na/Cl ratio increases above the background precipitation or seawater value.

On the other hand, the reverse ion exchange process, as shown in the following geochemical reaction, can decrease Na^+ concentration in groundwater:

$2Na^+ + Ca(Mg)_{Clay} \leftrightarrow (Na^+)_{Clay} + Ca^{2+} + Mg^{2+}$

vi) The reverse ion exchange causes a decrease in the Na/Cl ratio

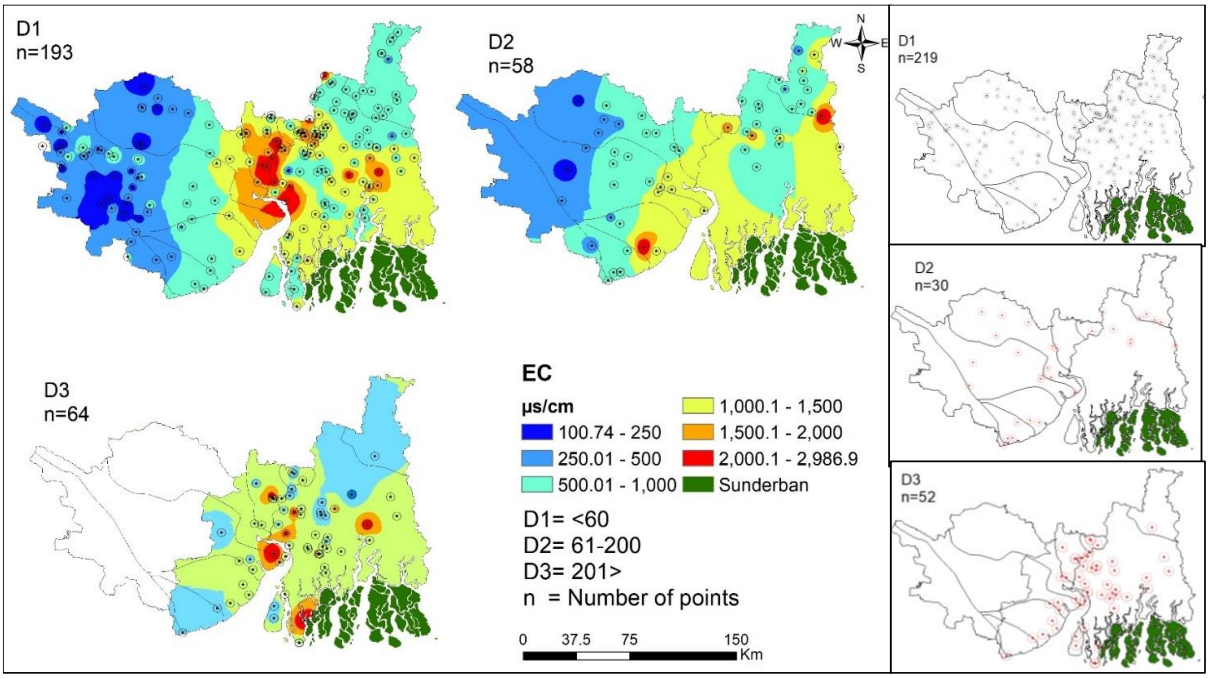

Figure 60: Spatial variation of EC at three depths D1(<60m), D2 (60m-200m), and D3 (>200m); and sampling locations at these three depths.

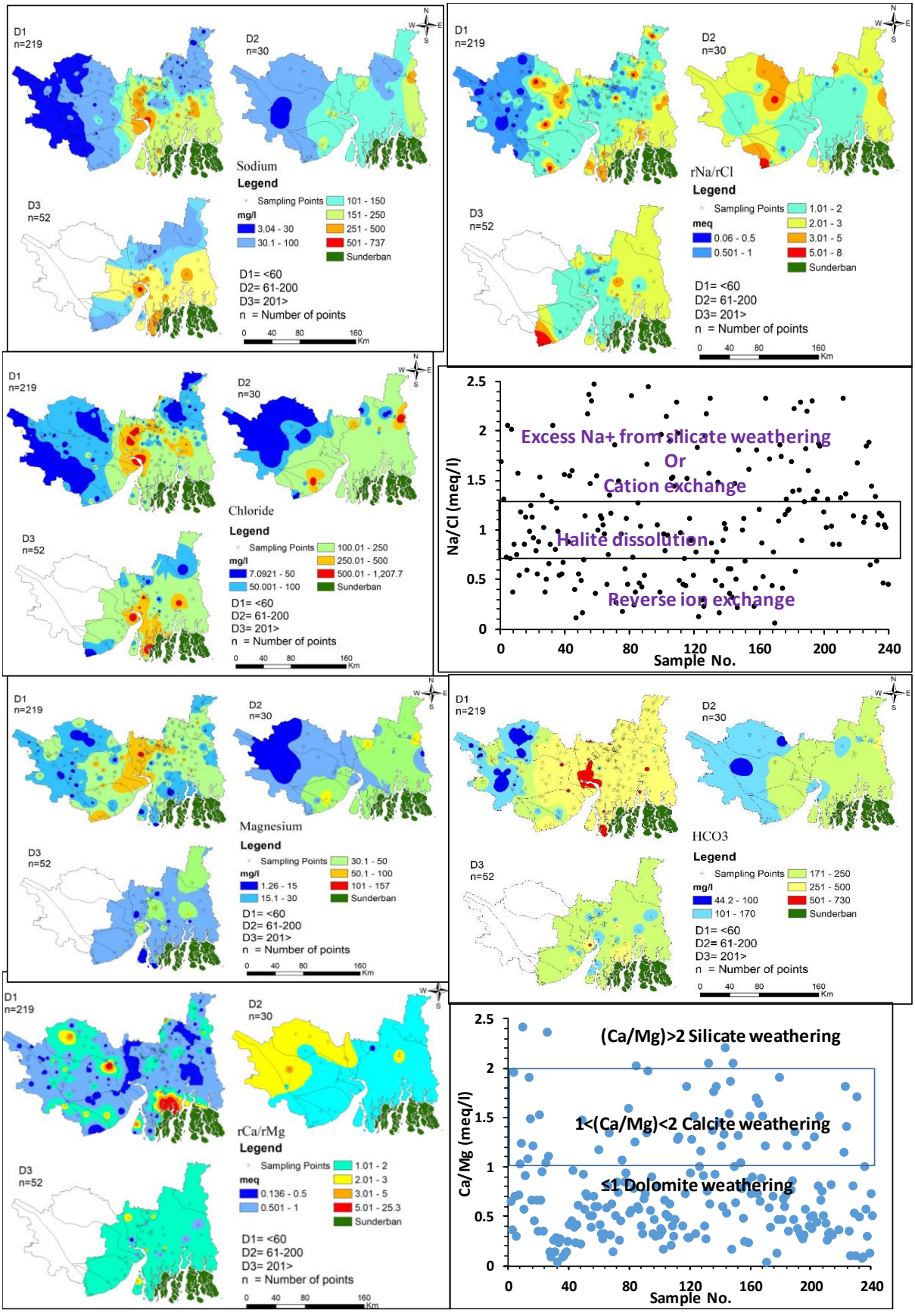

Figure 61: Spatial variation of Mg and HCO_3 in groundwater at three depths D1(<60m), D2 (60m-200m), and D3 (>200m)

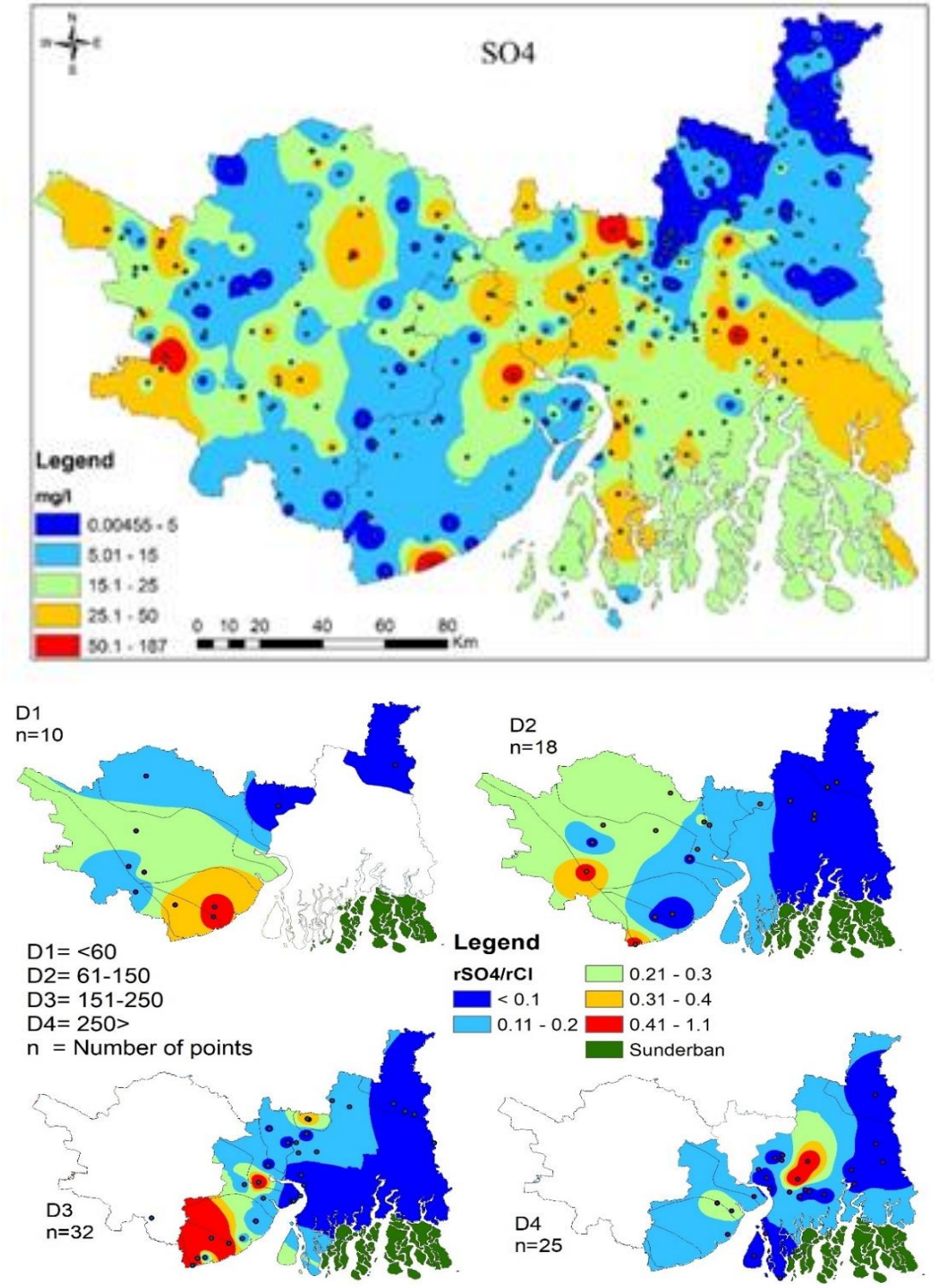

Figure 62: Spatial variation of Mg and HCO_3 in groundwater at three depths D1(<60m), D2 (60m-200m), and D3 (>200m)

In the present study, six samples have Na/Cl values (in epm/l) ranging from 0.846 to 0.869, which is close to the seawater composition of 0.859. Seventy-three data points have values less than 0.84, indicating a possible reverse ion exchange process. Twenty-six samples have Na/Cl values in the range of 0.91 to 1.1, suggesting halite as the possible source of Na and Cl ions.

One hundred data points have Na/Cl values greater than 1.3, indicating either silicate weathering or a cation exchange geochemical process. In the spatial distribution map of Na/Cl, the northwest region shows values less than 0.5, indicating lower sodium relative to chloride. This suggests a low sodium environment, likely dominated by calcium or magnesium-rich minerals. Downstream, the Na/Cl ratio increases, which could be indicative of mineralization processes such as silicate weathering or the mixing of groundwater with seawater.

Investigation of Seawater –Groundwater Interaction Using Isotopic Technique

The isotopic investigation of sweater-groundwater interaction is carried out on the premise that (i) the $\delta^{18}O$ of seawater is near zero whereas the continental groundwater is negative due to it's origin from the rainfall which is of depleted isotopic composition with respect to the seawater (ii) evaporation leads to enrichment in the stable isotopic composition as well as the salinity, but the rate of change of isotopic composition due to evaporation is much higher than the increase in the salinity (for example: a 50% evaporation may reduce $\delta^{18}O$ from -3‰ to -1.5‰ and a corresponding change in EC from 1500µS/cm to 3000µS/cm change) (iii) mixing with seawater changes also changes both the $\delta^{18}O$ and EC but the change in EC is much more than that observed in the evaporation (for example, a 50% mixing of seawater with groundwater of $\delta^{18}O$ = -3‰ can result in the isotopic composition of the mixed water to be -1.5‰; but the EC will change from 1500 µS/cm to 18,000 µS/cm). Therefore, a simple cross plot between EC and $\delta^{18}O$ can fingerprint seawater intrusion in groundwater. With this premises a plot is drawn and is shown in the **Figure 63**. In the figure, the red circles indicate evaporation enrichment.

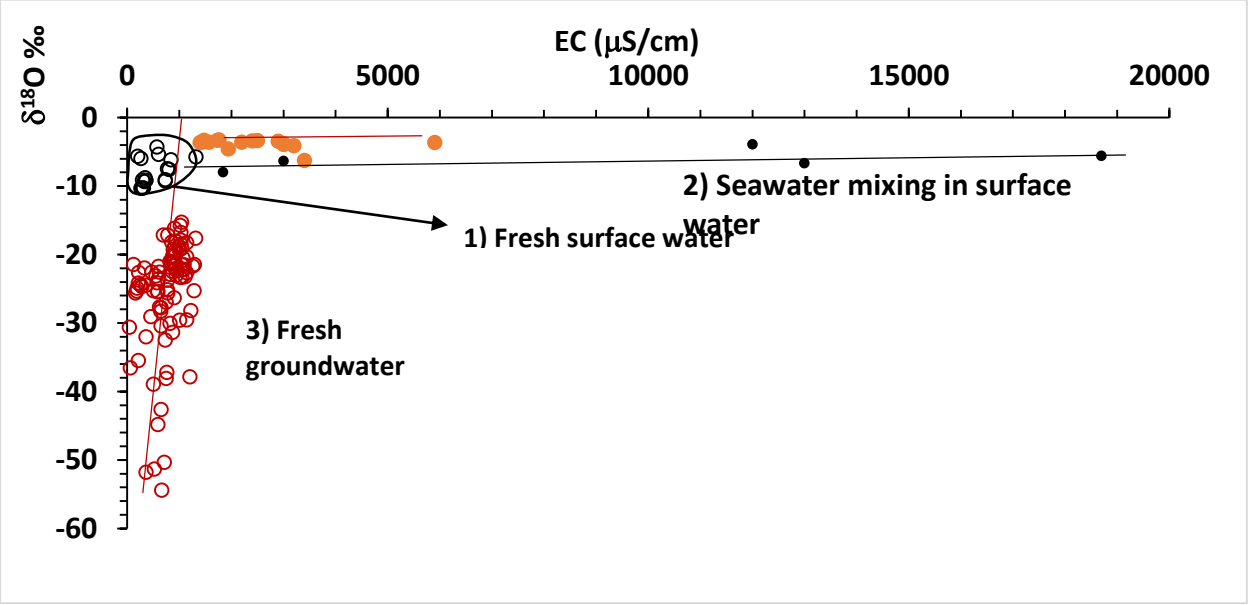

Figure 63: Identification of source of salinity in groundwater using stable isotope and EC cross plot. Red circles indicate groundwater salinity increased due to evaporation enrichment process and those in filled yellow circle indicate salinity enrichment due to seawater intrusion.

The range of enrichment in the red circled points is observed to be from -50‰ to -16‰ in $\delta^{18}O$ scale ((16/50)=0.32)) and the corresponding increase in salinity from 360µS/cm to 1040µS/cm ((360/1040)=0.35). On the contrary, the filled yellow circle indicates seawater intrusion. The isotopic composition of these points although did not change to any appreciable value but the EC changed from 1570µS/cm to 5900µS/cm.

Using conventional chemistry, the isotopic based data interpretation is validated and is shown in the **Figure 64** . The figure is prepared by isolating data that show NaCl type facies in Piper Diagram and Chaddha diagram and also have EC more than 1550µS/cm. The identified points matche exactly with those observed from the isotope-EC cross plot, and indicate seawater intrusion. The blue arrows indicate no intrusion zone or in other-words fresh groundwater outflow to marine zone which commonly termed as Sub-marine Groundwater Discharge (SGD).

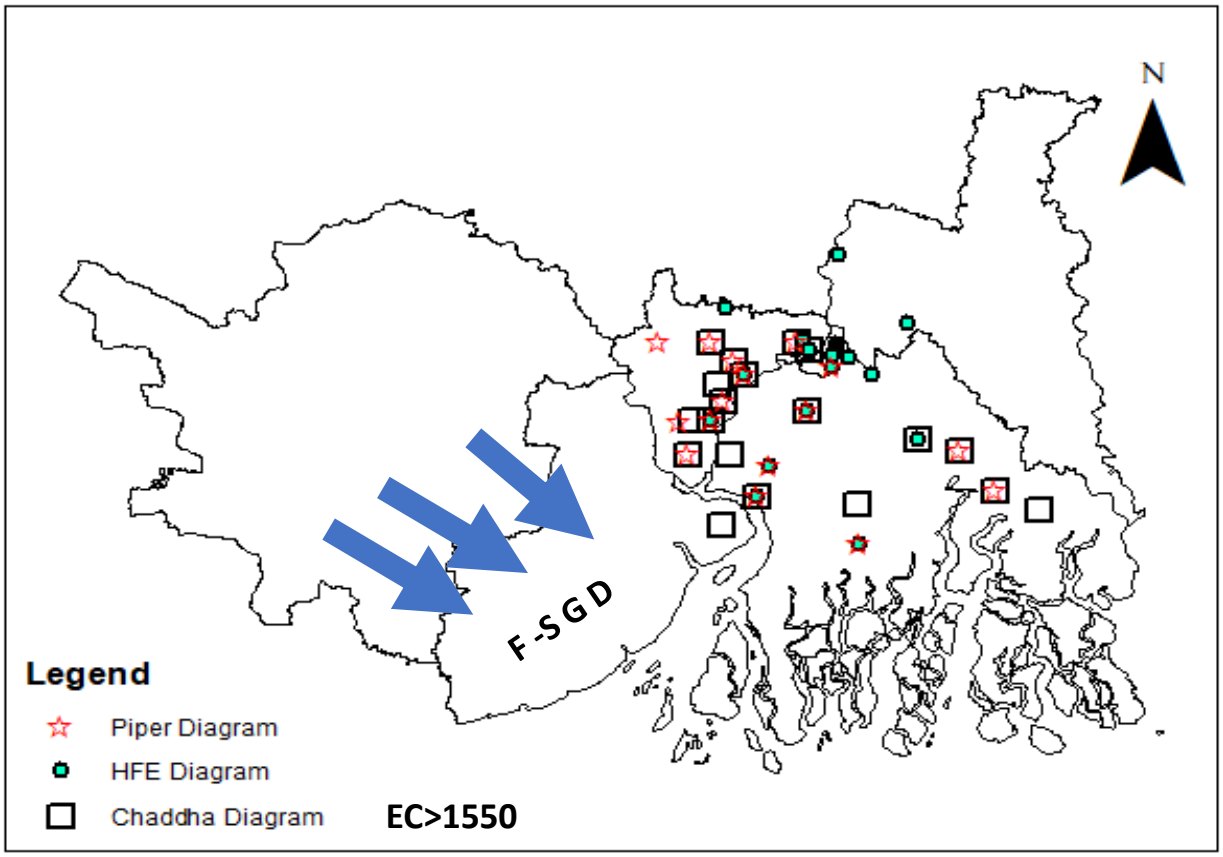

Figure 64: Identified seawater intrusion and SGD zones by hydrochemical characterization of groundwater.

4.7 Seawater Intrusion and Groundwater Contamination: Impacts on Urbanization and Population Growth in Coastal Areas

As population growth occurs, fresh-groundwater demand increases. An increase in the groundwater withdrawal can accelerate seawater intrusion if there exist groundwater seawater interaction or the interaction between tidal water- groundwater. The demographic vulnerability to saline groundwater can be assessed by combining tidal drainage map, seawater intrusion map and population density distribution map. The population density distribution for the Census year 2011 is shown in Fig 65. The map shows dense population in Kolkata and Howrah districts and its growth in the southern direction towards Haldi river. It may be noted that the southern region is spanned with dense network of tidal rivers that carry seawater during high tides. Also, In the direction south of Howrah district towards Haldi river seawater intrusion is noticed (as seen from isotopic and hydrochemical data). Therefore, if suitable measures are not taken the expanding built-up and economic growth in the southern region is expected to increase vulnerability for freshwater reserve in the region if immediate measures are not taken-up.

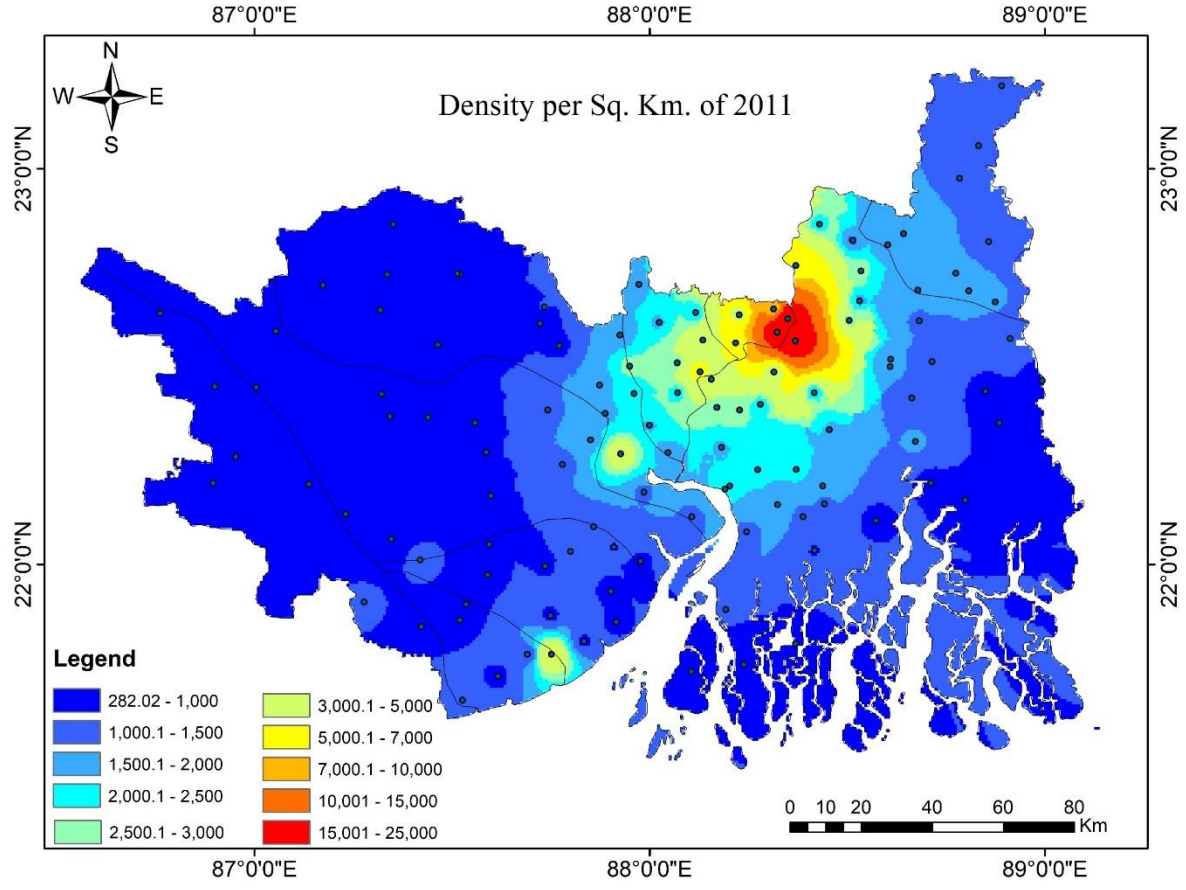

Figure 65: Distribution of population density (Based on Census data 2011)

4.7.1 Long-term Change in the Quality of Groundwater and River Water

Long term variation in salinity (EC and chloride data) in groundwater specially in the coastal region provides valuable insights into inland salinity change due to combined effect from (i) interaction of sea with local groundwater and surface water sources, (ii) anthropogenic influence on water resources, and (iii) impact of climate change on freshwater resources. Such an information is useful for assessing the sustainability of water resources particularly in coastal areas that are vulnerable to salinization. Spatial variation of long-term data helps identifying vulnerable rivers and groundwater pockets for salinization, and to evolve mitigation measures to ensure the health of aquatic ecosystem, supply of drinking water, and ecology sustenance.

Groundwater and River water quality data for pre-monsoon and post-monsoon seasons for the period 2010 to 2022 were collected from the State Department's website and the water quality variations are plotted **(Figure 66 and Table26).**

Table 26: Statistical values of groundwater quality data

Code	Location	EC Value in the Series			Chloride Value in the Series		
		µs /cm			mg/l		
		Min	Avg.	Max	Min	Avg.	Max
1	North 24 Parganas (Basirhat)	827.8	1834.1	2250	313.09	450.8	594.66
2	North 24 Parganas (Barasat)	368	922.7	1224	21.21	80.18	107.08
6	South 24 Parganas (Central Kolkata)	482.3	914.89	1395	29.99	123.1	429.87
8	South 24 Parganas (Sonarpur)	729	1067.92	2040	54.98	107.06	344.89
11	Howrah (Domjur Howrah)	634.2	837.1	1225	16	66.84	165.12
13	Howrah (Uluberia College)	909.1	993	1118	65.02	135.81	194.26
14	East Medinipur (Geokhali Bunglow)	804	1012.73	1154	67.99	117.01	209.93

The salinity (EC) of groundwater is the lowest in the western parts (at Kharagpur Industrial area is less than 150 µS/cm), followed by North 24 Parganas (at Barrackpur it is ~400 µS/cm), followed by Purba Medinipur (Geokhali, Haldia: 1000 µS/cm); followed by Howrah and Kolkata districts (Domjur: ~750 µS/cm, Central Kolkata: 1000 µS/cm, Sonarpur and Uluberia : 1000 µS/cm, Barasat it is near 1100 µS/cm. However, at some locations, exceptionally high salinity is also observed. For example, at Basirhat, North 24 Parganas it is 2000 µS/cm, and at IOC refinery, Haldia it is 2200 µS/cm.

A decreasing EC trend in groundwater is also observed at some sites during the period from 2010 to 2020 indicating freshening of groundwater in the study area. For example at Basirhat EC decreased from 2100 to 1600), at Barasat EC decreased from 1000 to 700; and at Sonarpur EC decreased from 1500 to 1000.

The chloride concentration also exhibited a trend similar to EC

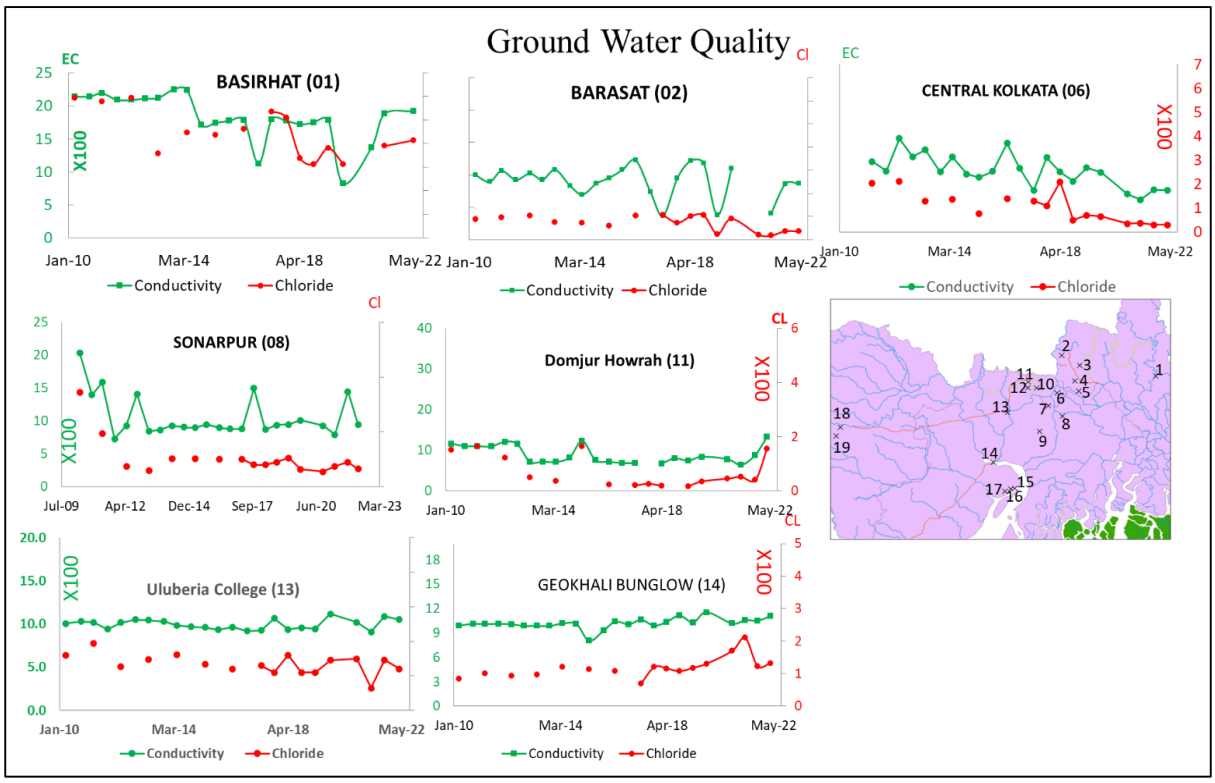

Figure 66. Groundwater quality for the period 2010-2020

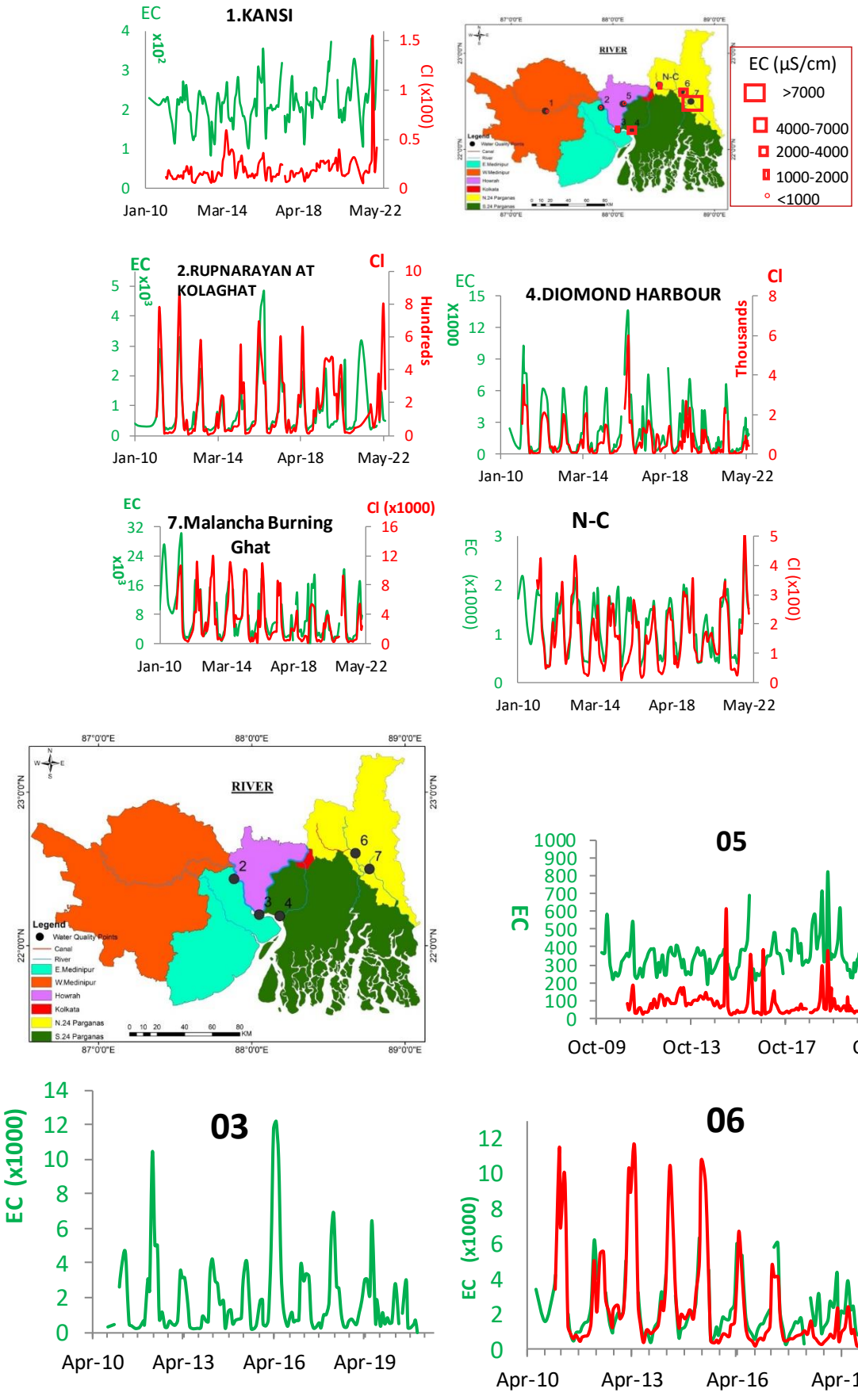

Figure 67: River water quality for the period 2010-2020

Water quality of all the river water show (**Figure 67**) seasonal fluctuation in EC. Amongst the river, similar to the groundwater, western rivers are the freshest in the study area. EC of Kansai river at Gandhi Ghat (Midnapore) is observed to fluctuate between 114μS/cm to 240±20μS/cm; River Ganga at Uluberia shows fluctuation in EC between 270±30 μS/cm to 575±25μS/cm; NC canal (near airport) shows fluctuation in EC from 505 μS/cm to 2000 μS/cm; Rupanarayan river just before its confluence to Haldi river (in East Medinipur District) shows EC fluctuation in the range 660±330 μS/cm to 5570±1435 μS/cm; the same Rupnarayan river near Kolaghat shows flusctuation between 330μS/cm to 2870μS/cm; at Diamond Harbour the river Haldi shows EC fluctuation between 400μS/cm to 5200μS/cm, and the Malancha river in the north 24 Parganas shows EC fluctuation from 2190 μS/cm to 27,200 μS/cm. A few of these rivers, over the period from 2010 to 2020 have shown a decreasing EC trend. For example, at Haroa bridge the extreme EC value of the river Ganga decreased from 13,000μS/cm to 4,300 μS/cm; EC of the river Malancha also decreased from 27,200 μS/cm to 18,500 μS/cm. However, the river Haldi at Diamond Harbour has shown an increase in EC from 5,200 μS/cm to 7,200 μS/cm during this period.

In general, over the years, water quality of groundwater and the river water is observed to getting freshened.

Assessing heavy metal concentrations in groundwater is crucial for determining the suitability of water for drinking purposes. Heavy metals such as arsenic (As), manganese (Mn), aluminum (Al), and copper (Cu) are known to cause serious health effects when present in concentrations above permissible limits. Long-term exposure to contaminated groundwater can lead to severe health issues, including neurological disorders, liver damage, and various forms of cancer. Therefore, monitoring and mapping heavy metal concentrations are essential to ensure water safety for human consumption and to mitigate potential public health risks.

The coastal region of West Bengal, where the study is conducted, is densely populated and highly industrialized. The presence of heavy metal industries, power plants, and chemical and fertilizer factories in the region contributes significantly to environmental pollution. Industrial effluents, coupled with urban runoff, introduce heavy metals into the groundwater, making the region particularly vulnerable to contamination. Given the area's economic importance and population density, assessing heavy metal contamination is critical to

safeguarding both human health and the local ecosystem, while also guiding future regulatory measures.

Spatial distribution patterns of dissolved heavy metal concentrations were prepared. The areas within the contours were analyzed to determine the percentage of the region falling within safe limits and those exceeding permissible limits.

Table 27: Acceptable and permissible limits for dissolved heavy metal concentrations in drinking water (Abbreviations: AL: Acceptable limit; PL: Permissible Limit; W: WHO standard; I: Indian Standard (BIS: IS-10500 (2012)); E: EU standard)

Parameters	**Limits: AL, PL**	**Parameters**	**Limits: AL, PL**
As	W: 10; I: 10, 50	Cu	E-20; I:50 -1500
Fe	W=I=300; 0%	Mn	W:20; I: 100, 300
Al	W-200; I:30, 200	Zn	W:3000; I:5000,15000

The distribution patterns of dissolved heavy metals indicate that (**Figure 68**) arsenic, aluminum, and manganese are the major contaminants in the groundwater of the study area. Arsenic is within the acceptable limit in only 25% of the study area. Dissolved aluminum is within the acceptable limit in just 11% of the area, while it exceeds the permissible limit in 30% area. Dissolved copper is above the acceptable limit in 13% of the study area. Manganese is within the acceptable limit in 50% of the area but exceeds it in 2% area. In contrast, dissolved zinc and iron remain within safe limits across nearly the entire study area.

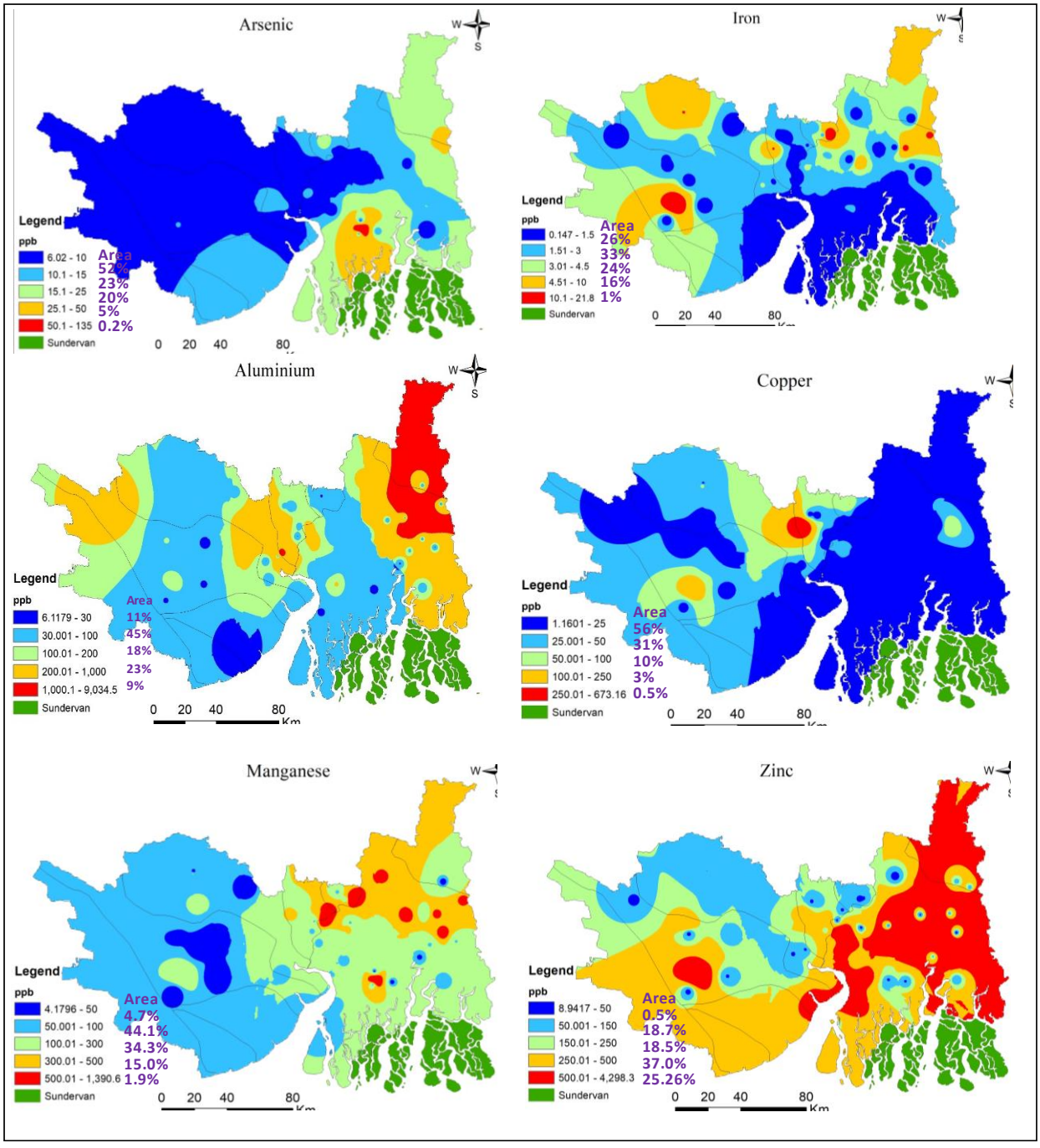

Figure 68: Concentration of dissolved heavy metals and the area covered within different concentration ranges (contour intervals) in groundwater in the study area.

4.8 LITHOLOGY OF AQUIFER OF THE STUDY AREA

The groundwater storage capacity of an area is determined by the total aquifer thickness and the area it covers. Direct measurement of aquifer thickness is challenging, but an estimate can be derived by integrating aquifer material thickness using strata chart data. The methodology for this study was as follows:

Marking Locations: Strata chart locations were identified and marked on the study area map.

Data Digitization and Classification: Strata chart details were digitized and categorized into aquifer and aquitard based on their composition (e.g., clay, sand, silt, gravel). Using this classification, the total aquifer thickness for each stratum at depths of 100 m and 200 m was calculated and expressed as a percentage of the total depth (100 m and 200 m).

Isopach Contour Plot Preparation: Using the latitude and longitude of each strata chart location and the corresponding aquifer thickness percentage, an isopach aquifer contour plot was generated. Contours were drawn at five intervals: <20%, 20%–40%, 40%–50%, 50%–60%, and >60%.

A contour interval of <20% for a depth of 100 m indicates that less than 20 m of the top 100 m consists of aquifer material. For a depth of 200 m, it means less than 40 m consists of aquifer material. A contour interval of 50%–60% at a 100 m depth indicates that the aquifer material is between 50 m and 60 m thick, while for a depth of 200 m, it indicates a thickness of 100 m–120 m.

These contours provide a visual representation of the spatial variation in aquifer thickness across the study area at total depths of 100 m and 200 m.

Watershed Subdivision: The study area was subdivided into respective watersheds to facilitate detailed analysis.

Aquifer Volume Estimation: For each watershed, the aquifer thickness contour value was multiplied by the area covered between adjacent contour intervals to estimate the aquifer volume. The groundwater storage capacity for each watershed can be calculated by multiplying the specific yield by the estimated aquifer volume.

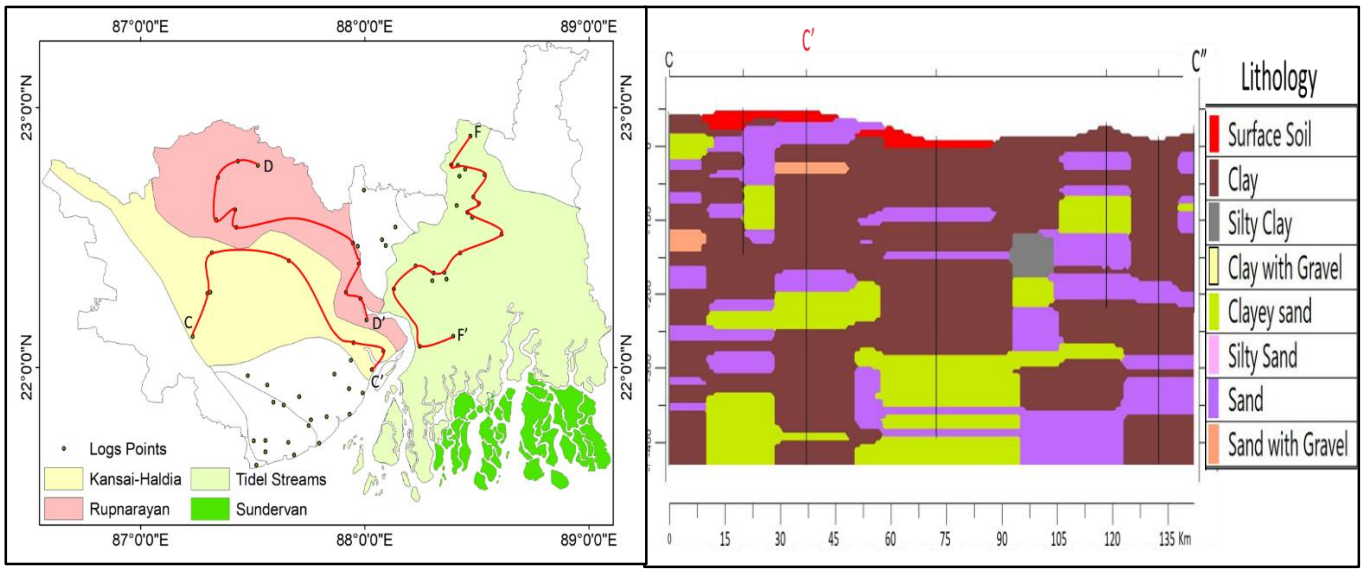

(a) (b)

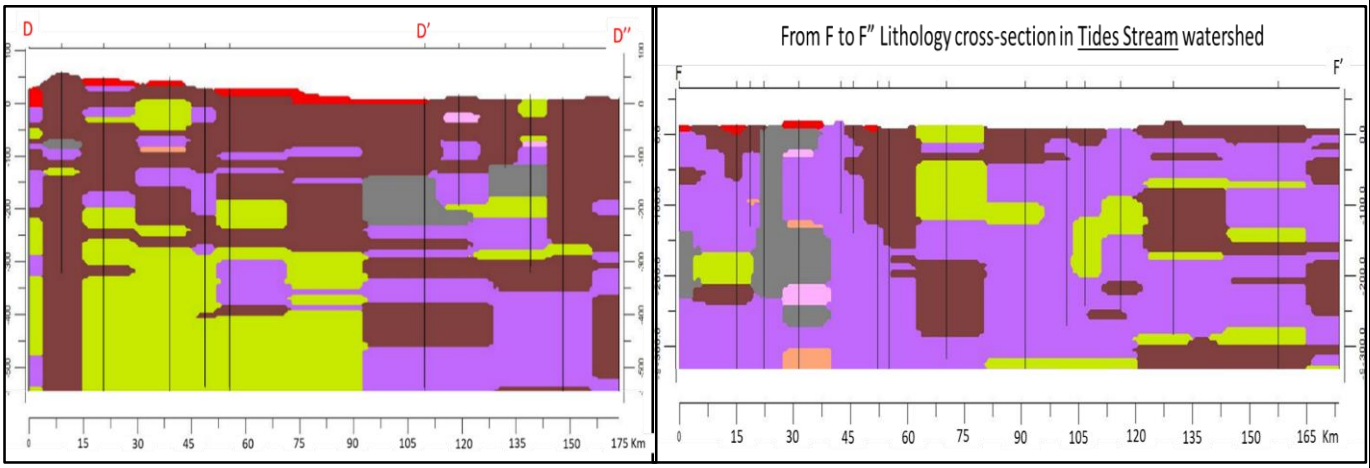

(c) (d)

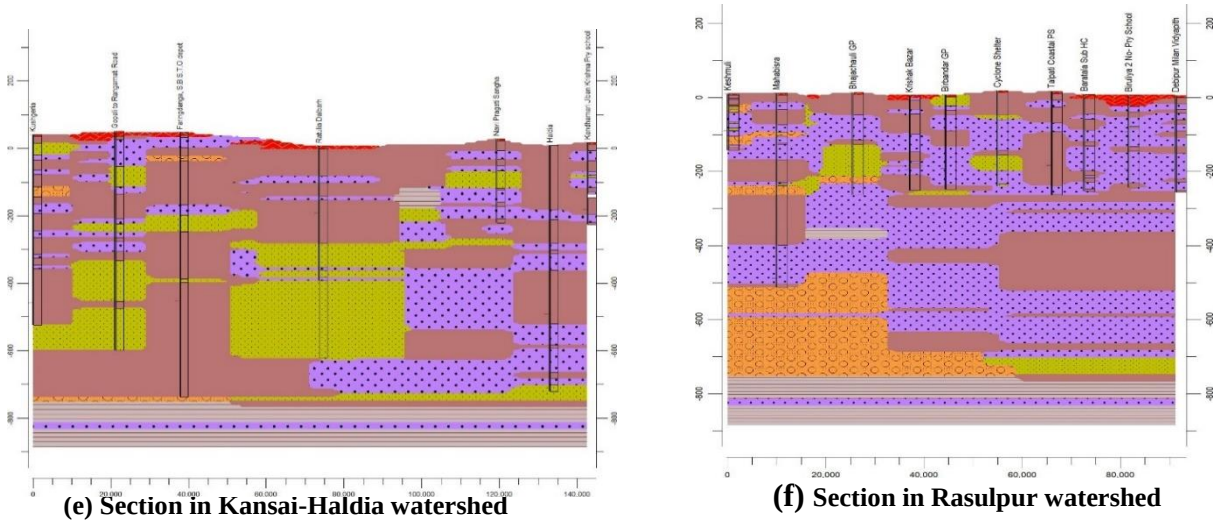

(e) Section in Kansai-Haldia watershed

(f) Section in Rasulpur watershed

Figure 69 Aquifer disposition map. (a) Watersheds in the study area and sectional lines for constructing the cross sections. Dots indicate location of strata charts. The cross sections along the sectional lines are shown in (b), (c), (d), (e) and (f).

Table 28:.Watershed and the estimated aquifer volume

Sr. No.	Watershed and the districts	Estimated aquifer volume (Km^3)	
		Up to 100m bgl	Up to 200m bgl
1.	Pichhabani (East Medinipur)	20.88	54.73
2.	Rasulpur (East Medinipur)	44.78	118.77
3.	Kansai-Haldia (East & West Medinipur)	123.00	249.74
4.	Rupnarayan (East & West Medinipur, and Howrah)	90.17	178.68
5.	Damodar (Howrah)	28.33	52.56
6.	Tidal-Stream (South 24 Parganas)	349.79	869.51

The vertical distance between groundwater under surface and surface at time of observation is known as aquifer thickness, the aquifer thickness of the study area is shown in the **(Figure 70).**

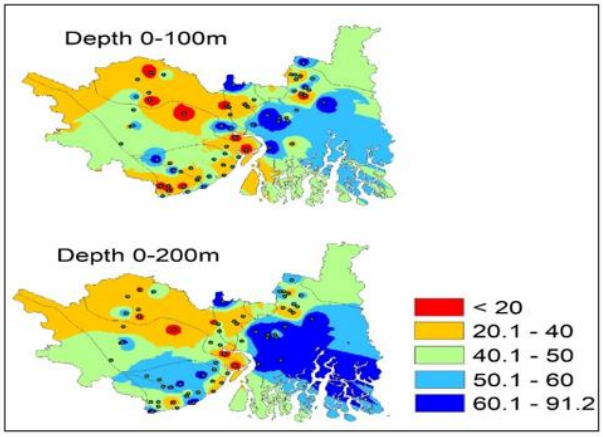

Depth of bore well	Area(km2)	Aquifer (%)
0-100 meter	807.8083	<20
	7888.4	20-40
	10825.18	40-50
	5699.873	50-60
	1131.483	>60
0-200 meter	308.7868	<20
	7220.097	20-40
	8635.002	40-50
	5491.994	50-60
	4696.868	>60

Figure 70. Depth of aquifer

The iso-patch map of aquifer suggests that the aquifer thickness varies significantly across the region. In particular:

- South 24 Parganas has the thickest aquifers, followed by North 24 Parganas and East Medinipur, and the thinnest aquifers in West Medinipur.
- Aquifer thickness in South 24 Parganas and East Medinipur increases substantially with depth, especially beyond 100 meters.
- If these deeper aquifers are affected by seawater intrusion, it could lead to widespread salinization, impacting not only South 24 Parganas and East Medinipur, but also extending into the south-eastern parts of Howrah district.

This highlights the vulnerability of the region's deeper aquifers to potential salinization from seawater intrusion, especially if an interaction between the sea and groundwater occurs due to a negative pressure gradient. Such intrusion could lead to long-term consequences for groundwater quality across a wide area, potentially resulting in freshwater shortages in this economically fast-growing region.

For dating groundwater using environmental tritium (^{3}H) activity, 19 samples were collected from 2019 to 2022 from hand pumps (shallow aquifers) and deep tube wells. These samples were analyzed for tritium content at NIH, Roorkee, using electrolytic enrichment and beta counting via an ultra-low-level liquid scintillation counter ('Quantulus'). The measured tritium content in groundwater ranged from close to zero to about 3.15 TU.

As per the **Figure 71**, 88% of the samples had tritium levels below 1.5 TU, indicating older groundwater, while 22% exhibited tritium activity above 1.5 TU, suggesting modern groundwater recharge. Areas with higher tritium activity are located in saline groundwater zones, particularly in the southwest of Howrah district near the Haldi River and the vicinity of Salt Lake City. This indicates that groundwater in these regions is likely receiving recharge from surface water sources such as the Haldi River and other nearby surface water bodies.

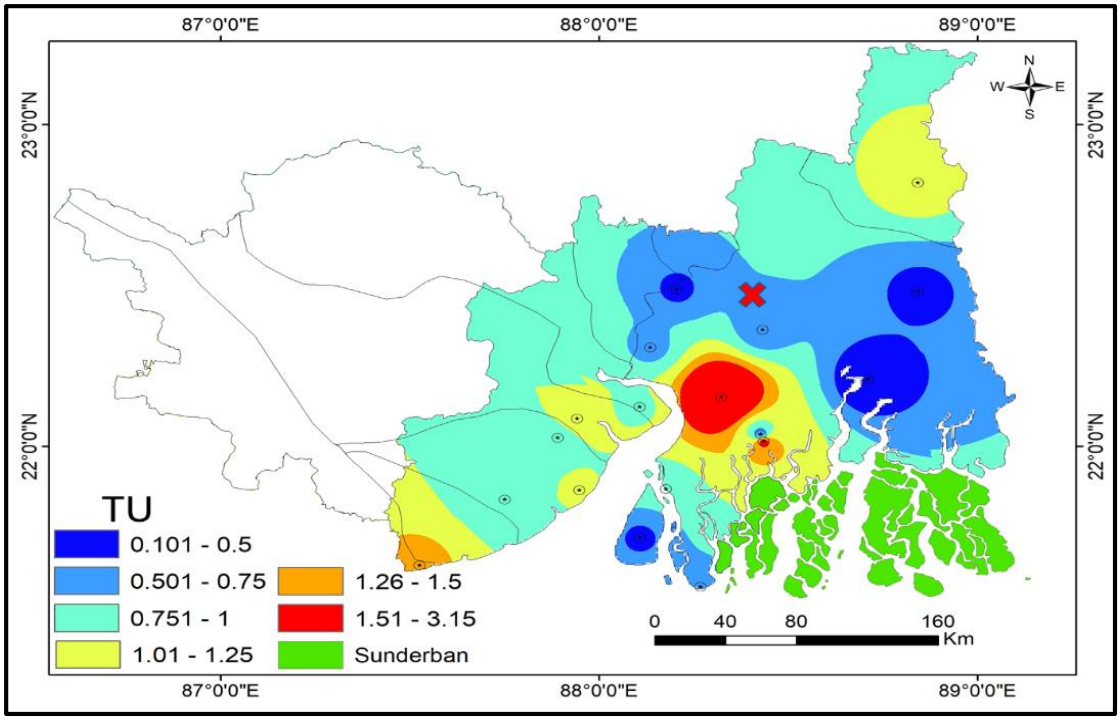

Figure 71. Groundwater dating using environmental tritium activity. Tritium activity greater than 1.5 TU, represented by red regions and red crosses, indicates the presence of modern recharge to the groundwater. Light blue and blue regions represent old groundwater (age >50 years), while yellow and brown regions indicate areas of mixing and transition between old and sub-modern groundwater. Dots with circles denote groundwater sampling locations. As the area is a final discharge zone (coastal area), the blue regions representing old groundwater indicate the ultimate discharge areas to the sea or surface water bodies.

5 SUMMARY AND CONCLUSIONS

5.1 Summary

Coastal zones, home to approximately 40% of the global population, are increasingly challenged by rapid urbanization and climate change. These regions, characterized by diverse geomorphic features like estuaries and tidal flats, are vital for their resources and strategic locations. However, they face threats from sea-level rise, pollution, and seawater intrusion. In India, the government has implemented Coastal Regulation Zone (CRZ) notifications to manage land use and protect ecologically sensitive areas.

The Bengal Basin, encompassing the Ganges-Brahmaputra delta, is geologically significant due to its tectonic activity and sediment deposition. This area supports dense populations and agriculture but is under threat from sea-level rise, sediment deposition, and coastal erosion. Hydrological studies in West Bengal's coastal districts reveal the adverse effects of seawater intrusion and excessive groundwater extraction on water quality, highlighting the need for a comprehensive understanding of these dynamics.

West Bengal's coastal region spans 220 km (325 km including islands) and covers approximately 9,630 square kilometers, including districts such as East Medinipur, South 24 Parganas, Howrah, West Medinipur, and North 24 Parganas. This area features diverse physiographic zones, including the Sundarbans and deltaic plains, which face challenges from land reclamation, urban development, and climate impacts. The climate is characterized by hot summers, high humidity, and seasonal rainfall patterns, resulting in significant rainfall variations across districts. Urban areas frequently encounter issues such as drainage congestion and industrial pollution.

Objectives

1. Assess Rainfall Patterns: Examine long-term rainfall data to understand precipitation variations in Coastal West Bengal and their impact on groundwater recharge.
2. Evaluate Runoff Characteristics: Estimate runoff percentages in various watersheds using GIS and remote sensing data for flood risk management.
3. Determine Groundwater Potential: Assess groundwater potential using GIS and remote sensing to identify zones suitable for recharge and optimize resource management.
4. Analyze Water Quality: Evaluate water quality from various sources by analyzing parameters such as electrical conductivity (EC), pH, and heavy metals for pollution levels.

5. Examine Groundwater Dynamics: Study changes in groundwater depth and flow patterns over time, focusing on the impact of seawater intrusion.
6. Investigate Surface Water Quality Trends: Assess long-term trends in surface water salinity and chloride concentrations to identify the effects of seawater intrusion.
7. Explore Groundwater Chemistry: Analyze spatial variations in groundwater chemistry to understand influences from seawater intrusion and rock-water interactions.
8. Study Seawater-Groundwater Interaction: Use isotopic techniques to differentiate between seawater and continental groundwater, identifying the extent of seawater intrusion.
9. Assess the Impact of Population Growth: Investigate the relationship between rising population densities and seawater intrusion to identify areas at risk of freshwater depletion.
10. Analyze Aquifer Lithology: Examine aquifer thickness and coverage to assess their storage capacity and susceptibility to seawater intrusion.
11. Measure Tritium Levels: Analyze tritium content in groundwater samples to determine groundwater age and identify areas with recent recharge.

Result Highlights:

Rainfall Analysis:

An analysis of 26 years (1993-2018) of rainfall data from 50 locations revealed:

- **Average Annual Rainfall**: Approximately 1,728 ± 293 mm.
- **Drought Extremes**: Two severe droughts occurred between 2010 and 2012, lowering average rainfall to 1,786.2 ± 216.08 mm when excluded.
- **Regional Variability**: Significant fluctuations noted in North and South 24 Parganas, with rainfall ranging from 377 mm during droughts to over 2,300 mm in wet years.
- **Coastal Trend**: Higher rainfall amounts were observed near the coast, decreasing towards the northeast and northwest, particularly in East Medinipur compared to West Medinipur.

Soil Types and Physiographic Zones: The study identified five major soil types and six physiographic zones. These are tabulated below:

Soil Types & Area %	**Physiographic zones**
Loamy: 44.82%	1. Sundarbans 2. Deltaic Plain 3. Degraded Plateau 4. Plateau Fringe Fan
Clayey: 34.48%	
Clay Skeletal: 12.18%	

	5. Reclaimed Coastal Zones **6.** Medinipur Coastal Plains
Sandy: 2.38%	
Loamy Skeletal: 1.29%	

Land Use and Land Cover (LULC)

The region's land use is predominantly agricultural:

Land-use type	**Area (%)**	**Land-use type**	**Area (%)**
Agricultural Fields	46.6%	Forest Cover	29%
Cultivated Land	10.1%	Mangrove Forests	7.6%
Inland Rivers	4.8%	Open Land and Built-up Areas:	6.1%
Wet Land	1.9%	Dry Land	0.7%
Ponds (Agricultural and inland ponds)			0.11%

Main Crops in the area: Rice, maize, pulses, oilseeds, and wheat, reflecting the region's agricultural focus.

Runoff Estimation

Using the Soil Conservation Service Curve Number (SCS-CN) method and GIS data from Sentinel images, watershed-wise the following runoff percentage is obtained:

- **Damodar River Watershed**: 52.53% (highest)
- **Rupnarayan Watershed**: 47.03%
- **Kasai-Haldi Watershed**: 44.57%
- **Rasulpur Watershed**: 28.83%

Groundwater Potential Assessment

Using GIS and SENTINEL-2B satellite imagery, the region was classified into four groundwater potential zones:

- **Very High**: 16.78%
- **High**: 53.48%
- **Moderate**: 29.52%
- **Low**: 0.22%

Flat or gently sloping areas were identified as more suitable for groundwater recharge, indicating a need for focused management in low-potential areas.

Groundwater Levels and Potential

Groundwater levels were assessed across Howrah, North and South 24 Parganas, Purba Medinipur, and Paschim Medinipur, with a recorded low of 10.07 m below ground level in Purba Medinipur (2016). A weighted overlay analysis of seven thematic layers (geology, geomorphology, soil, drainage density, rainfall, and land use) delineated groundwater potential zones: 53.48% in high-potential areas, 29.52% in moderate zones, 16.78% in very high-potential zones, and 0.22% in low-potential areas. The study recommends developing new well fields in high-potential zones to mitigate over-extraction and prevent seawater intrusion.

Water Quality Assessments (2019-2022)

Water quality assessments revealed critical insights into groundwater and surface water characteristics during pre- and post-monsoon seasons. Key parameters analyzed included electrical conductivity (EC), pH, isotopic composition, and major ions. Groundwater contour maps from 2001 to 2019 indicated a significant 15-meter rise in depth, attributed to natural outflow, anthropogenic withdrawals, and tidal influences. Although rainfall remained stable, groundwater levels declined, suggesting higher extraction rates and risks of seawater intrusion.

Surface Water Quality

Surface water quality from 11 river locations (2010-2022) exhibited high salinity levels, particularly during pre-monsoon periods, with EC values exceeding 10,000 µS/cm due to seawater intrusion. Post-monsoon, EC values dropped significantly due to freshwater influx, with chloride concentrations reducing from 11,000 mg/L to 3,000 mg/L after 2016. However, some areas, like Howrah, maintained stable salinity levels, while tidal impacts were more pronounced at elevations below 10 meters.

Groundwater Quality

Groundwater quality varied considerably, classified into five regions based on EC, ranging from freshwater to saline. Zone 3 had the highest ionic concentrations, with sulfate levels generally low. Hydrochemical analyses using Parsons Plot and Piper Diagram revealed influences from seawater intrusion and rock-water interactions, with 35% of samples in the Na-Cl zone and 65% in the Ca-Mg-Cl zone. TDS analysis indicated that 65% of groundwater samples had low mineral content (TDS < 1000 mg/L), while 35% had higher mineral content. Gibbs and Chadha plots supported findings of rock-water interactions and base-ion exchange processes, with evidence of seawater contamination in some areas.

Salinity and Chloride Variability

Surface water analysis showed a significant range in EC, with minimum values of 175 µS/cm at the Shitalatala River and maximum values of 29,990 µS/cm at the Bidyadhari River. Groundwater chloride levels varied between 16 mg/L in Howrah and 594.66 mg/L in North 24 Parganas during pre- and post-monsoon seasons, with 57.15% of samples within permissible limits and 42.85% exceeding them. Surface water chloride concentrations ranged from 11.31 mg/L at the Shitalatala River to 3,090.2 mg/L at the Bidyadhari River, with 60% of samples exceeding permissible limits.

Aquifer Characteristics

Groundwater quality varied spatially and with depth, indicating that shallow aquifers (D1) near the Haldi River are more contaminated with sodium and chloride, while deeper aquifers (D2 and D3) exhibit lower salinity. Na/Cl ratios suggested diverse salinity sources, including seawater intrusion and mineralization, with lower ratios in the northwest indicating calcium or magnesium dominance. Isotopic analysis effectively differentiated seawater from groundwater, while population growth exacerbated seawater intrusion in areas like Kolkata and Howrah, which face increasing freshwater demand.

Long-Term Trends and Health Risks

Long-term trends from 2010 to 2022 indicated the lowest groundwater salinity in Kharagpur and the highest in Howrah and Kolkata, with some areas demonstrating freshening trends. Seasonal river salinity fluctuations and high concentrations of heavy metals, including arsenic, manganese, and copper, posed significant health risks. Aquifer thickness varied, with South 24 Parganas and East Medinipur featuring the thickest, more vulnerable aquifers. Tritium analysis revealed that 88% of samples contained older groundwater, while 22% showed recent recharge, particularly near saline zones.

Recommendations and Climate Vulnerability

To combat these challenges, recommended coastal management strategies include constructing groins, porcupine structures, and movable flood barriers. Rising sea levels, averaging 0.24 cm/year (1915-2021) and accelerating to 0.96 cm/year (2010-2021), combined with tidal influences, particularly in the Hooghly estuary, highlight the region's vulnerability. This underscores the urgent need for integrated management to address seawater intrusion, population pressure, and climate change in Coastal West Bengal.

5.2 Conclusion

This study provides a comprehensive understanding of the hydrological dynamics and water quality challenges facing Coastal West Bengal, underscoring the critical need for sustainable water resource management in a region marked by significant environmental pressures. The findings emphasize the intricate relationships between rainfall variability, groundwater dynamics, seawater intrusion, and human activities, all of which have profound implications for the water security of the region. Additionally, the research highlights the vulnerability of both surface and groundwater resources to contamination, particularly from salinity and other pollutants resulting from natural and anthropogenic factors.

Adaptive Water Resource Management

The analysis reveals substantial variability in rainfall patterns, characterized by extreme fluctuations that render the region susceptible to both droughts and flooding. To address these challenges, adaptive water resource management strategies are urgently needed. This includes the development of flexible irrigation systems and water storage solutions capable of withstanding unpredictable weather patterns. Integrating advanced meteorological models for improved rainfall forecasting will enhance preparedness for extreme events, thereby reducing the risks associated with water shortages or flood damage. By aligning water management practices with climate variability, both agricultural and urban settings can achieve increased resilience.

Groundwater Potential and Quality Challenges

The classification of groundwater potential zones across Coastal West Bengal offers valuable insights into areas most vulnerable to depletion and seawater intrusion. Regions with high potential for groundwater recharge require targeted management efforts, including the development of new well fields and recharge initiatives. The study's findings on groundwater quality variability, particularly regarding salinity and contamination, demonstrate the necessity for continuous monitoring and management. The Water Quality Index (WQI) developed in this study serves as a standardized tool for assessing and monitoring water quality, facilitating the identification of pollution sources and trends over time. Furthermore, the innovative use of stable isotopes for water source tracing provides a nuanced understanding of groundwater dynamics, enhancing the accuracy of identifying seawater intrusion and other contamination risks.

Addressing Seawater Intrusion and Population Pressures

As coastal populations grow, the demand for freshwater increases, exacerbating the risks associated with seawater intrusion and resource depletion. This study highlights the urgent need

for improved water management practices, particularly in urbanized and densely populated areas such as Kolkata and Howrah, where groundwater depletion and salinization pose significant threats. Coastal management strategies, including the construction of groins, movable flood barriers, and seawalls, are recommended to mitigate the impacts of rising sea levels and increasing salinity. Engaging local communities in water management initiatives is equally vital, fostering sustainable practices and promoting resilience against the impacts of climate change.

Policy Recommendations and Future Research

This study lays a foundation for future research and policy development by providing a comprehensive dataset on the hydrological and water quality conditions in Coastal West Bengal. Policymakers can leverage these findings to develop evidence-based strategies that address pressing water challenges in the region. Incorporating data-driven policies and engaging communities in decision-making processes will make water management strategies more effective and sustainable. Continuous long-term monitoring is crucial, particularly in the context of climate change and urbanization, to adapt to evolving environmental conditions and safeguard water resources for future generations.

Summary

In conclusion, this study not only advances the understanding of the complex hydrological challenges in Coastal West Bengal but also provides actionable insights for stakeholders and policymakers. The recommendations for adaptive water resource management, groundwater potential mapping, and water quality monitoring, combined with the innovative use of isotopic techniques, offer a robust framework for addressing the region's water security challenges. By implementing integrated management strategies and promoting community engagement, Coastal West Bengal can enhance its resilience to climate change, urbanization, and water quality degradation, ensuring the sustainability of its vital water resources for the long term.

REFERENCES

1. Alexakis, D. E. (2021). Water quality indices: Current and future trends in evaluating contamination of groundwater resources. Water , 13 (4), 401.

2. Ali, S., Ghosh, N.C., Singh, R. and Sethy, B.K. (2013). Generalized explicit models for estimation of wetting front length and potential recharge. Water Resources Management, 27:2429-2445. DOI 10 1007/s11269-013-0295-2.. Water Resources Management. 27. 2429-2445. 10.1007/s11269-013-0295-2

3. Ali, Sk Ajim. (2018). Status of solid waste generation and management practice in Kolkata municipal corporation, West Bengal. 6. 1173- 1186. 10.6088/ijes.6112.

4. Amiri, Vahab & Berndtsson, R.. (2020). Fluoride occurrence and human health risk from groundwater use at the west coast of Urmia Lake, Iran. Arabian Journal of Geosciences. 13. 10.1007/s12517-020-05905-7.

5. Andreo, B., Vías, J., Durán, J. J., Jiménez, P., López-Geta, J. A., & Carrasco, F. (2008). Methodology for groundwater recharge assessment in carbonate aquifers: application to pilot sites in southern Spain. Hydrogeology Journal , 16 , 911-925.

6. Appelo C.A.J. and Postma D. (2005) Geochemistry, Groundwater and Pollution, 2^nd^ Edition, CRC Press.

7. Banerjee M (1996), Manual of Integrated Coastal Zone Management, p.229-239, (1996), (A. K. Ghosh and P. Sanyal eds, Dept. of Environment, Govt. of W. Bengal and Dept. of Ocean Development, Govt. of India)

8. Benavides M. M., C. Eberle, L. Narvaez (2023) Water Depletion Technical Report, UN EHS

9. Benhamiche, N., Sahi, L., Tahar, S., Bir, H., Madani, K., & Laignel, B. (2016). Spatial and temporal variability of groundwater quality of an Algerian aquifer: the case of Soummam Wadi. Hydrological Sciences Journal , 61 (4), 775-792.

10. Bharati, L; Jayakody, P (2010) Hydrology of the upper Ganga river. Colombo, Sri Lanka: International Water Management Institute. http://publications.iwmi.org/pdf/H043412.pdf

11. Binda, G.; Frascoli, F.; Spanu, D.; Ferrario, M.F.; Terrana, S.; Gambillara, R.; Trotta, S.; Noble, P.J.; Livio, F.A.; Pozzi, A. (2022) Geochemical Markers as a Tool for the Characterization of a Multi-Layer Urban Aquifer: The Case Study of Como (Northern Italy). Water, 14, 124. https://doi.org/10.3390/w14010124

12. Boulton, A. J., and P. J. Hancock (2006). Rivers as groundwater-dependent ecosystems: a review of degrees of dependency, riverine processes and

management implications. Australian Journal of Botany, vol. 54, No. 2, pp. 133--44. DOI: 10.1071/BT05074

13. CGWB (2022) Groundwater Year Book Uttar Pradesh (2021 -2022), CGWB, MoWR,RD &GR, GoI

14. Chakraborti, Dipankar & Mukherjee, Subhash & Pati, Shyamapada & Sengupta, Mrinal & Rahman, Mohammad Mahmudur & Chowdhury, Uttam & Lodh, Dilip & Chanda, Chitta & Chakraborti, Anil & Gautam Kumar, Basu. (2003). Arsenic Groundwater Contamination in Middle Ganga Plain, Bihar, India: A Future Danger?. Environmental health perspectives. 111. 1194-201. 10.1289/ehp.5966.

15. Chakraborty, M., Tejankar, A., Coppola, G. et al. (2022) Assessment of groundwater quality using statistical methods: a case study. Arab J Geosci 15 , 1136 https://doi.org/10.1007/s12517-022-10276-2

16. Chanda S and A. K. Hait, Paleobotanist 45: 117-124, (1996)

17. Chow V.T., Maidment, D.R., and Mays, W. (1988). Applied Hydrology, Mc Graw Hill, New York

18. Dar, T., Rai, N., & Bhat, A. (2021). Delineation of potential groundwater recharge zones using analytical hierarchy process (AHP). Geology, Ecology, and Landscapes , 5 (4), 292-307.

19. Das, R. & Granat, L. & Leck, C. & Praveen, P.s & Rodhe, H.. (2010). Chemical composition of rainwater at Maldives Climate Observatory at Hanimaadhoo (MCOH). Atmospheric Chemistry and Physics Discussions. 10. 10.5194/acpd-10-17569-2010.

20. Datta, P.S., Tyagi, S.K. (1996) Major ion chemistry of groundwater in Delhi area: Chemical weathering processes and groundwater flow regime. Jour.Geol. Soc. India v.47, pp.179-188.

21. Dutta V, D. Dubey, S. Kumar (2020) Cleaning the River Ganga: Impact of lockdown on water quality and future implications on river rejuvenation strategies. Sci Total Environ., 743: 140756. [https://doi.org/10.1016/j.scitotenv.2020.140756](https://doi.org/10.1016%2Fj.scitotenv.2020.140756)

22. Elumalai V, Brindha K, Lakshmanan E. (2017) Human Exposure Risk Assessment Due to Heavy Metals in Groundwater by Pollution Index and Multivariate Statistical Methods: A Case Study from South Africa. Water .; 9(4):234. https://doi.org/10.3390/w9040234

23. Eyankware, Moses & Akakuru, Obinna & Eyankware, Emmanuel. (2022). Interpretation of hydrochemical data using various geochemical models: a case

study of Enyigba mining district of Abakaliki, Ebonyi State, SE Nigeria. Sustainable Water Resources Management. 8. 10.1007/s40899-022-00613-4.

24. Fallahi, M.M., Shabanlou, S., Rajabi, A. et al. (2023) Effects of climate change on groundwater level variations affected by uncertainty (case study: Razan aquifer). Appl Water Sci 13 , 143. https://doi.org/10.1007/s13201-023-01949-8

25. Fatima, S. U., Khan, M. A., Siddiqui, F., Mahmood, N., Salman, N., Alamgir, A., & Shaukat, S. S. (2022). Geospatial assessment of water quality using principal components analysis (PCA) and water quality index (WQI) in Basho Valley, Gilgit Baltistan (Northern Areas of Pakistan). Environmental Monitoring and Assessment , 194 (3), 151.

26. Feist, S.E., Hoque, M.A. & Ahmed, K.M. (2023) Coastal Salinity and Water Management Practices in the Bengal Delta: A Critical Analysis to Inform Salinisation Risk Management Strategies in Asian Deltas. Earth Syst Environ 7, 171--187. https://doi.org/10.1007/s41748-022-00335-9

27. Fistikoglu, Okan & Gunduz, Orhan & Simsek, Celalettin. (2016). The Correlation Between Statistically Downscaled Precipitation Data and Groundwater Level Records in North-Western Turkey. Water Resources Management. 30. 10.1007/s11269-016-1313-y.

28. Freeze R.A. and J. A. Cherry (1979) Groundwater. Prentice-Hall Inc., New Jersey

29. Gao, Zongjun & Liu, Jiutan & Jianguo, Feng & Wang, Min & Wu, Guangwei. (2019). Hydrogeochemical Characteristics and the Suitability of Groundwater in the Alluvial-Diluvial Plain of Southwest Shandong Province, China. Water. 11. 1577. 10.3390/w11081577.

30. Ghosh A, Schmidt S, Fickert T, Nüsser M (2015) The Indian Sundarban mangrove forests: History, utilization, conservation strategies and local perception. Diversity 7(2): 149--169.

31. Ghosh, A., Mukhopadhyay, S. (2016) Quantitative study on shoreline changes and Erosion Hazard assessment: case study in Muriganga--Saptamukhi interfluve, Sundarban, India. Model. Earth Syst. Environ. 2 , 75 https://doi.org/10.1007/s40808-016-0130-x

32. Gonçalves, Carlos M., Joaquim CG Esteves da Silva, and Maria F. Alpendurada. "Evaluation of the pesticide contamination of groundwater sampled over two years from a vulnerable zone in Portugal." Journal of agricultural and food chemistry 55.15 (2007): 6227-6235.

33. Gopinath, G., Seralathan, P. Rapid erosion of the coast of Sagar island, West Bengal - India. Environ Geol 48 , 1058--1067 (2005). https://doi.org/10.1007/s00254-005-0044-9

34. Gunduz, Orhan & Simsek, Celalettin. (2011). Influence of Climate Change on Shallow Groundwater Resources: The Link Between Precipitation and Groundwater Levels in Alluvial Systems. 10.1007/978-94-007-1143-3_25. Chapter in NATO Security through Science Series C: Environmental Security

35. Gupta A (2022) Intra-Municipal Infrastructural Disparities --A Case Study of Howrah Municipality, WB And Its Selected Wards. Journal of Pharmaceutical Negative Results, 13

36. Hailu, Birhane & Mehari, Hagos. (2021). Impacts of Soil Salinity/Sodicity on Soil-Water Relations and Plant Growth in Dry Land Areas: A Review. Journal of Natural Sciences Research. 12. 1-10.

37. Han Jiqin, Fikiru Temesgen Gelata, Samerawit Chaka Gemeda; Application of MK trend and test of Sen's slope estimator to measure impact of climate change on the adoption of conservation agriculture in Ethiopia. Journal of Water and Climate Change 1 March 2023; 14 (3): 977--988. doi: https://doi.org/10.2166/wcc.2023.508

38. Handa, B.K. (1969), Chemical composition of monsoon rains over Calcutta. Part I. Tellus, 21: 95-100. https://doi.org/10.1111/j.2153-3490.1969.tb00421.x

39. Hauer M.E., Fussell E., Mueller V., Burkett M., Call M., Abel K., McLeman R., Wrathall D. Sea-level rise and human migration. Nat. Rev. Earth Environ. 2020;1(1):28--39.

40. Hem John D. (1985) Study and interpretation of the chemical characteristics of natural water, John D. Hem, Third Edition, USGS, Water-Supply Paper 2254

41. Hewitt C.N. (1992) Methods of Environmental Data Analysis. Springer Science +Business Media, B.V.

42. Horton, R.K. (1965) An Index Number System for Rating Water Quality. Journal of the Water Pollution Control Federation, 37, 300-306.

43. Hussin, Nur & Yusoff, Ismail & Raksmey, May. (2020). Comparison of Applications to Evaluate Groundwater Recharge at Lower Kelantan River Basin, Malaysia. Geosciences. 10. 289. 10.3390/geosciences10080289.

44. IMD, 2008: Climate of the West Bengal Controller of Publications, Government of India, New Delhi

45. Jha, V.C. and Bairagya, H.P (2011) Flood plain evaluation in the Ganga-Brahmaputra Delta: A tectonic review. Ethiopian Jrn of Environ. Stud. & Managem. 4 12-24

46. Joshi S. K., S. P.Rai, R.Sinha, S. Gupta, A. L. Densmore, Y. S Rawat, S. Shekhar (2018) Tracing groundwater recharge sources in the northwestern Indian

alluvial aquifer using water isotopes (δ18O, δ2H and 3H), Journal of Hydrology, [559,]{.underline} 835-847, https://doi.org/10.1016/j.jhydrol.2018.02.056.

47. Khan, Ramsha & Saxena, Abhishek & Shukla, Saurabh & Goel, Pooja & Bhattacharya, Prosun & Li, Peiyue & Ali, Esmat & Shaheen, Sabry. (2022). Appraisal of water quality and ecological sensitivity with reference to riverfront development along the River Gomti, India. Applied Water Science. 12. 10.1007/s13201-021-01560-9.

48. Krishnaswami, S. & Singh, Sunil. (2005). Chemical weathering in the river basins of the Himalaya, India. Current Science. 89.

49. Kumar, Rajesh & Rani, Seema & Maharana, Pyarimohan. (2021). Assessing the impacts of Amphan cyclone over West Bengal, India: a multi-sensor approach. Environmental Monitoring and Assessment. 193. 10.1007/s10661-021-09071-5.

50. Li, P., Karunanidhi, D., Subramani, T., & Srinivasamoorthy, K. (2021). Sources and consequences of groundwater contamination. Archives of environmental contamination and toxicology , 80 , 1-10.

51. Liebman, H. (1969). Atlas of water quality methods and practical conditions. Munich: R. Oldenburg.

52. Lu C, Li L, Xu J, Zhao H, Chen M. (2024) Research on the Critical Value of Sand Permeability Particle Size and Its Permeability Law after Mixing. Water . 16(3):393. https://doi.org/10.3390/w16030393

53. Machiwal, D., Cloutier, V., Güler, C., & Kazakis, N. (2018). A review of GIS-integrated statistical techniques for groundwater quality evaluation and protection. Environmental Earth Sciences ,

54. Mandal, R.N. & Das, Chandan & Naskar, K.R.. (2010). Dwindling Indian Sundarban mangrove: the way out. Sci. & Cult. 76 (7-8). 275-282.

55. Margat, Jean, and Jac Van der Gun (2013). Groundwater around the World: A Geographic Synopsis, 1st edition, Hoboken: CRC Press

56. Mazor E (2003) Chemical and Isotopic Groundwater Hydrology: The Applied Approach. Third Edition, CRC Press

57. Mishra V., A Soka, K Vatta, U Lall (2018) Groundwater Depletion and Associated CO~2~ Emissions in India. Earth's Future, 6 , 1672-1681

58. Mitra, A.; K. Mondal and K. Banerjee (2011) Spatial and Tidal Variations of Physico-Chemical Parameters in the Lower Gangetic Delta Region, West Bengal, India. Journal of Spatial Hydrology Vol.11, 52-69

59. Möller, Detlev. (2002). The Na/CL ratio in rainwater and the seasalt chloride cycle. Tellus B. 42. 254 - 262. 10.1034/j.1600-0889.1990.t01-1-00004.x.

60. Mondal, Ismail & Bandyopadhyay, Jatisankar. (2014). Coastal Zone Mapping through Geospatial Technology for Resource Management of Indian Sundarban, West

Bengal, India. International Journal of Remote Sensing. 4. 10.14355/ijrsa.2014.0402.04.

61. MoWR (2014) Ganga Basin, Ministry of Water Resources, Government of India (www.india-wris.nrsc.gov.in)

62. MoWR (2022) Water Security. 21 MAR 2022 7:57PM by PIB Delhi

63. MoWR (2023) Union Minister For Jal Shakti Releases Dynamic Ground Water Resource Assessment Report For The Country For The Year 2023. PIB, 1^st^ Dec 2023

64. Mukherjee, A., Bhanja, S.N. & Wada, Y. (2018) Groundwater depletion causing reduction of baseflow triggering Ganges river summer drying. Sci Rep 8 , 12049. https://doi.org/10.1038/s41598-018-30246-7

65. Mukherjee, Prasun & Das, Subhasish & Mazumdar, Asis. (2020). Evaluating volatility in quality indexing of saline water during tidal backwater incursion in Western Canals of South 24-Parganas, West Bengal. Journal of the Indian Chemical Society. 97. 577-586.

66. Nandy, S. & S. Bandyopadhyay (2011). Trend of sea level change in the Hugli estuary, India. Indian Journal of Geo-Marine Sciences. 40. 802--812.

67. Panda DK, Ambast SK, Shamsudduha M (2021) Groundwater depletion in northern India: Impacts of the subregional anthropogenic land-use, socio-politics and changing climate. Hydrological Processes. 35:e14003. [https://doi.org/10.1002/hyp.14003.]{.underline}

68. Passarella, G., & Caputo, M. C. (2006). A methodology for space-time classification of groundwater quality. Environmental monitoring and assessment , 115 , 95-117.

69. Paul A. K., Mondal D. (2021) Coastal urbanization and population pressure with related vulnerabilities and environmental conflicts - A case study at Medinipur littoral tract, West Bengal. Item: http://inet.vidyasagar.ac.in:8080/jspui/handle/123456789/5748; Vidyasagar University, Midnapore, West Bengal, India,

70. PLFS (2022-2023): Annual Report Periodic Labour Force Survey (PLFS) July 2022 -- June 2023 , Ministry of Statistics and Programme Implementation, Government of India.

71. Rai S. P. , K V Akpataku, Jacob Noble, A Patel, S K Joshi (2023) Hydrochemical evolution of groundwater in northwestern part of the Indo-Gangetic Basin, India: A geochemical and isotopic approach, Geoscience Frontiers, 14, 101676, https://doi.org/10.1016/j.gsf.2023.101676.

72. Rodella, Aude-Sophie, Esha Zaveri, and François Bertone (2023). The Hidden Wealth of Nations: The Economics of Groundwater in Times of Climate Change. Washington, DC: World Bank. Available at

https://www.worldbank.org/en/topic/water/publication/the-hidden-wealth-ofnations-groundwater-in-times-of-climate-change.pdf

73. Rosu, Cristina & Pistea, Ioana & Roba, Carmen & Nes, Monica & Ozunu, Alexandru (2014). Groundwater quality and its suitability for dinking and agriculture use in rural area from Cluj County (Floresti Village) Scientific Papers Series : Management, Economic Engineering in Agriculture and Rural Development. 14.

74. Roy A, S. B. Dhar (2021) Chapter 20 - Forest land degradation and reclamation process in Indian Sundarbans: a case study, Ed.(s): G S Bhunia, U Chaterjee, A. Kashyap, P. K Shit, Modern Cartography Series, Academic Press, 10 , 435-464, https://doi.org/10.1016/B978-0-12-823895-0.00001-4.

75. S.K. Ambast, N.K. Tyagi, S.K. Raul (2006) Management of declining groundwater in the Trans Indo-Gangetic Plain (India): Some options. Agricultural Water Management, 82, 279-296, https://doi.org/10.1016/j.agwat.2005.06.005.

76. Sarkar, A., Shekhar, S., & Rai, S. P. (2017). Assessment of the spatial and temporal hydrochemical facies variation in the flood plains of North-West Delhi using integrated approach. Environmental earth sciences , 76 , 1-12.

77. Schoeller H (1965) Qualitative evaluation of groundwater resources. In: methods and techniques of groundwater investigations and development. In: Proceedings of the UNESCO, pp 54--83

78. Schoeller H (1967) Geochemistry of groundwater. An international guide for research and practice UNESCO, chap 15, pp 1--18

79. Sharma K, N. J Raju, N Singh, S. Sreekesh (2022) Heavy metal pollution in groundwater of urban Delhi environs: Pollution indices and health risk assessment, Urban Climate, [45]{.underline} , 101233, https://doi.org/10.1016/j.uclim.2022.101233.

80. Singh J, S. M. Das, A Kumar (2015) Forecasts of Rainfall (Departures from Normal) over India by Dynamical Model, Aquatic Procedia, [4]{.underline}, 764-771, https://doi.org/10.1016/j.aqpro.2015.02.159.

81. Sinha R. S. (2021) State of Groundwater in Uttar Pradesh -A Situation Analysis with Critical Overview and Sustainable Solutions, Water Aid, Groundwater Action Group, Lucknow, Uttar Pradesh, India

82. Soltan, M. E. (1999). Evaluation of groundwater quality in Dakhla Oasis (Egyptian Western Desert). Environmental Monitoring and Assessment, 57(2), 157--168. doi:10.1023/A:1005948930316.

83. Stephanie Fraser (2021) Water Quality: Analysis and Interpretation. Syrawood Publishing House.

84. Stigter, T. Y., Ribeiro, L., & Carvalho Dill, A. M. M. (2006). Application of a groundwater quality index as an assessment and communication tool in

agroenvironmental policies--Two Portuguese case studies. Journal of Hydrology (Amsterdam), 327, 578--591

85. Susanne M., S. and D.O. Tréguer (2018) Beyond Crop per Drop Assessing Agricultural Water Productivity and Efficiency in a Maturing Water Economy. World Bank.

86. Tafasca, S., Ducharne, A., and Valentin, C.: Weak sensitivity of the terrestrial water budget to global soil texture maps in the ORCHIDEE land surface model, Hydrol. Earth Syst. Sci., 24, 3753--3774, https://doi.org/10.5194/hess-24-3753-2020, 2020.

87. UN (2022) World Population Prospects 2022: Summary of Results July 2022 www.un.org.development.desa.pd/files/undesa_pd_2022_wpp_key-messages.pdf

88. USDA (1951, 2017) Soil Survey Division Staff; Soil Conservation Service Volume Handbook 18, U.S. Department of Agriculture (2017)

89. USDA (1969) US Department of Agriculture Soil Conservation Service (1969) Engineering field manual for conservation practices

90. USDA (1986): Urban Hydrology for Small Watersheds. USDA, Technical Release-55, Manual, 1986

91. Wen, Yao, Jiahao Qiu, Si Cheng, Changchang Xu, and Xiaojiang Gao. 2020. "Hydrochemical Evolution Mechanisms of Shallow Groundwater and Its Quality Assessment in the Estuarine Coastal Zone: A Case Study of Qidong, China" International Journal of Environmental Research and Public Health 17, no. 10: 3382. https://doi.org/10.3390/ijerph17103382

92. Yuan, H., Yang, S., & Wang, B. (2022). Hydrochemistry characteristics of groundwater with the influence of spatial variability and water flow in Hetao Irrigation District, China. Environmental Science and Pollution Research , 29 (47), 71150-71164.

93. Zaveri E, J Russ, R Damania (2020) Rainfall anomalies are a significant driver of cropland expansion. PNAS 117(19) 10225-10233 https://doi.org/10.1073/pnas.1910719117

94. Zeinalzadeh, K., & Rezaei, E. (2017). Determining spatial and temporal changes of surface water quality using principal component analysis. Journal of Hydrology: Regional Studies , 13 , 1-10.

95. Zewdie, M.M., Kasie, L.A. & Bogale, S. (2024) Groundwater potential zones delineation using GIS and AHP techniques in upper parts of Chemoga watershed, Ethiopia. Appl Water Sci 14 , 85. https://doi.org/10.1007/s13201-024-02119-0